NTNU
Norwegian University of
Science and Technology

Corrosion of Nickel-Aluminium Bronze

How does the different alloying elements
effect the corrosion properties?

Ellen Synnøve Skilbred

Abstract

This thesis examines the effect of copper, aluminium, iron and nickel on the corrosion properties of Nickel-Aluminium bronze (NAB) in seawater. NAB has a complex microstructure consisting of a copper-rich phase, α, and several intermetallic phases, κ. NAB is documented to be susceptible to selective phase corrosion (SPC), where different phases corrode at different pH levels. The stability of aluminium oxide is assumed to cause this pH-dependency. However, the behaviour of aluminium is known to be generally unstable in seawater, thus a more thorough examination of the issue is of interest. The NAB alloy examined was characterized to find the amount of each element in each phase and the volume fraction of copper-rich and intermetallic phases. Several corrosion experiments were performed in synthetic seawater (SSW) to shed light on the corrosion behaviour of NAB at different potentials and pH, as well as the effect of the main alloying elements on the corrosion properties of NAB. Aluminium oxide was established to be unstable in SSW with pH<6, whereas partially hydrated nickel oxide displayed stability in the same region as NAB. This indicates that nickel may contribute to passivity of NAB. It is thus suggested that the passivity of NAB is attributed the formation of a passive layer of aluminium oxide that is stabilized by the presence of nickel. When the passive film is stable, the corrosion properties are dominated by corrosion of copper. When the film is unstable, intermetallic phases corrode actively which decreases the open circuit potential (OCP). At pH<4, the copper-rich phase is galvanically protected until the surface is depleated from iron-rich intermetallic phases, or as long as the potential of the surface is kept below the OCP of copper. The alloy's iron is mainly situated in small, iron-rich intermetallic particles and these have not appeared detrimental for NAB, as they are embedded in other phases that are not iron-rich. Iron is thus not concidered to inflict singificant corrosion problems for the microstructure examined in this thesis. The main concern of corrosion at pH<4 is the continuous intermetallic phase, κ_{III}, which is nickel- and aluminium-rich. If NAB is to be used in seawater and there is a possibility that it will be subject to pH<4, like during crevice corrosion or if covered by marine debris, heat treatment is suggested to make sure all intermetallic phases are discontinuous near the surface. Then, the corrosion propagation will probably to a greater extent be determined by the copper-rich phase, which has a slower corrosion rate than the intermetallic phases.

Keywords: Nickel-Aluminium bronze (NAB), selective phase corrosion (SPC), passivation, static polarization, polarization curves, characterization, copper, aluminium, nickel

Sammendrag

Denne avhandlingen undersøker hvordan kobber, aluminium, jern og nikkel influerer korrosjonsegenskapene til nikkel-aluminium bronse (NAB) i sjøvann. NAB har en kompleks mikrostruktur, som består av en kobberrik fase, α, og flere intermetalliske faser, κ. NAB er mottakelig for selektiv korrosjon (SPC), hvor ulike faser korroderer ved ulike pH. Stabiliteten til aluminiumoksid antas å være grunnen til denne pH-avhengigheten. Men, aluminiumoksid er generelt kjent for å oppføre seg ustabilt i sjøvann og en mer inngående undersøkelse er av interesse. NAB legeringen, som undersøkes i denne avhandlingen, ble karakterisert for å finne andelen kobber, aluminium, jern og nikkel i hver fase, samt volumfraksjonen av kobberrik fase og intermetalliske faser. Flere korrosjonsforsøk ble utført i syntetisk sjøvann (SSV) for å belyse korrosjonsegenskapene til NAB ved ulike potensial og pH, samt innflytelsen hvert hovedlegeringselement har på korrosjonsegenskapene til NAB. Aluminiumoksid viste seg å være ustabilt i SSV med pH<6, mens delvis hydrert nikkeloksid var stabilt i samme område som NAB. Dette indikerer at nikkel bidrar til passivitet for NAB. Denne avhandlingen foreslår at passiviteten til NAB oppstår ved dannelsen av en aluminiumoksidfilm som er stabilisert av nikkel. Når filmen er stabil er korrosjonsegenskapene kontrollert av kobber. Når filmen er ustabil vil de intermetalliske fasene korrodere aktivt og gjøre åpen krets potensialet (OCP) lavere. Ved pH<4 er den kobberrike fasen galvanisk beskyttet til overflaten er utarmet av de jernrike intermetalliske fasene, eller så lenge potensialet er lavere enn OCP for kobber. Jernet i legeringen befinner seg for det meste i små intermetalliske partikler og disse ser ikke ut til å være skadelige for NAB, siden de er innkapslet i andre faser som ikke er jernrike. Jernet i legeringen ser altså ikke ut til å skape betydelige korrosjonsproblemer for mikrostrukturen som undersøkes i denne avhandlingen. Hovedproblemet med korrosjon ved pH<4 er den sammenhengende intermetalliske fasen, κ_{III}, som er rik på nikkel og aluminium. Hvis NAB skal brukes i sjøvann og det er mulig at materialet blir utsatt for pH<4, for eksempel i forbindelse med spaltkorrosjon eller marin groe, foreslås det å benytte seg av en varmebehandling som sørger for at alle de intermetalliske fasene er ikke-kontinuerlige nær overflaten. Da vil trolig korrosjonsutviklingen i større grad bli bestemt av den kobberrike fasen, som har lavere korrosjonshastighet enn de intermetalliske fasene.

Preface

This thesis is submitted in partial fulfillment of the requirements for degree Master of Science (MSc) at the Norwegian University of Science and Technology (NTNU).

The thesis is based on my research in the course *Materials, Specialization Project* (TMM4511), which was submitted in December 2015 [1].

First of all I will thank my supervisors, Professor Roy Johnsen and Ph.D Candidate Hedda Nordby Krogstad, for guidance, support and encouragement.

A lot of laboratory work have been conducted in association with this thesis. I thank the employes at the SINTEF corrosion laboratory at NTNU for being of assistance whenever I needed help. I also thank Cristian Torres Rodriguez for interesting discussions and good advice in the corrosion laboratory, and Hedda Nordby Krogstad for accompanying me and guiding me in unconventional corrosion experiments.

Finally, I would like to thank my familiy and Espen Skjong, for support, guidance and proofreading.

Trondheim, 1. June 2016.

Ellen Synnøve Skilbred

iii

Contents

List of Figures

List of Tables

Nomenclature

Abbreviations and symbols

η	Overpotential
b_a	Anodic Tafel slope
b_c	Cathodic Tafel slope
E	Potential
i	Current density
i_{corr}	Corrosion current density
Ag/AgCl	Silver/silver chloride electrode
BCC	Body centered cubic
Cu**Al**10**Fe**5**Ni**5	NAB alloy with 80% copper, 10% aluminium, 5% iron and 5% nickel
EDS	Energy-dispersive X-ray spectroscopy
FCC	Face centered cubic
IIR	Infinite impulse response
NAB	Nickel-Aluminium bronze
OCP	Open circuit potential
SEM	Scanning electron microscopy
SHE	Standard hydrogen electrode
SPC	Selective phase corrosion
SSW	Synthetic seawater

Chapter 1

Introduction

This chapter is an introduction to the scope of this thesis. A short literature review is given in Section 1.1 to illuminate the composition and corrosion performance of the Nickel-Aluminium Bronze (NAB) alloy examined in this thesis. A summary of experiments previously conducted by the author on NAB and its main alloying elements is given in Section 1.2 [1]. Finally the thesis outline is given in Section 1.3.

1.1 Background

NAB alloys are commonly used in underwater structures where good mechanical properties and corrosion resistance are required. NAB is a multi-phase alloy consisting of a copper rich phase, α, and several intermetallic phases, κ, with higher contents of aluminium, nickel and iron. The intermetallic phases improve the mechanical properties and the alloy has excellent corrosion resistance, especially to cavitation and corrosion fatigue [3]. The composition of the constituent phases of NAB has been documented several times, with varying results [2, 4–8]. The documented compositions of the intermetallic phases are often inconsistent and NAB is often described as a complex alloy. The NAB alloy discussed in this thesis contain 80 % copper, 10 % aluminium, 5 % iron and 5 % nickel, and is commonly denoted as Cu**Al**10**Fe**5**Ni**5.

The good corrosion properties of NAB in seawater is attributed the formation of a passive film. Schüssler and Exner [9] examined the formation and character of this film and identified aluminium and copper oxides as the main compounds. However, the content of nickel within the film was not examined in this examination. The passive film of aluminium bronzes may be degraded during prolonged exposure in stagnant seawater, especially in the presence of sulphide [3]. Nakhaie et al. and Song et al. [8,10] measured the Volta potentials of the NAB phases and documented that the κ phases were less noble than the α matrix. Thus, the α phase is galvanically protected by the corrosion of κ, when κ corrodes actively. However, the κ phases have been documented to contain more aluminium than α. When aluminium oxide has been formed on the NAB surface κ is protected while α is susceptable to corrosion [1,8]. Neodo et al. [4] documented that α corrodes at pH>4.0, while κ preferentially corrode for pH<4.0, due to the stability of the aluminium oxide.

Selective phase corrosion (SPC) of NAB has been documented at welds, crevices and under marine growth [11]. Crevice corrosion in NAB is rare, but may cause severe damage when it occurs [3]. Development of an acidic environment during crevice corrosion reverses SPC, so the κ phases are corroding actively while α is galvanically

protected. The corrosion rates are increased almost ten times in these conditions. Wharton and Stokes [12, 13] studied the formation and propagation of NAB crevice corrosion in seawater. They found that the lamellar κ phase was the most vulnerable phase, with corrosion attacks as deep as 80 μm after only a month. The propagation of such an attack depends on the formation of an acidic environment within the crevice.

1.2 Preliminary project

In the preliminary project work to this master project the corrosion behaviour of NAB and the main alloying elements copper, aluminium, iron and nickel, was investigated [1]. The main objective of the project was to examine how the main alloying elements effect the corrosion properties of NAB. The corrosion experiments conducted were a two week immersion test and polarization tests, for samples exposed one hour in the electrolyte before polarization. Both types of tests were performed for each material in synthetic seawater (SSW) with pH≈3.5 and pH≈8. The surfaces were grinded shortly before immersion. The most important observations from the project are listed in the following:

- The most copper rich phase of NAB corroded at pH≈8 while the intermetallic phases corroded at pH≈3.5, see Figure 1.1.

- The polarization curves for copper and iron were seemingly independent of pH.

- Aluminium suffered from pitting to a larger degree at pH≈3.5 than pH≈8, had five times higher corrosion current density at pH≈3.5 than pH≈8, but had a similar open circuit potential (OCP) in both environments.

- The polarization curves of nickel at pH≈8 and pH≈3.5 differed in both OCP and corrosion current density.

- Nickel was passively protected at pH≈8, while active corrosion occured at pH≈3.5.

- Both NAB and nickel had considerably lower OCP at pH≈3.5 than pH≈8.

- The OCP of NAB in SSW with pH≈3.5 increased during the first 24 hours of exposure. From then, NAB kept an OCP above -235 mV vs silver/silver chloride electrode with saturated KCl concentration, short hand notation mV vs Ag/AgCl, until the test finished after two weeks. The NAB sample was exposed in the same container as samples of pure aluminium and nickel and the validity of this test may thus be questioned.

The small difference in corrosion properties for aluminium in the two environments suggests that the passive protection of NAB at high pH is enhanced by the presence of other elemets as well. Nickel is a possible candidate, given the very different behaviour in the two environments. Iron exhibited similar corrosion behaviour in SSW with

pH≈3.5 and pH≈8, and further investigations of the corrosion properties of iron are not prioritized in this work.
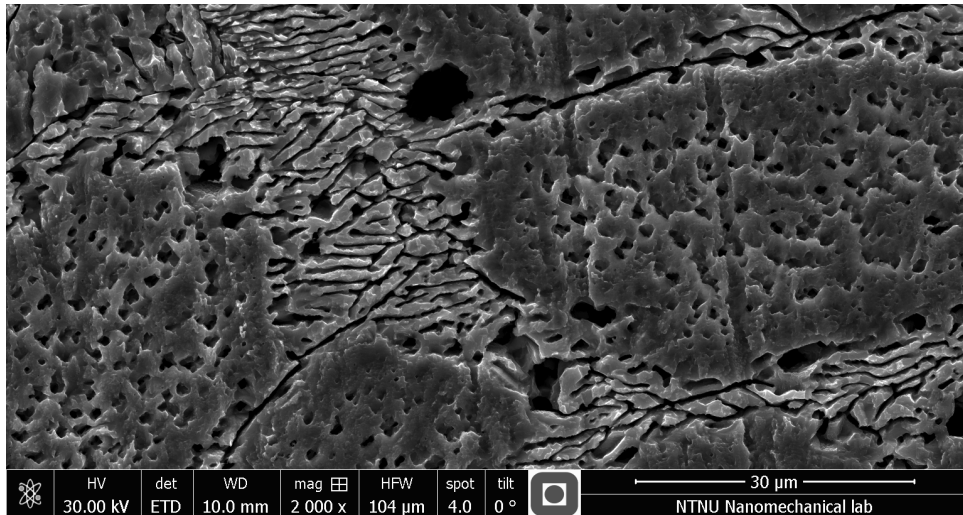
(a) NAB exposed two weeks in SSW with pH≈3.5.
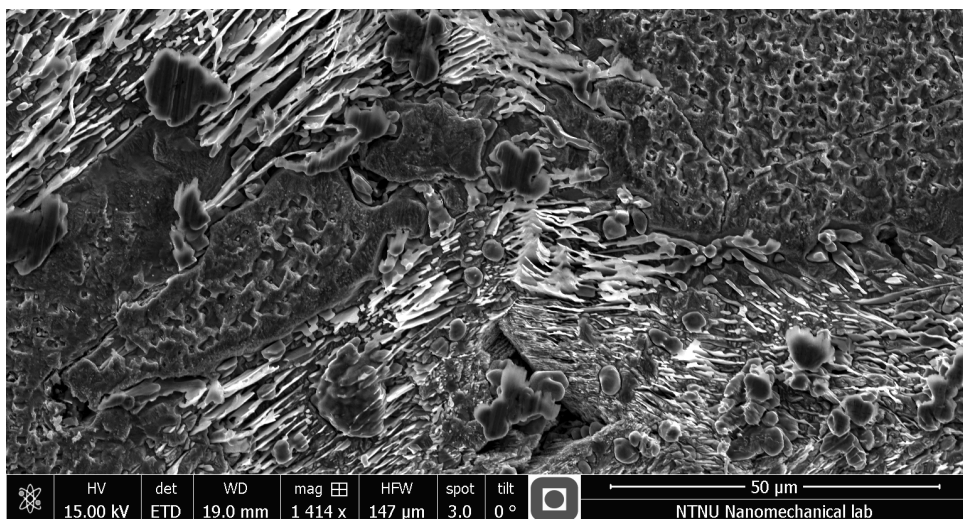
(b) NAB after cathodic and anodic polarization in SSW with pH≈8.2.

Figure 1.1: SEM images of NAB test samples from the project work prior to this thesis.

1.3   Thesis outline

The aim of this thesis is to acchieve a good understanding on how the alloying elements effect the corrosion properties of NAB and how the phases in the material behave at different potentials and pH. The corrosion properties at low pH are of special interest and determining whether nickel plays a significant role in the pH-dependent behaviour of NAB corrosion.

The main objectives of interest are:

- To examine the stability of aluminium oxide at different pH levels.

- To determine whether nickel effect SPC of NAB.

- To examine the corrosion behaviour of NAB and its constituent phases at different potentials and pH levels.

- To connect the corrosion behaviour of the NAB phases to their main elements.

- To evaluate the extent of corrosion attacks on NAB at low pH.

Several tests were conducted to shed light on the objectives above. Corrosion tests were conducted and corroded surfaces observed by scanning electron microscopy (SEM). Energy-dispersive X-ray spectroscopy (EDS) analyses were performed to identify the amount of the elements in the phases of un-corroded NAB and for examining the surfaces of the corroded samples. Image analyses were used to determine the relative amount of copper-rich phase vs intermetallic phases. Corrosion experiments were performed to determine whether it is likely that nickel has a larger part in SPC of NAB than it is credited for. The stability of aluminium was also tested in SSW with varying pH. NAB was immersed in SSW with pH$\in$<3,4> for periods up to eight weeks, to examine the corrosion development of NAB at low pH. Polarization tests have been performed for NAB, copper, aluminium and nickel in SSW with pH=8.2 and SSW with pH=3.5.

The original project description is given in Appendix D.

Chapter 2

Theoretical Background

This chapter is an introduction to the microstructure of NAB and the corrosion properties of NAB, copper, aluminium and nickel. Some attention is also given the copper alloys Cu-Ni and Cu-Al to shed some light on the effect of nickel and aluminium in copper.

2.1   The microstructure of NAB
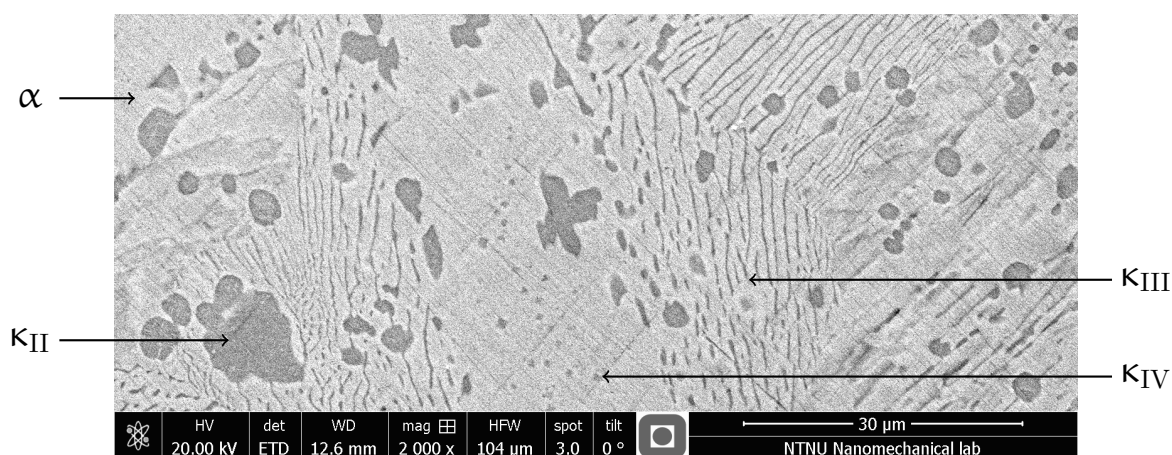
Figure 2.1: Microstructure of as-cast NAB.

The equilibrium phases of Cu**Al**10**Fe**5**Ni**5 at room temperature are named α and κ [3]. α is a copper rich phace with face centered cubic (FCC) structure. κ is a number of intermetallic phases with high contents of nickel, iron and aluminium. The κ-phases are distinguished by morphology, location and distribution in the microstructure [12]. The location and contents of the κ particles are defined differently in the literature, hence some care should be taken before comparing written material about the NAB phases. A main distinction between the phases is whether it is based on NiAl or Fe_3Al. Both the NiAl and Fe_3Al structures have an ordered body centered cubic (BCC) structure [3]. Iron, nickel or copper may substitute the nickel in NiAl and the iron in Fe_3Al. In this thesis the definition given by Hasan et al. [2] is used. Hasan et al. investigated the contents of alloying elements in as-cast NAB phases. The results for α and the κ-phases are given in Table 2.1. According to [2], κ_I, κ_{II} and κ_{IV} are based on Fe_3Al, whereas κ_{III} is based on NiAl. The position and morphology of the particles are correlated to the phase transformations that occur in the alloy during cooling. For that reason a brief summary about the phase transformations is included. The summary is based on the works of A. Jahanafrooz et al. [6] on phase transformation of Cu-Al-Fe-Ni alloys. Between about

1000°C and 900°C, κ_{II} nucleate in a copper-rich phase called β. The κ_{II} particles are dendritic in shape and have diameters of 5 to 10 μm [2]. The κ_{II} particles that nucleate at the α/β-grain boundaries may be enveloped in the α phase as α grows. Between 940°C and 840°C, κ_{IV} particles start to form in the α phase as a result of low solubility of iron in α at such temperatures. Thus, κ_{IV} particles only appear in the centre of the α-phase in as-cast material. Between 840°C and 800°C, depending on alloy composition, the remaining β will transform to a lamellar structure of α and κ_{III}. κ_{III} is often described as continuous in nature [12]. Some of the initially formed κ_{III} is globular in shape, but most of the κ_{III} phase is lamellar. Heat treatments may result in spheroidization of κ_{III}, but these treatments are rarely applicable to large castings [5]. At normal cooling rates, some β will remain and form a martensitic structure.
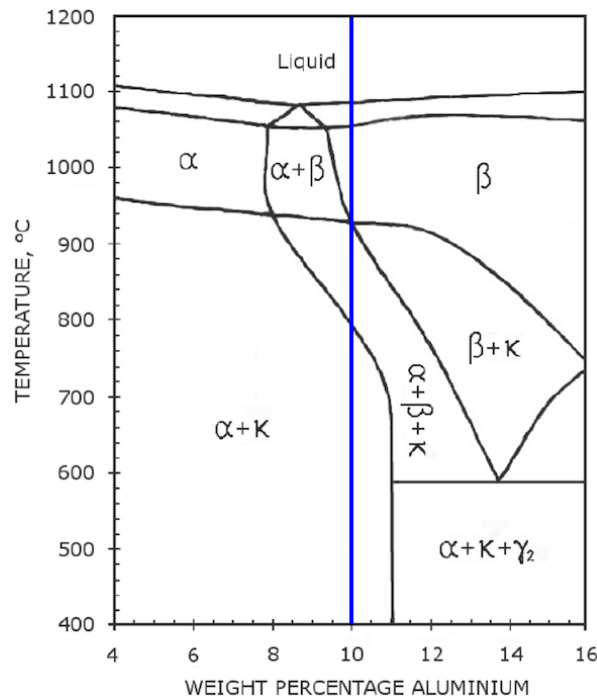
Figure 2.2: NAB phase diagram [3].

Table 2.1: Alloying content of κ-phases (wt%) found by Hasan et al. [2].

Phase	Copper	Aluminium	Iron	Nickel	Other elements
α	85.8	7.2	2.8	3.0	1.5
κ_I	10.5	9.3	72.2	3.5	4.5
κ_{II}	12.1	12.3	61.3	8.0	6.3
κ_{III}	17.0	26.7	12.8	41.3	2.2
κ_{IV}	2.6	10.5	73.4	7.3	6.2

2.2 Role of the alloying elements

NAB alloys are attractive due to their good mechanical properties and corrosion resistance. Aluminium is the element with the most significant effect on the corrosion resistance of aluminium bronzes, and also the element in NAB with the most pronounsed effect to mechanical properties [3]. The elongation of aluminium bronzes increases with increasing content of aluminium until 8 wt% is reached. The elongation decreases rapidly for aluminium contents above 8 wt% until it reaches zero at about 13 wt% aluminium, due to formation of a corrodible phase called γ_2. The tensile strength of aluminium also increases with increasing aluminium content until 10 wt% is reached. Iron acts as a grain refiner in NAB and improves the strength, hardness, toughness and fatigue. The corrosion resistance, however, is decreased when iron is added. By adding nickel together with iron the corrosion properties are improved. The best corrosion resistance is achieved when the nickel content is higher than the iron content. Nickel expands the $\alpha+\kappa$ field of the phase diagram to a higher aluminium content, which makes it possible to create alloys of higher strength without the very corrodible γ_2 phase. The maximum content of aluminium, possible without risking γ_2 formation, is thus dependent on the nickel content. Nickel also improves the hardness, but reduces the elongation. Aluminum bronzes with approximately 5 wt% of both iron and nickel, like the Cu**Al**10**Fe**5**Ni**5 alloy, have good corrosion properties and high strength, and are widely used.

2.3 Passivation

NAB creates a passive film when exposed to seawater, which reduces the corrosion rate by a factor of 20-30 [9]. Aluminium is concidered to be the element in NAB that contributes the most to passivity. An Al_2O_3 layer restrains ionic transport across the corrosion product. However, long time corrosion resistance is dependent on the subfilm structure [3]. The formation of Cu_2O in the outer part of the protective layer reduces the charge transfer of the oxygen reduction and decreases the cathodic reaction rate. The passive film formed during anodic polarization is 15 nm thick and consists of a compact Al_2O_3 layer of $\sim$9 nm. A typical polarization curve for NAB in seawater is given in Figure 2.3, indicating an OCP of about -290 mV vs Ag/AgCl for an active surface, and -240 mV vs Ag/AgCl for a passive surface. The anodic Tafel slopes for NAB is +60 mV/decade in the initial stage and +210 mV/decade in 0.6M NaCl electrolyte [4]. The passive layer of a freshly prepared NAB surface in seawater is formed in three stages [9]. First, the corrosion rate is constant and controlled by surface reactions. In the second stage the corrosion current is considerably decreased to a linear relation with the square root of exposure time. This dependence indicates that diffusion determines the corrosion rate. Since the passive layer is aluminium rich, the corroson process is most likely controlled by the aluminium ion transportation in the Al_2O_3 phase. In the last stage the corrosion current is again constant and determined by metal ion dissolution at a constant layer thickness. The growth of Al_2O_3 is assumed completed. The reduced diffusion of aluminium ions through the passive layer makes copper preferentially oxidized on the

oxide surface. This theory is supported by significant copper enrichment found in the outer part of the fully developed corrosion layer.

The oxidized copper ions react with chloride to form a dichlorocuprous anion complex. This reaction is generally simplified to [12]

$$Cu + 2Cl^- \rightarrow CuCl_2^- + e^-, \tag{2.1}$$

where $CuCl_2^-$ may be transformed to Cu_2O to some extent, depending on the pH and chloride concentration of the electrolyte. This process is more thoroughly decribed in the section about corrosion of pure copper, Section 2.5.1. Investigations of α-Al-bronze have documented very early formation of Cu_2O, which grew progressively over time, under open-ciruit conditions [14]. The dissolution of copper starts in the α phase within the α/κ_{III} eutectoid [4].
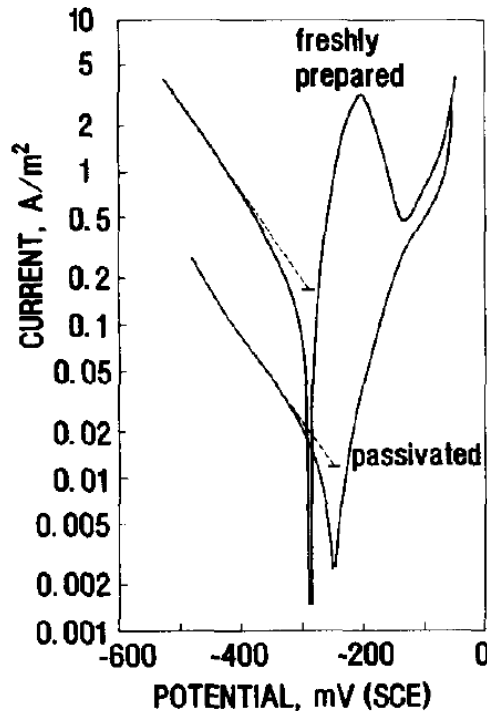
Figure 2.3: Typical polarization curve of NAB in seawater [9].

2.4 SPC

In neutral chloride containing electrolytes, the copper rich α phase of NAB corrodes while the κ phases are cathodically protected [3, 4, 10]. α-Al-bronze, which has composition close to that of α in NAB, suffers from corrosion shortly after immersion in chloride media, leading to general corrosion and pit nucleation, growth and merging

of neighboring pits [14]. The corrosion products on α-Al-bronze create a duplex layer with Al_2O_3 on the inner surface and an outer layer of Cu_2O, $Cu(OH)_3Cl$ and $Cu(OH)Cl$. $Cu(OH)Cl$ may be detected on the surface after nine days, while $CuCl$ is only detected on samples subject to anodic potentials conciderably higher than the OCP. The electrochemical behaviour of NAB has however been observed to be pH-dependent. In chloride containing electrolytes with pH<4 the corrosion performance appears to be controlled by the dissolution of the κ_I-, κ_{II}- and κ_{IV}-phases [4]. However, when exposed to the low pH environment for 5 hours, the NAB polarization curve at pH<4 is similar to that at pH>8. This is reflected both in OCP and the shape of the linear polarization curve, as can be seen in Figure 2.4. Above pH=4.0 the OCP remains stable at -210 mV vs Ag/AgCl, whereas at pH<4.0 the OCP decreases markedly after a few minutes, to a potential dependent on the H^+ concentration [4]. α dissolves at about the same potential as pure copper while the κ dissolves at approximately -300 V vs Ag/AgCl [4].

The SPC of NAB is important in environments where the local environment at the NAB surface is subject to pH alteration. Such an environment is created during crevice corrosion of NAB. Crevice corrosion is a corrosion type that takes place in and near crevices and other structures where mixing of electroyte and ion transportation is significantly limited. Crevice corrosion may lead to severe failures due to the extreme chemical conditions generated locally within the confined space [4]. Copper alloys are usually only susceptable to crevice corrosion when cathodically protected, but NAB has been reported to be susceptable also when not cathodically protected [12]. Wharton and Stokes [12, 13] studied the crevice corrosion properties of NAB. Two SEM images from their crevice experiments are given in Figure 2.5. Among their research is investigations of the solution chemistry development during crevice corrosion of NAB, with analyses of metallic cations and inorganic anions [13]. The solution within the crevice has a chloride concentration four times that of the bulk solution and is subject to metal cation accumulation, especially cupric ions. Wharton and Stokes [13] propose that chloride accumulation results from an initial copper(I) chloride complex formation and subsequent oxidisation to the less stable copper(II) complexes, which allows the chloride ions diffusion from the surface back to the bulk solution. The locations of crevice corrosion initiation are dependent on variations of metal-ion concentration. The hydrolysis of metal cations within the crevice alters the concentrations and thus the locations of corrosion activity. This complicates the crevice corrosion mechanism. Initially, corrosion is confined to the eutectoid regions with a slight attack of α in the $\alpha+\kappa_{III}$ eutectoid. The location of the crevice corrosion initiation appears to be controlled by a copper-ion concentration cell, similar to the mechanism normally associated with copper-based alloys. However, propagation of crevice corrosion depends on formation of an acidic environment within the crevice. Due to its continuous character the κ_{III} phase is especially vulnerable to crevice corrosion. After a month κ_{III} had corroded to a depth of about 80µm. At cathodic sites on the corroded surfaces within the eutectoid regions copper had redeposited, see Figure 2.5.
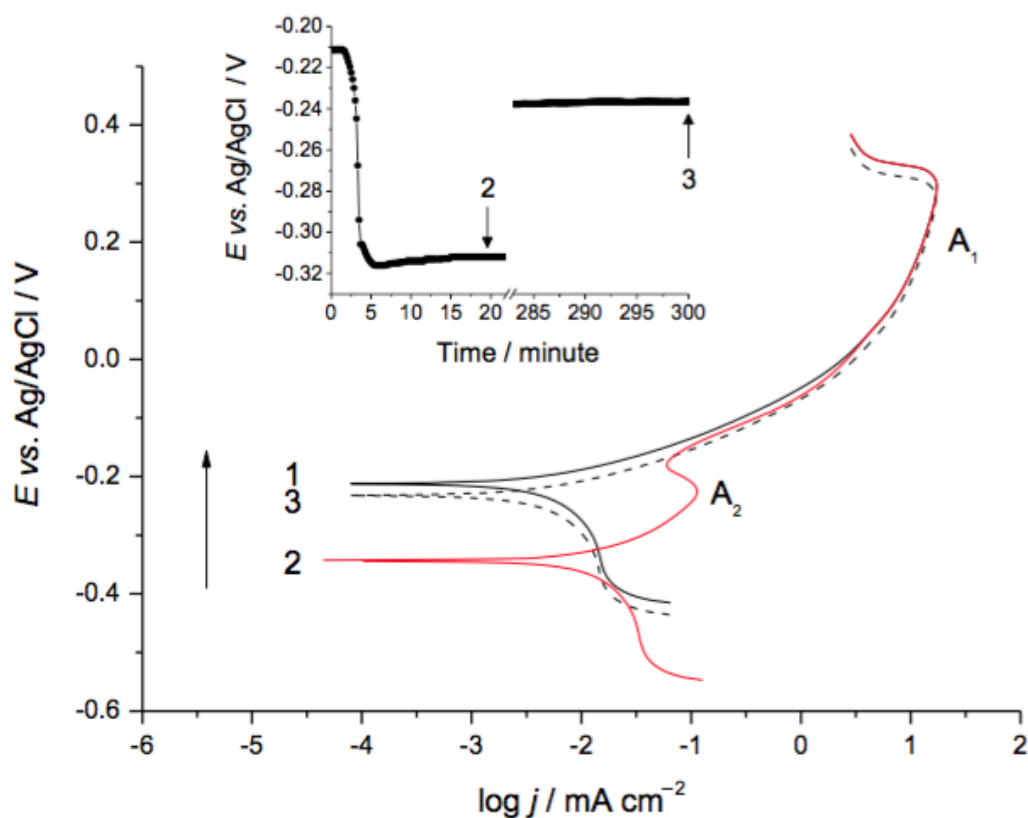
Figure 2.4: Polarization curves for NAB at scan rate 1 mV/s in 0.6M NaCl: (1) at pH=6.2, (2) and (3) at pH=3.5. Tests (1) and (2) were conducted after 20 minutes of immersion, whereas (3) was conducted after 5 hours of immersion. The inset shows the OCP trend of (2) and (3) before polarization. The long arrow indicates direction of scan rate [4].

(a) The centre of a crevice zone.

(b) Deposited copper in previous κ_{III} location.
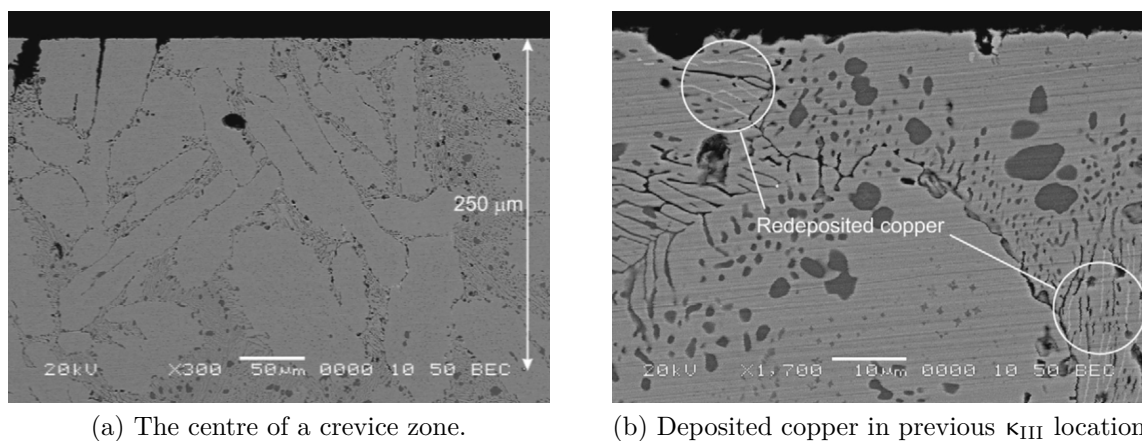
Figure 2.5: NAB after 6.5 months of crevice corrosion while immersed in 3.5% NaCl solution [12].

2.5   The corrosion properties of the main alloying elements

The alloying elements in focus in this thesis are the elements that exhibited passive behaviour in SSW during experiments in the preliminary project. These materials are copper, aluminium and nickel. Pourbaix diagrams of these materials are given in figures 2.7, 2.9 and 2.10. The reader should note that the potentials in the pourbaix diagrams are given in V vs a Standard hydrogen electrode (SHE). This is 0.2 V higher than the potentials measured versus the saturated Ag/AgCl reference, which is the reference used in Chapter 4. The pourbaix diagrams are given for a certain activity of chloride ions and a certain temperature. Temperature and presence of agressive species like chloride ions are known to alter the passive behaviour of materials. Both increased temperature and increasing content of agressive species affect the polarization curves by increasing the passive potential, the critical current density and the passive current density, and reducing the pitting potential. Pitting is also facilitated by stagnant electrolytes.

The expected reduction reactions, for the environment and the potential range of the experiments conducted in this work, are H_2 evolution, as described in (2.2), or O_2 reduction, as described in (2.3) for acidic environment and in (2.4) for alkaline environment.

$$2H^+ + 2e^- \rightarrow H_2 \tag{2.2}$$

$$O_2 + 4H^+ + 4e^- \rightarrow 2H_2O \tag{2.3}$$

$$O_2 + 2H_2O + 4e^- \rightarrow 4OH^- \tag{2.4}$$

As the reactions display, both O_2 reduction and H_2 evolution increase the pH of the solution by producing OH^- or consuming H^+. The reduction reactions are drawn in the Pourbaix diagrams in figures 2.7, 2.9 and 2.10 as broken lines (a) and (b), where (a) is the H_2 evolution and (b) is O_2 reduction.
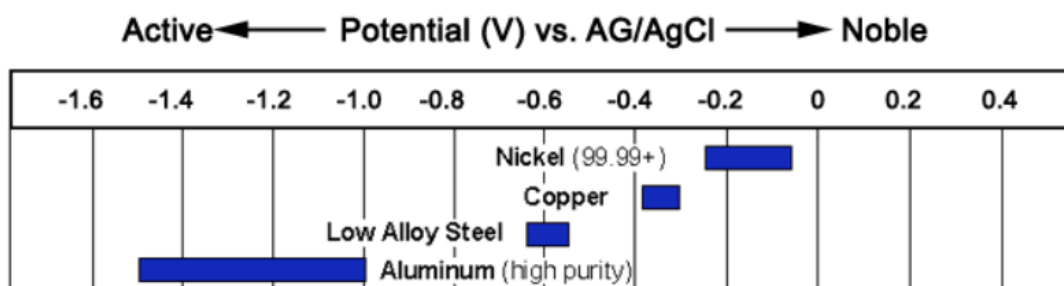
Figure 2.6: Galvanic series of metals and alloys in seawater [15].

A galvanic series of materials similar to the alloying elements is given in Figure 2.6. The potential range of pure elements is larger than alloyed materials, thus the range for pure iron probably spans more values than the bar for low alloy steels. The potential is also expected to be lower, as the common alloying elements of iron are positioned higher in the galvanic series. The observed potentials for pure iron in the preliminary project were about -700 mV vs Ag/AgCl [1].

2.5.1   Copper

Copper is a noble metal which forms passive protective films in marine environments [16]. The films can be composed of copper oxides, oxychlorides of copper, copper carbonate and calcareous material [17]. Copper and copper alloys are only long term corrosion resistant when in a passive state [18]. The corrosion rates of copper immersed in seawater is typically 0.0127-0.0508 mm/year [16]. $CuCl_2^-$ has been documented to be the main cuprous chloride complex in the passive layer, when copper is exposed to seawater and other saline electrolytes [18]. The passive layers are poorly conducting and the transport processes through the corrosion product layers are limited. Thus, the overall anodic and cathodic reaction rates are limited by the passive layer. According to Figure 2.6, the OCP of copper in seawater is between -400 and -300 mV vs Ag/AgCl. The pourbaix diagram in Figure 2.7 shows that copper is immune or passively protected at pH>7, and immune at potentials below 0 mV vs Ag/AgCl in electrolyte with 0.67 activity of Cl^-. The chloride ion has a strong influence on the corrosion mechanism of copper. Oxygen content, velocity of the seawater, temperature, metal ion concentration and biofouling also affect the performance of copper in seawater, including film formation [16]. In other porbaix diagrams of copper in seawater, with other chloride concentrations and activities of copper, a region of $Cu_2(OH)_3Cl$ is situated between the Cu^{2+} region and CuO region and the $CuCl_2^-$ region is replaced with a CuCl region [18, 19]. Anodic dissolution tests of copper in sodium chloride solutions indicate that the anodic process of copper is under diffusion control and that the anodic process independent of pH, but dependent of Cl^- concentration [20].

Anodic polarization curves have demonstrated Tafel behaviour with slopes equal to 60 mV/decade for room temperatures [20]. However, another Tafel region is apperant for filmed surfaces in aquatious chloride media at high potentials, starting about 0.2 V above the OCP, due to formation of Cu(II) species [18]. The initial oxidation reaction for copper alloys in unpolluted seawater is [19],

$$Cu \rightarrow Cu^+ + e^-.$$

The corresponding reduction reaction is O_2 reduction, which is described in equations (2.3) and (2.4). The anodic reaction is believed to involve the formation of a cuprous chlorocomplex, which subsequently reacts with hydroxyl ions to produce a Cu_2O layer.

$$Cu + 2Cl^- \rightarrow CuCl_2^- + e^-$$

$$2CuCl_2^- + 2OH^- \rightarrow Cu_2O + H_2O + 4Cl^-$$
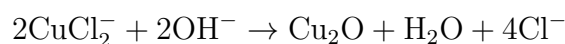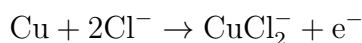
Cu_2O will transform to CuO as the oxide thickens,

$$Cu_2O + H_2O \rightarrow 2CuO + 2H^+ + 2e^-.$$
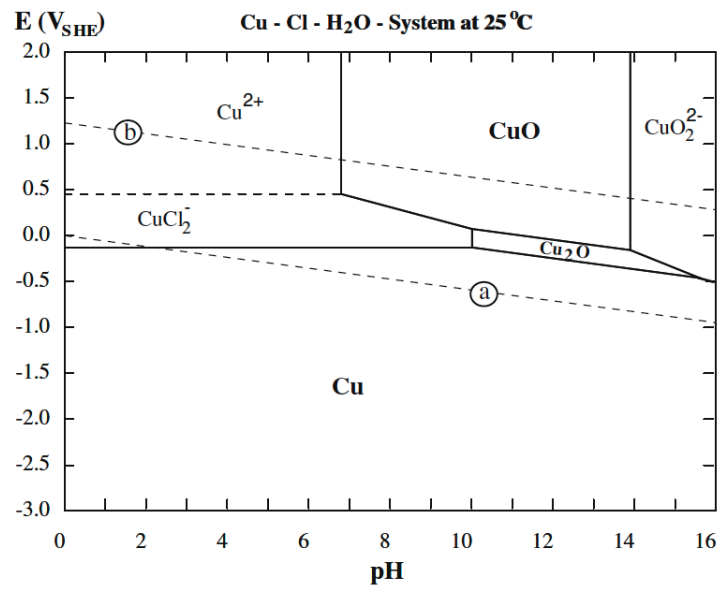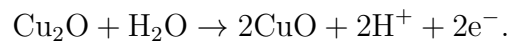
Figure 2.7: Pourbaix diagram of copper in the presence of 0.67 activity of Cl^- [21].

2.5.2 Cu-Al and Cu-Ni

Alfantazi et al. [21] investigated copper, Cu-Al and Cu-Ni alloys in chloride media. Cu-Al alloys suffer from dealloying of aluminium due to the difference of potential between copper and aluminium. The OCP first decreases when Cu-Al is immersed in chloride media with pH=6. Aluminium corrodes at this potential until the surface is depleated from aluminium. Copper in Cu-Al then starts corroding at a potential similar to that of pure copper. Cu-Ni alloys did not suffer from dealloying of nickel in the same way because the potential of nickel is more similar to the potential of copper. The OCP of Cu and Cu–Ni decreased upon immersion in chloride media with pH=6 before reaching a steady state value. The OCPs of all the alloys were stable after less than 20 minutes. Polarization curves for copper, Cu-Al and Cu-Ni are given in Figure 2.8. Two peaks were observed in the polarization curve of pure copper at pH=10, and one peak in Cu-Ni. The upper one, which was only found for pure copper, is caused by the formation of CuO, while the lower, which was observed for both pure copper and Cu-Ni, was caused by the formation of Cu_2O.
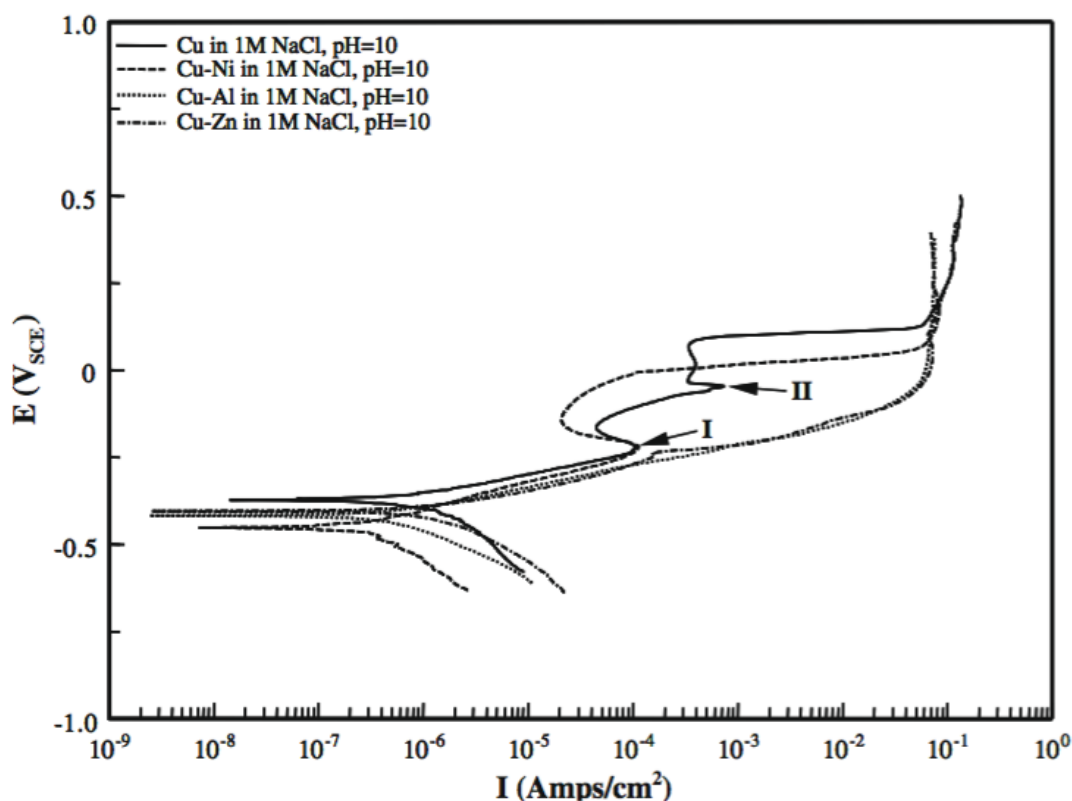
Figure 2.8: Polarization curves of Cu, Cu-Al and Cu-Ni in chloride solution with pH=10 [21].

2.5.3   Aluminium

Aluminium alloys usually have good resistance to corrosion in seawater, although pure aluminium is known to have unstable behaviour in seawater. According to the galvanic series in Figure 2.6, the OCP of pure aluminium in seawater spans a large range of values, from -1500 to -1000 mV vs Ag/AgCl. Aluminium forms Al_2O_3, when submerged in seawater. Due to low solubility of oxygen in water at 20°C and atmospheric pressure, the assumed reduction reaction accompanying the oxidation of aluminium is reduction of H^+ ions [22]. Al_2O_3 is insoluble in water and precipitates on the surface [22]. After complete film formation on the metal surface, the corrosion rate of aluminium decreases to a low passive current. Certain elements, such as magnesium, strengthen the protective properties of Al_2O_3 by forming mixed oxides [22]. This requires the structures of aluminium and the other element to be compatible. Other elements, such as copper, weakens the protective properties. Deposition of Cu^{2+} ions can cause severe pitting corrosion of aluminium alloys. The Cu^{2+} ions can also be reoxidised, i.e. dissolved as Cu^{2+} ions, and then be reduced again by the aluminium. On the other hand, the pitting potential of aluminium alloys increases with increasing copper content, at least for copper contents below 10% [23]. This suggests a beneficial effect from copper in aluminium, considering corrosion resistance properties. The pourbaix diagram of aluminium, given in Figure 2.9, shows that Al_2O_3 is stable above -1550 mV vs Ag/AgCl, and between pH 4.5 and 9.2 in an eletrolyte with 0.67 activity of Cl^-. The diagram also shows that active corrosion occurs at pH<4.5 when the potential is above -155 mV vs Ag/AgCl and the activity of Cl^- is 0.67. The breakdown of the passive layer is usually local and the corrosion mechanism of aluminium in seawater is often in the form of pitting [24].
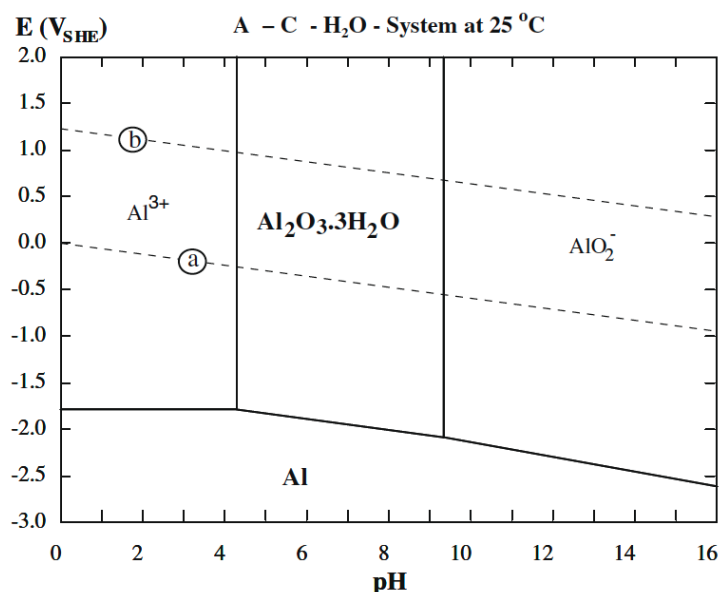
Figure 2.9: Pourbaix diagram of aluminium in the presence of 0.67 activity of Cl^- [21].

2.5.4   Nickel

Nickel is a passivation metal which efficiently protects the substrate material by passive oxide films that are only a few nm thick [25]. Films formed in acidic and neutral solutions consist of partially hydrated NiO, i.e. NiO and $Ni(OH)_2$. Passive surfaces exposed to cathodic conditions experience a gradual disolution of $Ni(OH)_2$ to Ni^+ or metallic nickel. At high anodic potentials before oxygen evolution, the layer mainly consists of Ni_2O_3 [26]. Nickel has low corrosion rates in rapidly flowing seawater. The calculated corrosion rates range from 0.00127 mm/year to 0.0254 mm/year [24]. In still seawater, deposits of biofouling may cover nickel surfaces, and passivity will be lost under the deposited material and at crevices [16]. The corrosion rate of nickel tends to decrease with exposure time. This is common for passive materials and may be the result of reduced pitting attack over time [24]. According to Figure 2.6, the OCP of pure nickel in seawater is between -250 and -50 mV vs Ag/AgCl. The pourbaix diagram of nickel in Figure 2.10 shows that nickel is immune to corrosion below -300 mV vs Ag/AgCl for pH<10 in water with 0.67 activity of Cl^-. Above -300 mV vs Ag/AgCl, passivity is achieved for pH>8.5 due to formation of nickel oxides. Long-time experiments of pure nickel and selected nickel alloys in two tropical environments (temperatures about 25°C) has to some degree clarified the effect of nickel in copper and copper in nickel [27]. The mass loss was most severe for pure nickel when submerged in tropical seawater. Copper-nickel (70-30) had better resistance in the seawater environments than both pure nickel and nickel-copper (monel). Nickel-copper was subject to a rapid, high-density pitting attack, however, the depth of these pits stopped increasing with time.
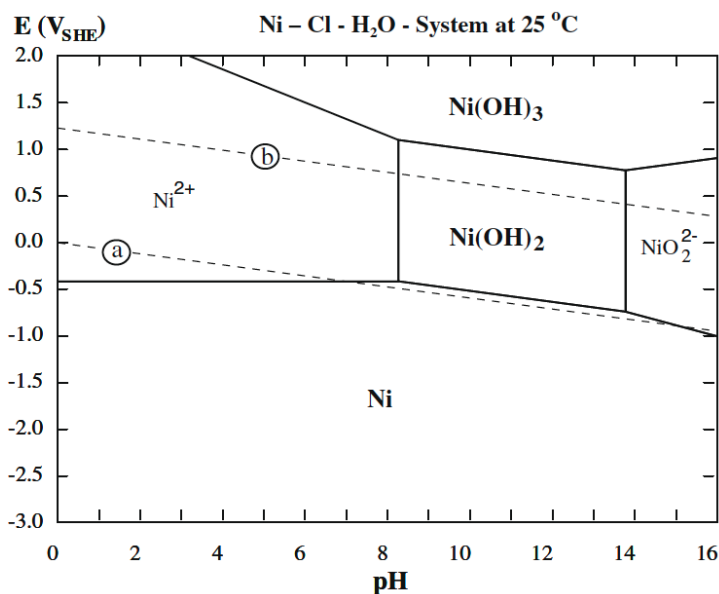
Figure 2.10: Pourbaix diagram of nickel in the presence of 0.67 activity of Cl^- [21].

Chapter 3

Experimental Work

This chapter contains descriptions of all the experiments in this work. The chapter is divided into four main sections. First, the material specifications and sample preparation is described in Section 3.1. Descriptions of instruments and corrosion test environment are given in sections 3.2 and 3.3, respectively. Finally the experimental configurations are decribed in Section 3.4.

Two main categories of experiments were conducted; charaterization of the NAB phases and corrosion experiments. The characterization consisted of EDS analyses of the NAB phases to find which phases each alloying element is likely to effect the most, and image analyses of the relative amount of α and κ phases, to find the active areas during selective corrosion of a certain phase. The corrosion experiments were conducted to shed light on the corrosion properties of NAB and how copper, aluminium and nickel effect the corrosion properties of NAB. All experiments were conducted at the Norwegian University of Science and Engineering during autumn 2015 and spring 2016. The experiments conducted during the autumn of 2015 were part of the preliminary project and it is stated in the experiment description if samples or results from the preliminaty project are used.

3.1   Materials and sample preparation

The composition of the NAB alloy used in the experiments in this thesis is given in Table 3.1. The NAB alloy was in as-cast condition and comes from a component that has been air-cooled in the sand form in which it was casted. The specifications for the other test materials are given in Table 3.2. The samples subject to corrosion experiments were treated as follows: A hole with diameter 0.2 cm was drilled through each sample for suspension purposes. The grinded samples were grinded with FEPA P500 silicon carbide paper using a Struers Rotopol-2 machine less than 30 minutes prior to immersion in the electrolytes, unless stated otherwise. The corners were rounded to reduce differences in corrosion current density over the sample surface.

Table 3.1: Chemical composition of the NAB samples in wt%.

	Al	Cr	Cu	Fe	Mg	Mn	Ni	Pb	Si	Sn	Zn
Minimum	9.0		79.0	4.0		0.5	4.5				
Maximum	10.0	0.005	81.5	5.0	0.04	1.0	5.5	0.02	0.05	0.08	0.20

3.2   Instruments

Most of the samples have been observed in a Quanta FEG 650 SEM and imaged by secondary electrons using an Everhart-Thornley detector. The parameters used for imaging are visible in the images, except the aperture size which was 30 µm. The SEM parameters for the EDS analyses are given in Table 3.3. The pH measurements were performed with a PHM210 Standard pH meter from Radiometer Analytical. Polarization and OCP measurement before polarization, were conducted by an Interface 1000 potensiostat from Gamry Instruments. Other OCP loggings were performed with software tailored for the lab, except the logging for the OCP variation with pH test for NAB and nickel.

Table 3.2: Properties of the copper, aluminium and nickel test samples.

Material	Purity	Heat treatment	Sample dimentions after cutting
Cu sheet	99.9 %	Temper half hard	2.5 cm × 5 cm × 0.2 cm
Al sheet	99.5 %	Temper half hard	2.5 cm × 5 cm × 0.2 cm
Ni sheet	99.0 %	Temper annealed	2.5 cm × 5 cm × 0.2 cm
Al rod	99.999 %	Temper as extruded	3.3 cm (diameter), 0.4 cm (thickness)

3.3   Corrosion test environment

The corrosion experiments were conducted in room temperature, 21±2°C. The SSW used was mixed according to the ASTM D141 standard and the composition is given in Table . The pH of the SSW was altered for some of the experiments by addition of HCl. If HCl was added it is stated in the experiment description. Without additional HCl, the pH of SSW is 8.2. The pCl of SSW is about the same for SSW with pH=3.5 and pH=8.2, a calculation is given in Appendix .

3.4   Test configurations

In this section the execution of the experiments are described. Sketches of some of the experimental configurations are given. Photographs of the same configurations are given in Appendix C.

3.4.1   EDS analyses of the constituent phases

The composition of the phases was determined using EDS in SEM with parameters as given in Table 3.3. Minimum 20 analyses were performed for each phase. EDS analyses where one or more of the counting errors were larger than 32 % were not used, except when the content of the element was below 3 wt%, since high errors have minor impact

for such low concentrations. For the elements which accounted for less that 3 wt% of a phase, the maximum error was 73 %. Three etched samples and two samples from the preliminary project were investigated by EDS. The etched samples examined were 1cm × 1cm × 1cm cubes of as-cast Cu**Al**10**Fe**5**Ni**5, with chemical composition given in the material specification in Table 3.1. The cube sides examined in SEM were grinded to grit size 5 μm using silicon carbide paper FEPA P4000, polished with a diamond particle suspension with particle size 3 μm and etched in a 10 wt% $FeCl_3$ solution for 5, 10 or 20 seconds. After etching, the samples were cleaned in ethanol and air dried. A SEM image of the cube etched for 20 seconds is presented in Figure 3.1. Two samples from the preliminary project were also used for the EDS analyses. One sample had been subject to cathodic and anodic polarization in SSW with pH=8.2. Mainly the α phase had corroded, and the κ phases were clearly visible on this sample. The other sample had been subject to cathodic and anodic polarization in SSW with pH=3.1. SEM images of these samples are portrayed in Figure 3.1. Because most of the κ_{IV} particles on the surface of the etched sample had suffered from corrosion, the analyses of the κ_{IV} phase were performed only on the sample from the preliminary project polarized at pH=8.2. The other phase analyses were conducted on both this sample and an etched sample. The sample from the preliminary project subject to polarization at pH=3.1 was only used for analyses of α.

Table 3.3: SEM parameters for EDS analyses.

Acceleration voltage	Working distance	Aperture size	Spot size
10-20 kV	9.7-12.1 mm	30 μm	5
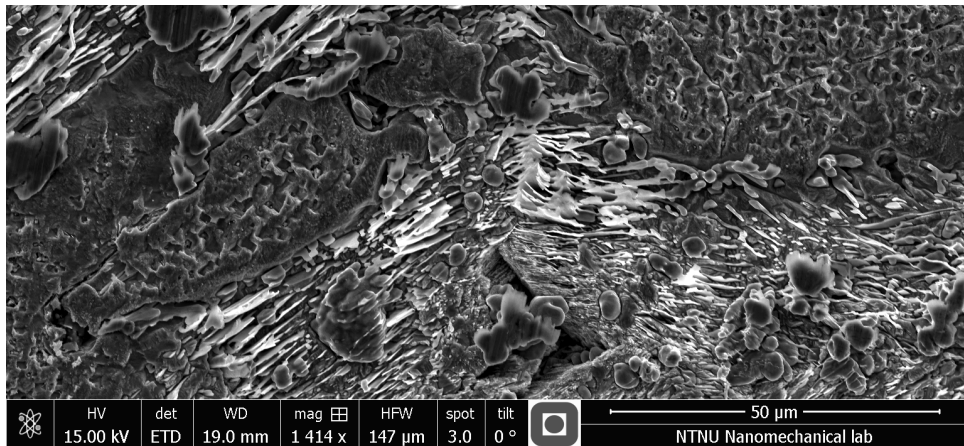
(a) Sample corroded at pH=8.
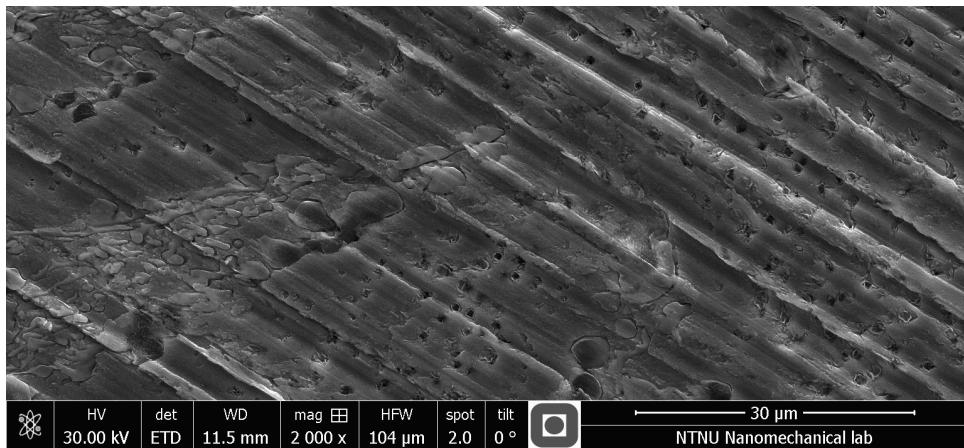
(b) Sample corroded at pH=3.5.
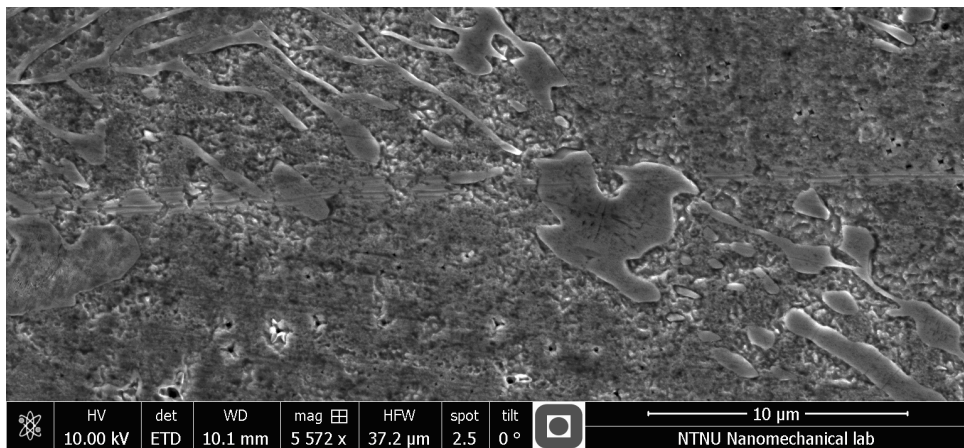
(c) Etched NAB sample

Figure 3.1: NAB samples used for EDS analyses of the NAB phases.

3.4.2   Image analyses for determining the amount of κ and α phases

The surface-area fraction of α and κ phases in the CuAl10Fe5Ni5 alloy were estimated using the image processing program ImageJ. The program created histograms of the light intensities of black-and-white images where the κ phases are dark. Light microscope images of etched samples and SEM images of uncorroded samples were analyzed. The colours of the images were first smoothed, making light parts in the κ particles dark and reducing the grinding marks. For each image, a histogram representing the number of pixels with each graytone was produced. For a certain graytone limit the lighter pixels were mainly found in α, while the darker pixels were mainly in the κ phase. The pixels on each side of the limit were counted and the ratio between the counts was used as an estimate of the amount of α phase and κ phase in the image. Since some pixels in the α phase were darker than some pixels in the κ phase, two graytone limits were set for each image, one where too few pixels were counted as κ phase and one where to many pixels were counted as κ phase. The image processing is illustrated in Figure 3.2. The estimated surface-area fractions of α phase and κ phase were based on 22 random images in magnification 500x to 2000x. None of the images portrayed overlapping areas. Each image contributed with two estimated ratios, since two threshold limits were used.

(a) Original image

(b) Smoothed image

(c) Lower limit for κ

(d) Upper limit for κ
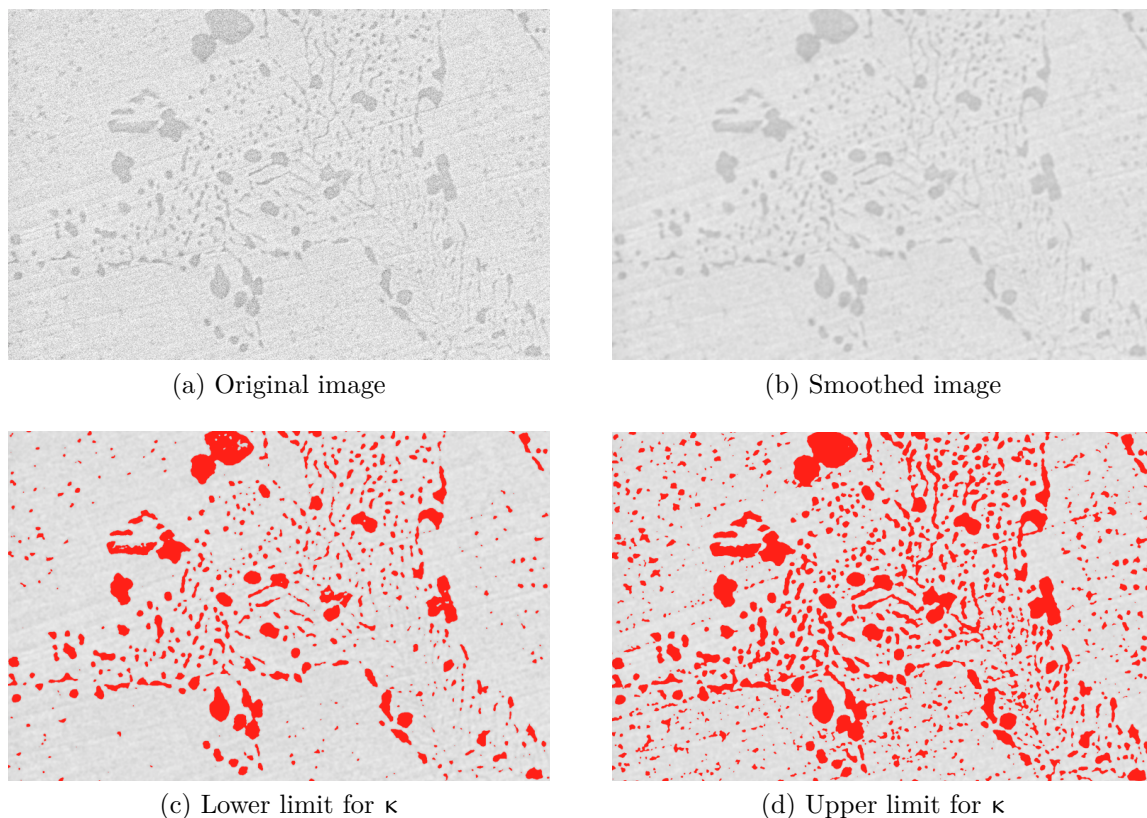
Figure 3.2: Illustration of the image processing for determining amount of phases. The red pixels represents κ phases.

3.4.3 Polarization curves of NAB, copper, aluminium and nickel

Polarization curves were conducted for NAB, copper, aluminium and nickel in SSW with pH=3.5 and unaltered pH, i.e. pH=8.2, to investigate the corrosion behaviour of the materials and their pH-dependency. The material specifications for the copper, aluminium and nickel samples are given in Table 3.2, and the material specification for the NAB sample is given in Table 3.1. Different samples were used for the anodic and cathodic polarization curves. The samples were exposed in the electrolyte for one hour before polarization. All curves were conducted to 300 mV away from the OCP, except the anodic polarization curves for aluminium which were conducted to +100 mV vs Ag/AgCl. The cathodic polarization curves were conducted in the preliminary project [1], except copper at pH=3.5 and NAB at pH=3.5 and pH=8.2. Originally, the plan was to conduct new cathodic curves for each of the anodic curves, because the exact deviation of the reference electrode in the preliminary project was unknown. The reference in the preliminary project was measured to be within acceptable limits, but since the exact deviation was unknown the OCP was inconclusive when matching curves from this thesis with curves produced in the preliminary project. However, the OCP was also inconclusive for some of the anodic curves matched with corresponding cathodic curves, where the exact deviation of the reference was known for both tests. It was then decided to find Tafel slopes and corrosion current density from overpotential curves. The accuracy of the reference electrode was then unimportant and cathodic curves from the preliminary project could be used.
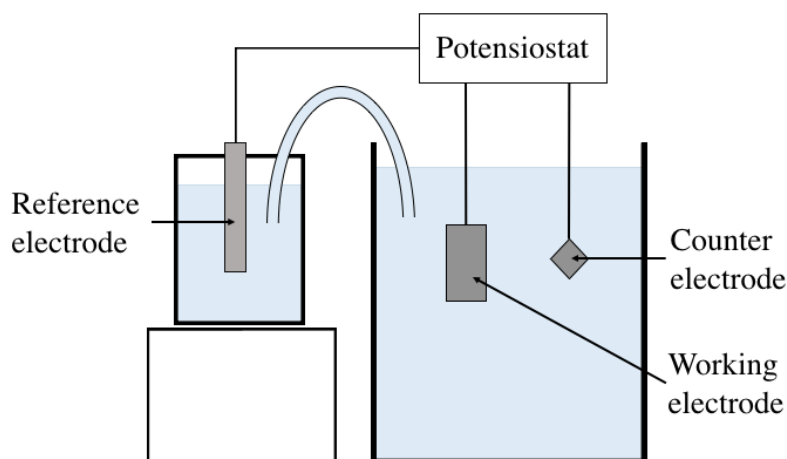
Figure 3.3: Experimental configuration of polarization experiments.

3.4.4 Polarization curves of the α phase

The corrosion properties of the α phase were investigated using NAB samples where the κ phases had corroded away from the surface. The experimental configuration of the test was similar to the configuration of the other polarization curves, as described in

Section 3.4.3 and displayed in Figure 3.3. Polarization curves were constructed in SSW with pH∈<3,4> and in SSW with pH=8.2. However, it was hard to determine whether κ had corroded to a significant extent for the sample exposed at low pH. The low pH curve was thus discarded. The sample used for anodic polarization at pH=8.2 was a sample from the preliminary project that had been exposed to SSW with pH∈<3,4> for two weeks. The sample used for cathodic polarization had been exposed in SSW for one week. Images of the surfaces before and after this test are given in Figure 4.12.

3.4.5   Static anodic polarization of NAB in SSW with pH=3.5

NAB was anodically polarized to -150, -250 and -300 mV vs Ag/AgCl for different time intervals, while submerged in SSW with pH=3.5, to investigate the corrosion properties of the different phases. The duration of the polarizations were 30 minutes, 24 hours and 48 hours for each of the potentials, i.e. one sample was polarized to -150mV for 0.5 hours, another to -250mV for 24 hours, etc. The material specification for the NAB sample is given in Table 3.1. Before polarization the samples were exposed to the electrolyte for one hour. The corroded samples were investigated in SEM to find whether a passive film had developed on the surface or not, and to see which phases had corroded. The experimental configuration is similar to the configuration for the polarization curves, see Figure 3.3.

3.4.6   Static anodic polarization of aluminium in SSW while pH is reduced

Aluminium samples were exposed to SSW and polarized to -200 mV vs Ag/AgCl, while HCl was added to the electrolyte. Samples cut from an aluminium rod were used. The material specification for the samples is given in Table 3.2. To ensure small concentration differences in the electrolyte an 800 mL container was used. The samples were exposed to the electrolyte one hour before the polarization started while the OCP was logged. Static polarization to -200 mV vs Ag/AgCl started automatically after the first hour of exposure. After five minutes of polarization HCl was added every second minute, total of six times, i.e. the anodic polarization lasted 17 minutes. In a non-sucsessful experiment the current of aluminium was stable after less than a minute in SSW with pH=4 and SSW with pH=6, and thus it was assumed that the current would be stabilized within two minutes after HCl addition, if the current would be stabilized at all. Electrolyte samples of 10 mL were taken out before each addition of HCl, for pH-measuring. The experiment was conducted twice with this proceedure. Since variations in current density may have other causes than the addition of HCl, the experiment was conducted once without HCl addition.

Electrolyte was also removed during this experiment, in the same manner as the others to ensure as similar conditions as possible. Only a few pH measurements were performed during the test without HCl, since stable pH was expected.

3.4.7 Long-time exposure of NAB in SSW with pH∈<3,4>

Four NAB samples were exposed to SSW with pH∈<3,4> for different periods to shed light on the corrosion development of NAB. The material specification for the samples is given in Table 3.1. The samples were exposed one day, one week, four weeks and eight weeks, and were weighed before and after the experiment to estimate the mass loss. Figure 3.4 show the experimental configuration as it looked when none of the samples had been removed. Distilled water was added regularly to add up for water evaporation from the electrolyte. To prevent the samples from being exposed to air when the water level was low, a tight glass bottle was put in two of the container corners to increase the electrolyte level. The water content never varied more than 1 L. The pH increased during the experiment and HCl was added to keep pH<4. After exposure, the samples were weighed and cut in two. One piece was cast in epoxy so the cross section could be more easily examined in SEM. The epoxy in the images has been coloured dark since it is of no interest. The surface of the other piece was examined. The piece in epoxy was grinded and polished with 3 µm suspension. Some silicon particles were left on the surface after polishing and these may be seen in some of the SEM images of the cross sections.
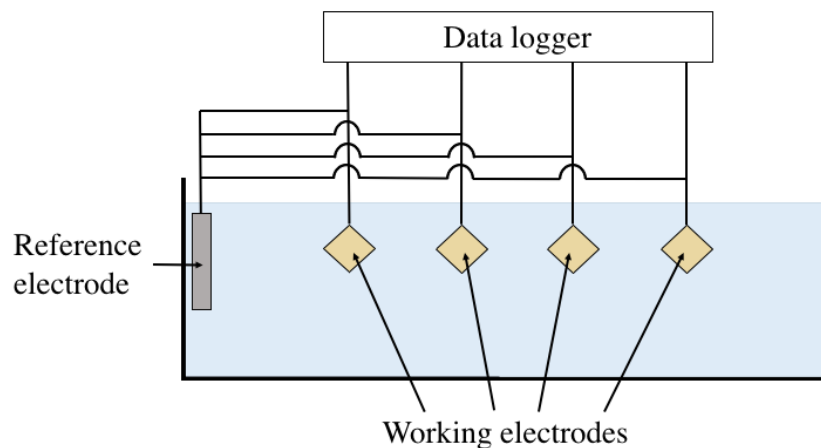
Figure 3.4: Experimental configuration of long-time exposure test of NAB in SSW with pH∈<3,4>.

3.4.8 OCP varation with pH for NAB and nickel

In the preliminary project nickel and NAB had a substantial decrease of OCP for exposure in low pH SSW compared to normal SSW pH [1]. Furher investigations of the pH-dependent behaviour of NAB and nickel were thus of interest. The pH-dependencies of the OCPs of nickel and NAB were investigated by exposing samples to SSW while gradually adding HCl and measuring the OCP. The material specification for the NAB test samples are given in Table 3.1 and the material specification for the nickel test

samples are given in Table 3.2. The samples were prepared as described in Section 3.1 and put in a beaker of 850 mL SSW 18 hours before the first drops of HCl were added. The first experiment for nickel was conducted with 20 minutes exposure time before HCl addition, due to seemingly stable OCP after this time. However the change of OCP was little prominent during this test. This suggested that a passive film had not been formed and the samples were exposed over night, i.e. 18 hours, to ensure passive film formation before the test. The test was performed twice in this manner for NAB and three times for nickel. An Ag/AgCl electrode or Standard calomel electrode (SCE) was used for reference and connected to the SSW in the beaker by a salt bridge. The references were checked against a known reference before every experiment, and the OCPs converted to mV vs Ag/AgCl. Between 1 and 5 drops of HCl were added at a time by a dropper. 10 minutes after the addition of HCl the OCP was logged and a 10 mL sample of the electrolyte was taken with a dropper. The pH of each sample was measured after the experiment was finished. The buffer capacity of the SSW and the volume variation, due to the electrolyte samples taken, made it difficult to calculate the pH before it was measured. Thus, there are few OCP values logged between 4<pH<5.
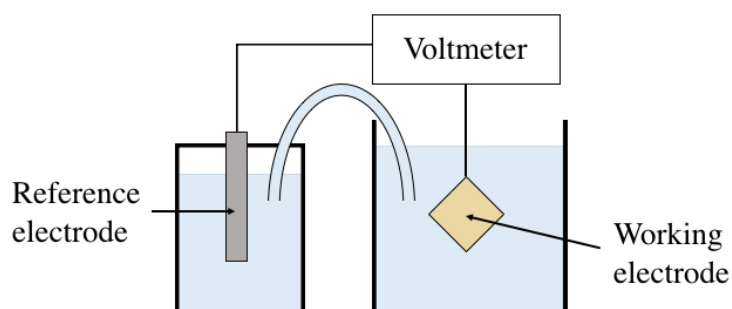
Figure 3.5: Experimental configuration of OCP variation with pH experiment.

Chapter 4

Results

In this chapter the results of the tests described in Chapter 3 are presented. Some additional information about the experiments is given in Appendix A.

4.1 Characterization of the NAB phases

The surface-area fractions of α and κ were estimated by image processing and analyses, while the composition of each phase was examined in SEM using EDS. The estimated amounts of α and κ phase are given in Figure 4.2, and the compositions of the phases are given in Figure 4.1.

Table 4.1: Composition of the NAB phases [wt%].

Element	α	κ_{II}	κ_{III}	κ_{IV}
Copper	85.6 ± 2.2	15.5 ± 4.1	27.1 ± 9.6	27.0 ± 6.7
Aluminium	9.1 ± 1.7	23.9 ± 5.9	28.1 ± 4.5	17.5 ± 2.5
Iron	1.6 ± 0.5	37.2 ± 13.0	12.4 ± 4.0	41.4 ± 8.3
Nickel	3.8 ± 0.7	23.4 ± 5.9	32.4 ± 5.7	14.2 ± 4.9

Table 4.2: Estimated amount of α and κ phases in as-cast Cu**Al**10**Fe**5**Ni**5.

Phase	Surface-area %	Standard deviation
κ	18 %	8 %
α	82 %	8 %

4.2 Polarization curves of NAB, copper, aluminium and nickel

Polarization curves for NAB, copper, aluminium and nickel are given in the following, as well as overpotential curves with suggested Tafel slopes drawn in red. Please note that the overpotential curves are the same curves as the corrosion curves plotted above them, only the back scan has been removed and the potentials, E, have been converted to overpotentials, η. Anodic and cathodic Tafel slopes, b_a and b_c respectively, and the corrosion current density, i_{corr}, have been estimated using Tafel extrapolation of the overpotential curves. The absolute value of the current density, i, is plotted in the polarization curves. For some curves, i was negative during parts of the anodic

polarization back scan. This is stated where it applies. The anodic polarization curves were used for estimating the OCP, except for NAB at low pH. At pH=3.5 the OCP of NAB varied a lot from test to test, and several OCP measurements before testing were used for estimating the OCP. The potentials of the pure metals at the OCP of NAB at pH=3.5 and pH=8.2 are presented in Table 4.3. All potentials have been estimated to the closest 10 mV. SEM images of the samples subject to anodic polarization are also included in this section. The cathodically polarized samples are of less interest and were not imaged in SEM.

Table 4.3: Current densities of alloying elements at the OCP of NAB in SSW with pH=3.5 and pH=8.2.

Material	i at the OCP of NAB, pH=3.5 [mA/m^2]	i at the OCP of NAB, pH=8.2 [mA/m^2]
Copper	78 (cathodic)	57 (at OCP)
Aluminium	1 300 (anodic)	41 000 (anodic)
Nickel	560 (anodic)	5.0 (cathodic)
Iron	44 000 (anodic)	100 000 (anodic)

The i values for iron were found using data from the preliminary project [1].

4.2.1   NAB

Polarization curves for NAB in SSW with pH=3.5 and pH=8.2 are given in Figure 4.1, with associated corrosion constants in Table 4.4. The cathodic polarization curve of NAB at pH=3.5 used in Figure 4.1 was not performed with a back scan. The OCP measurements of NAB at pH=3.5 varied to a much greater extent than the other materials at both pH levels tested and NAB at pH=8.2. The OCP of NAB at low pH was thus estimated on the basis of all the OCP measurements of NAB in SSW with pH=3.5, which are presented in Figure 4.2. The anodic polarization curve at pH=8.2 had negative i in the back scan for E<-185 mV vs Ag/AgCl. The anodic curve at pH=3.5 started with two negative i values, but i was otherwise positive for both the anodic curve and the back scan. SEM images of the anodically polarized NAB samples can be seen in Figure 4.3.
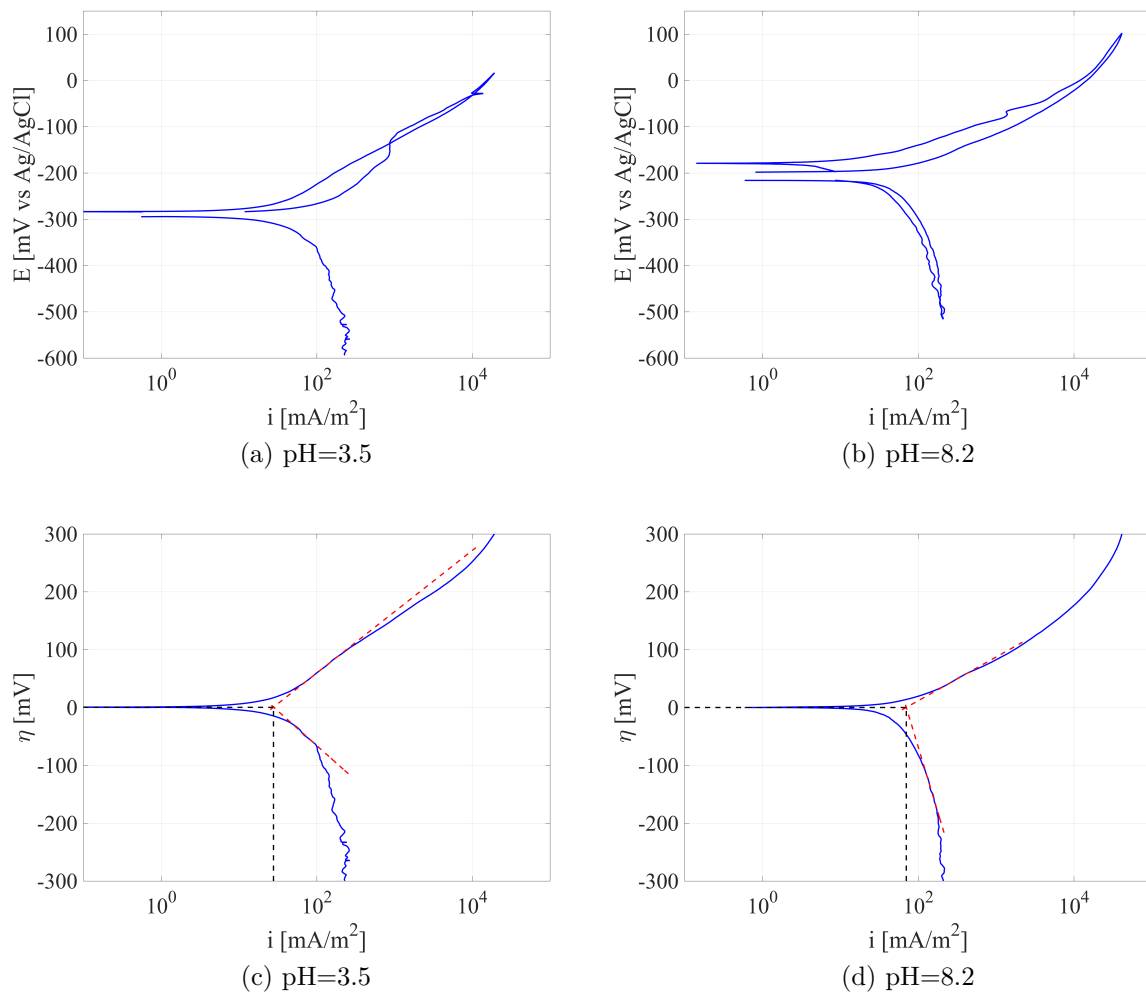
Figure 4.1: Polarization curves of NAB in SSW with pH=3.5 and pH=8.2.

Table 4.4: Corrosion constants for NAB in SSW with pH=3.5 and pH=8.2.

Constant	pH=3.5	pH=8.2
b_a [mV/decade]	106	76
b_c [mV/decade]	-120	-447
i_{corr} [mA/m^2]	28	70
OCP [mV vs Ag/AgCl]	-320	-210
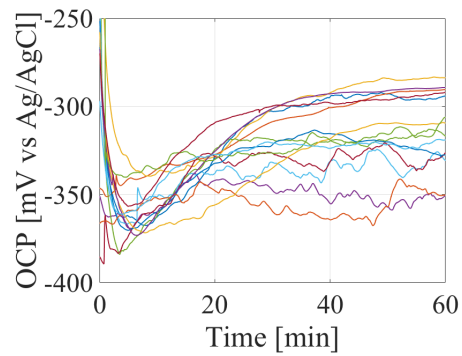
Figure 4.2: One hour OCP measurements of NAB in SSW with pH=3.5. Each colour represents one OCP measurement conducted for a freshly grinded sample.
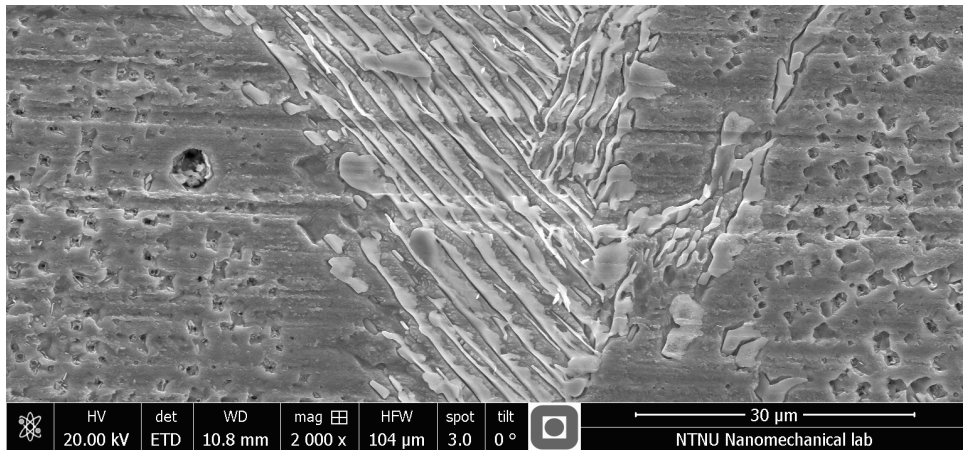
(a) SSW with pH=3.5
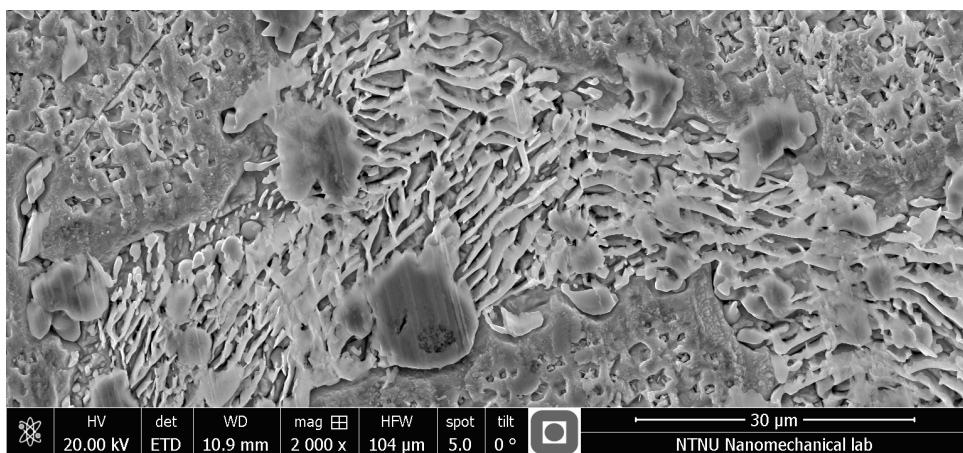
(b) SSW with pH=8.2

Figure 4.3: SEM images of anodically polarized NAB surfaces.

4.2.2   Copper

The polarization curves and corrosion constants for copper are portrayed in Figure 4.4 and Table 4.5, respectively. The anodic back scan at pH=8.2 had negative i for $E \in <$-84,-58$>$ mV vs Ag/AgCl and $E<$-180 mV vs Ag/AgCl. The anodic curve at pH=3.5 had negative i for $E<$-57 mV vs Ag/AgCl. Figure 4.5 show SEM images of anodically polarized samples.

(a) pH=3.5 (b) pH=8.2 (c) pH=3.5 (d) pH=8.2
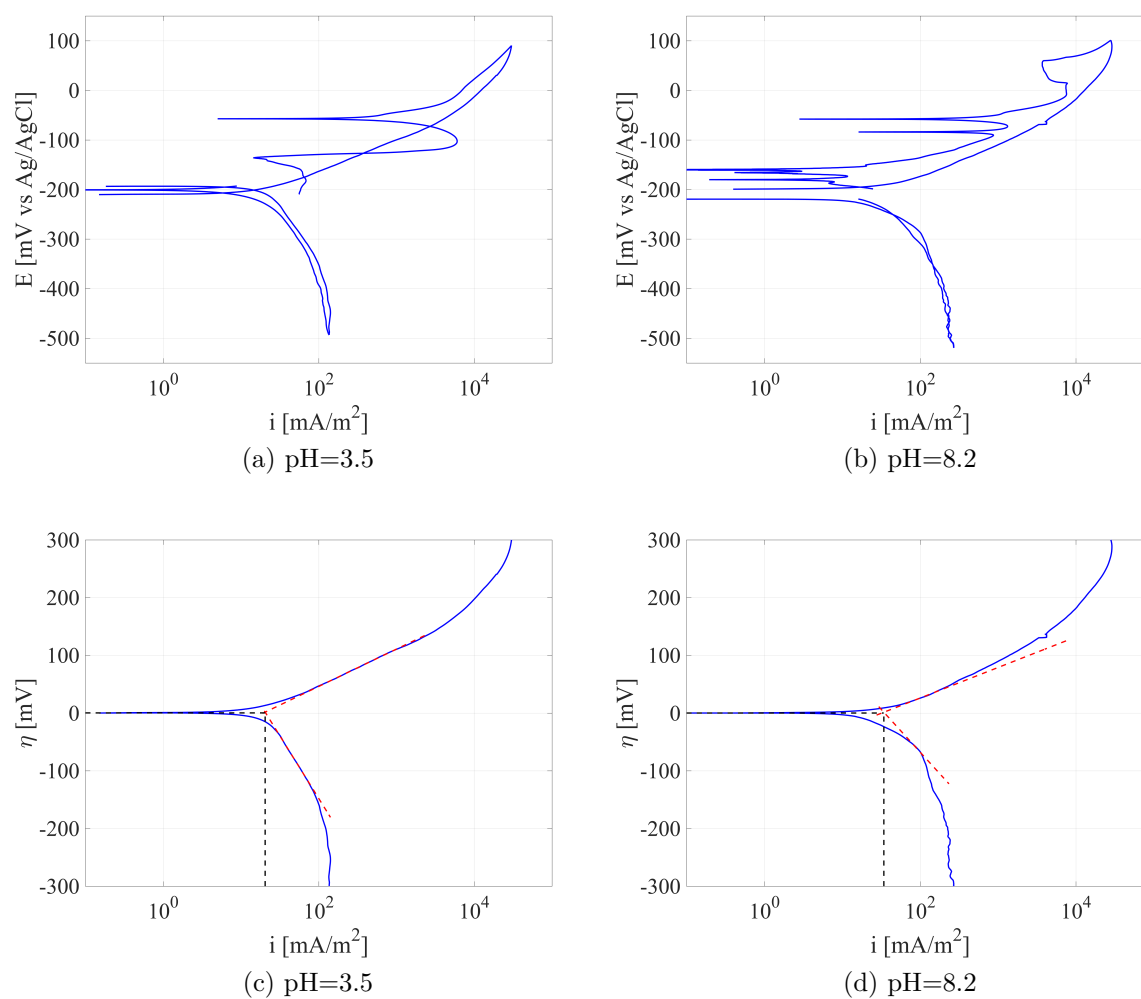
Figure 4.4: Polarization curves of copper in SSW with pH=3.5 and pH=8.2.

Table 4.5: Corrosion constants for copper in SSW with pH=3.5 and pH=8.2.

Constant	pH=3.5	pH=8.2
b_a [mV/decade]	65	71
b_c [mV/decade]	-217	-281
i_{corr} [mA/m^2]	21	57
OCP [mV vs Ag/AgCl]	-200	-210

	HV	det	WD	mag ⊞	HFW	spot	tilt			100 µm	
	10.00 kV	ETD	10.6 mm	500 x	414 µm	3.5	0 °			NTNU Nanomechanical lab	

(a) SSW with pH=3.5

	HV	det	WD	mag ⊞	HFW	spot	tilt			100 µm	
	20.00 kV	ETD	10.5 mm	500 x	414 µm	3.0	0 °			NTNU Nanomechanical lab	

(b) SSW with pH=8.2

Figure 4.5: SEM images of anodically polarized copper surfaces.

4.2.3   Aluminium

The polarization curves of aluminium are portrayed in Figure 4.7, with associated corrosion constants in Table 4.6. The anodic polarization curve of aluminium at pH=3.5 behaved strangely during the first mV of polarization. The OCP was lower for the anodically polarized sample compared to the cathodically polarized sample. However, when the potential increased above the OCP of the cathodically polarized sample, the current density of the anodically polarized sample started behaving like the OCP had been the same as for the cathodically polarized sample. The back scan also indicated that the OCP of the anodic sample was in fact about the same as OCP of the cathodically polarized sample. Also, the overpotential curve and Tafel slopes made little sense due to the strange shape of the anodic curve. The overpotential curve for pH=3.5 was therefor plotted without the first values of the anodic curve, hence the potential of the entire anodic overpotential curve was lowered. This was all done in an effort to make the OCP and the Tafel more meaningful. i was never negative for the anodic polarization curve back scan at pH=8.2. For the back scan of the anodic curve at pH=3.5 i was negative below $E < -706$ mV vs Ag/AgCl. During anodic polarization of aluminum, bubbles developed on the aluminium surface, rapidly as they drifted to the surface. This can be seen in Figure 4.6. SEM images of the anodically polarized aluminium samples are given in Figure 4.8.
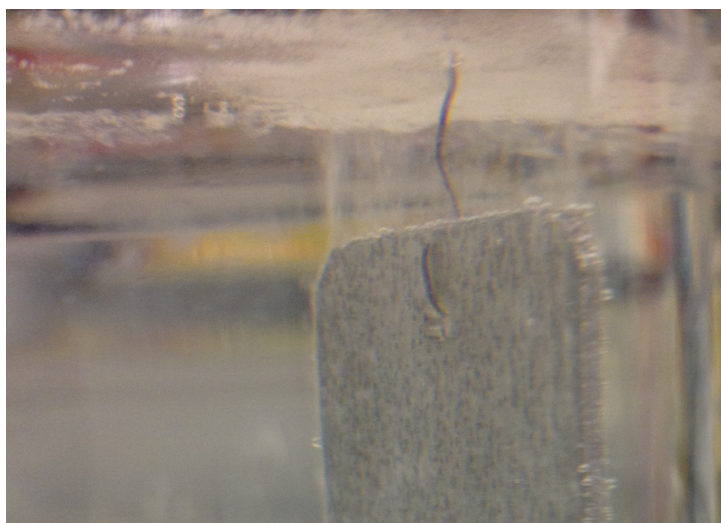
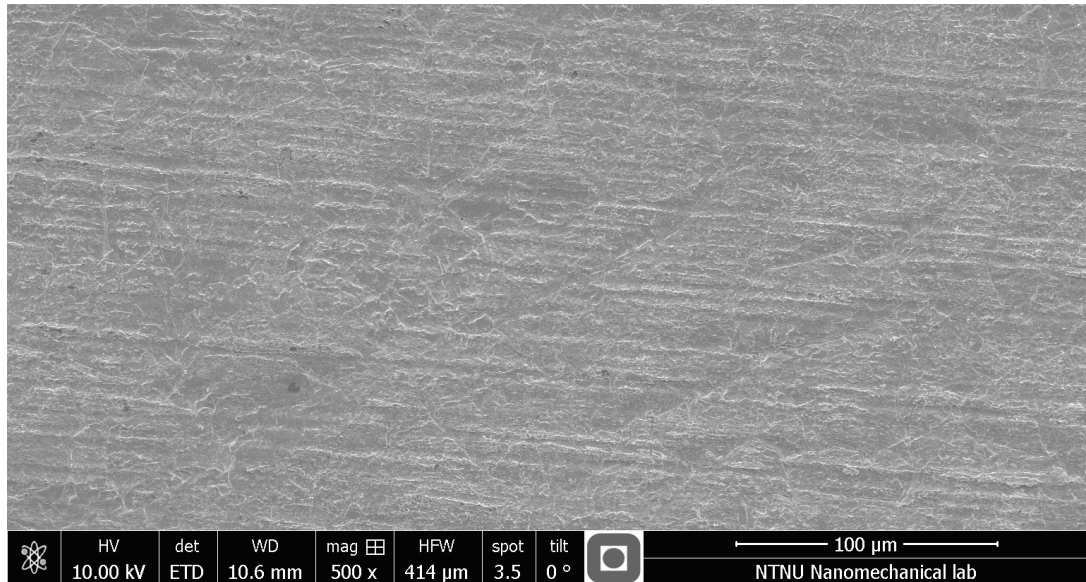Figure 4.6: Bubble formation on anodically polarized aluminium in SSW.
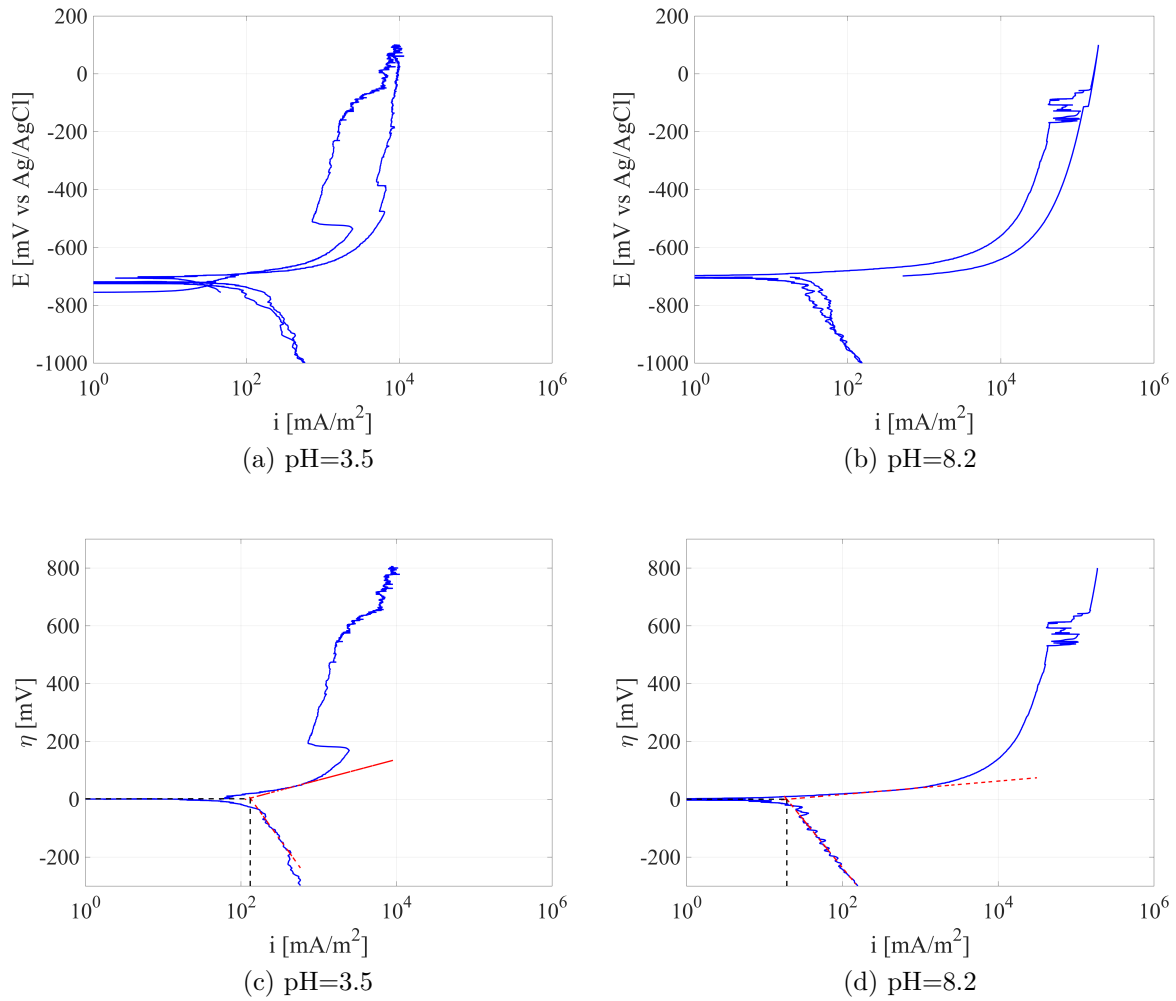
Figure 4.7: Polarization curves of aluminium in SSW with pH=3.5 and pH=8.2.

Table 4.6: Corrosion constants for aluminium in SSW with pH=3.5 and pH=8.2.

Constant	pH=3.5	pH=8.2
b_a [mV/decade]	71	23
b_c [mV/decade]	-374	-331
i_{corr} [mA/m^2]	132	19
OCP [mV vs Ag/AgCl]	-720	-700
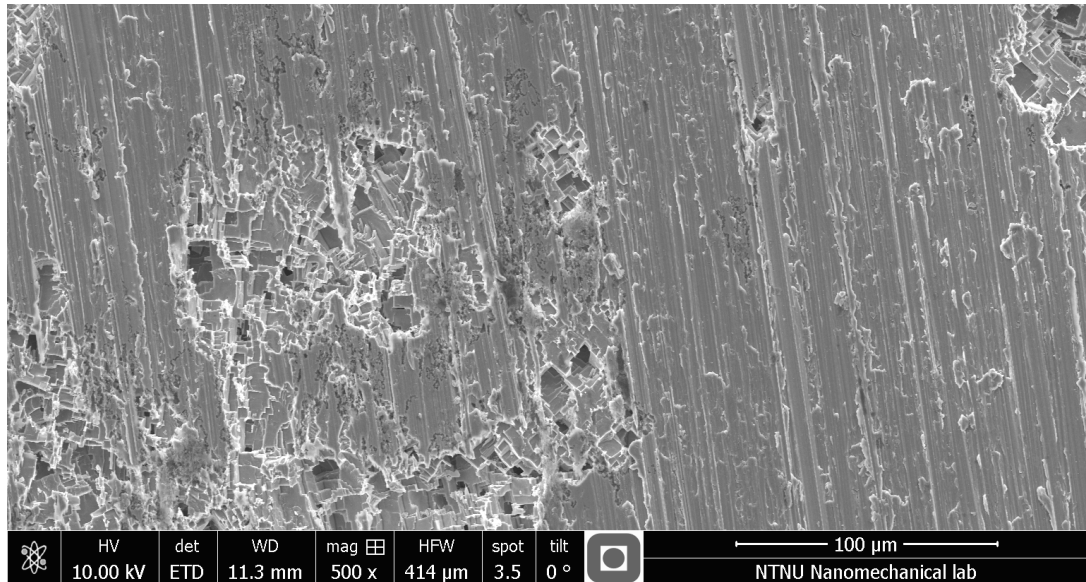
(a) SSW with pH=3.5
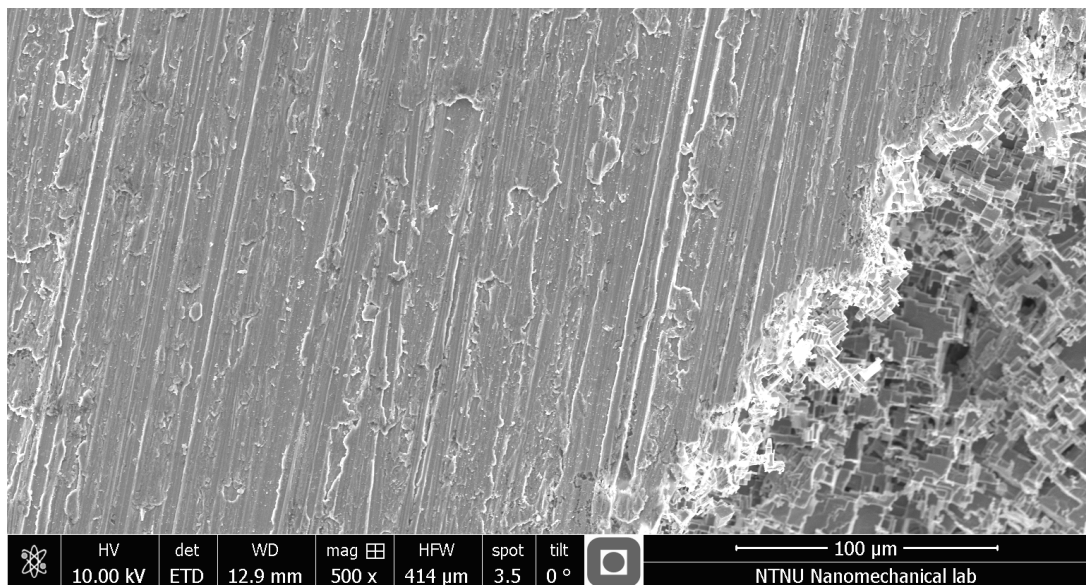
(b) SSW with pH=8.2

Figure 4.8: SEM images of anodically polarized aluminium surfaces.

4.2.4   Nickel

The polarization curves of nickel are given in Figure 4.9, with associated corrosion constants in Table 4.7. For the anodic polarization back scan at pH=8.2, i was negative for E<-71 mV vs Ag/AgCl. SEM images of the anodically polarized nickel surfaces are given in Figure 4.10.
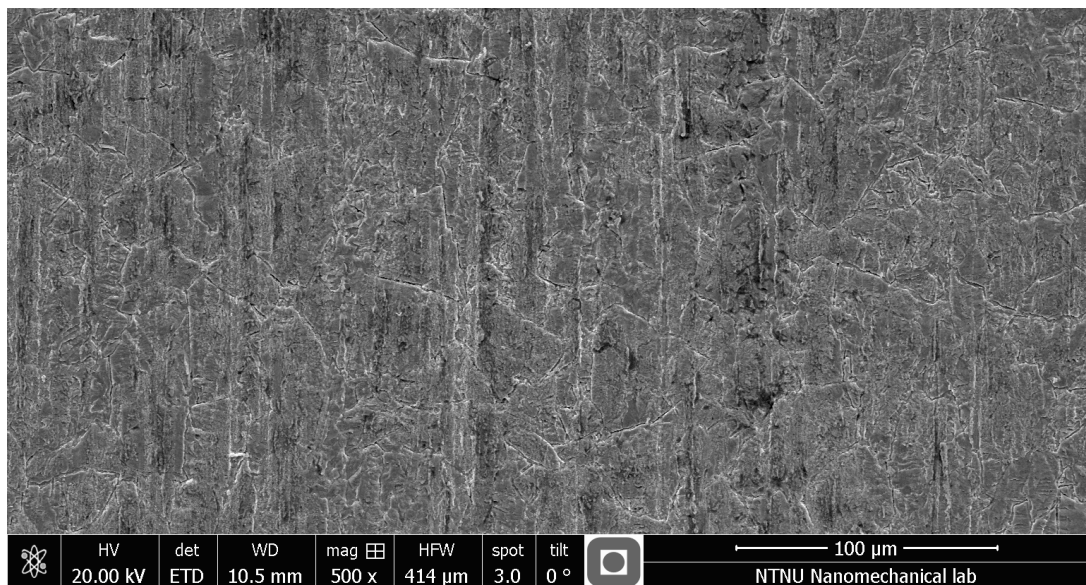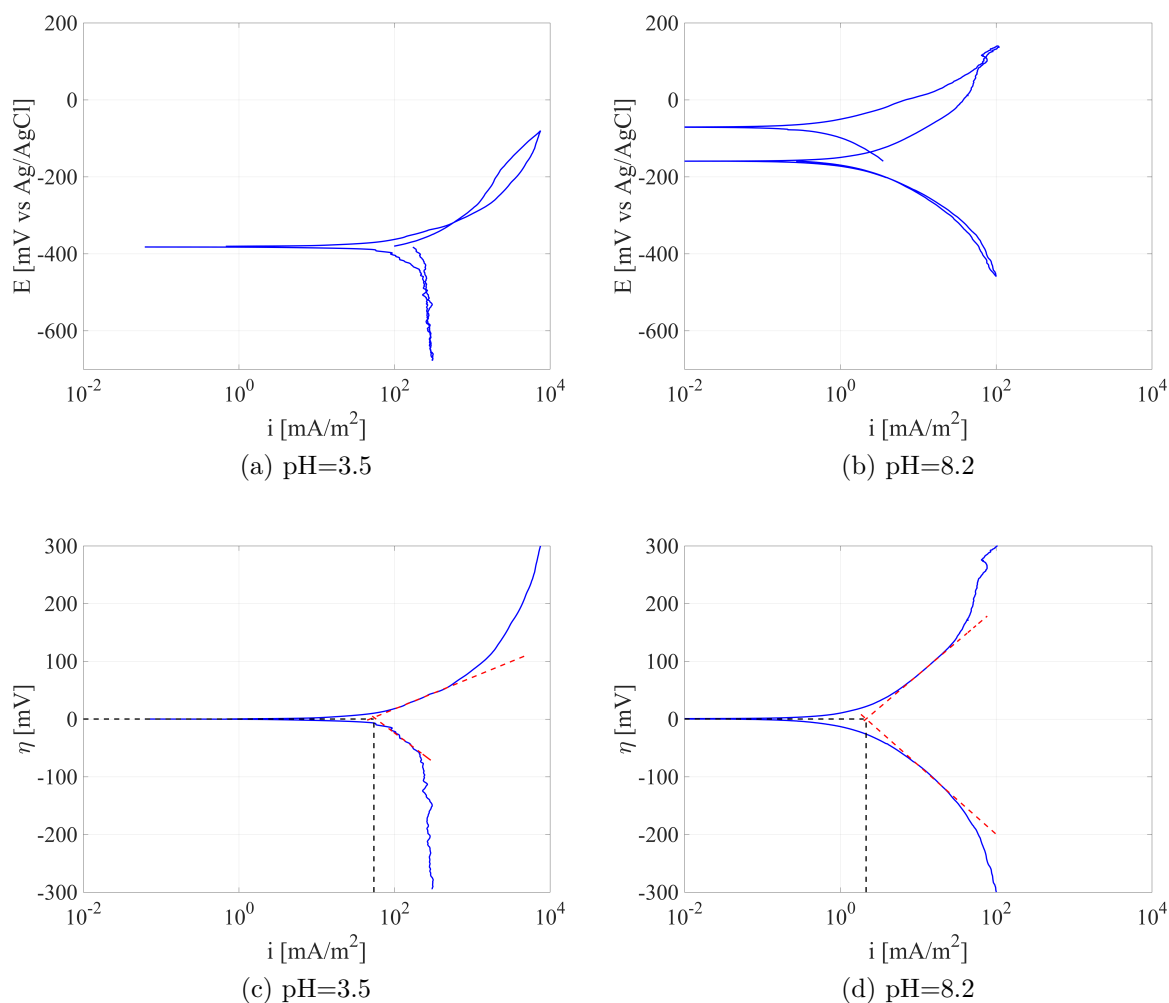

Figure 4.9: Polarization curves of nickel in SSW with pH=3.5 and pH=8.2.

Table 4.7: Corrosion constants for nickel in SSW with pH=3.5 and pH=8.2.

Constant	pH=3.5	pH=8.2
b_a [mV/decade]	55	115
b_c [mV/decade]	-101	-120
i_{corr} [mA/m^2]	54	2
OCP [mV vs Ag/AgCl]	-380	-160
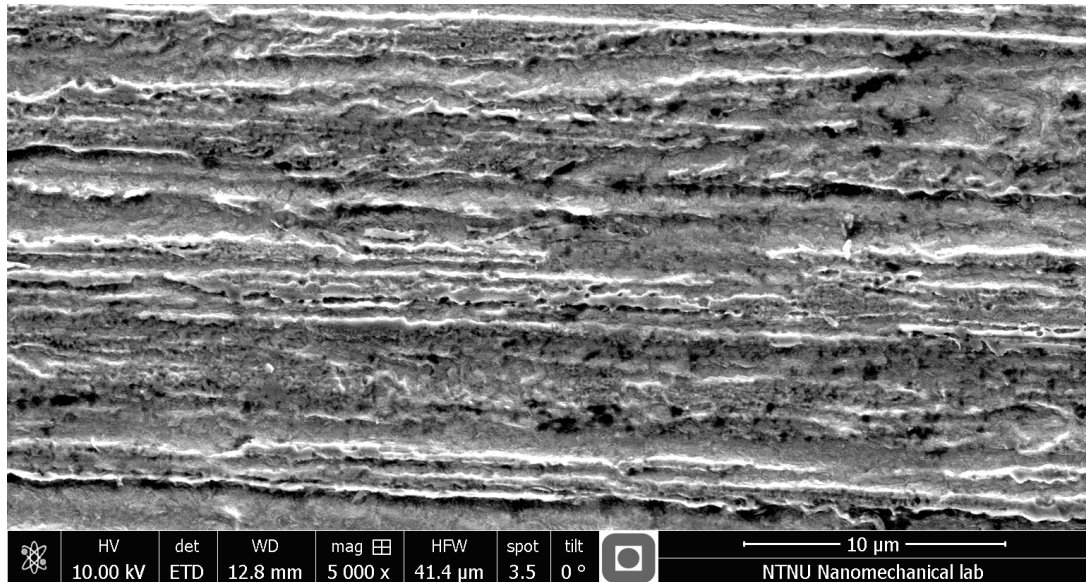
(a) SSW with pH=3.5
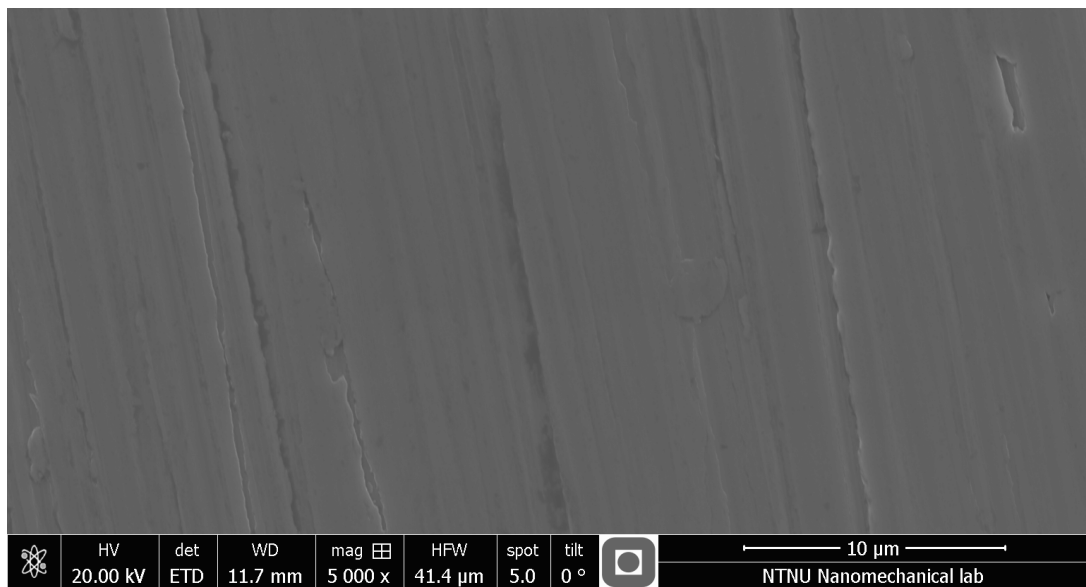
(b) SSW with pH=8.2

Figure 4.10: SEM images of anodically polarized nickel surfaces.

4.3   Polarization curve of the α phase

The polarization curve of α is presented and treated like the polarization curves in Section 4.2. Figure 4.11 illustrates the polarization curve and overpotential curve with suggested Tafel slopes. Corrosion constants are given in Table 4.8. The area of the α phase exposed to the electrolyte was unknown for all the experiments, as the depth of the corrosion attack of the κ phases before testing was unknown. The total sample area, including the areas previously occupied by κ phases, was used for calculating i. During the back scan of anodic polarization i was negative at E<-165 mV vs Ag/AgCl, and otherwise positive. The SEM images in Figure 4.12 show an NAB sample exposed to SSW with pH∈<3,4> for one week and the anodically polarized sample. As the polarized sample was exposed one week in SSW with 3<pH<4 before polarization, the sample in Figure 4.12 (a) represents the surface of the corroded surface in Figure 4.12 (b) before it was polarized.

(a) Polarization curves with back scan   (b) Overpotential curve with suggested Tafel lines
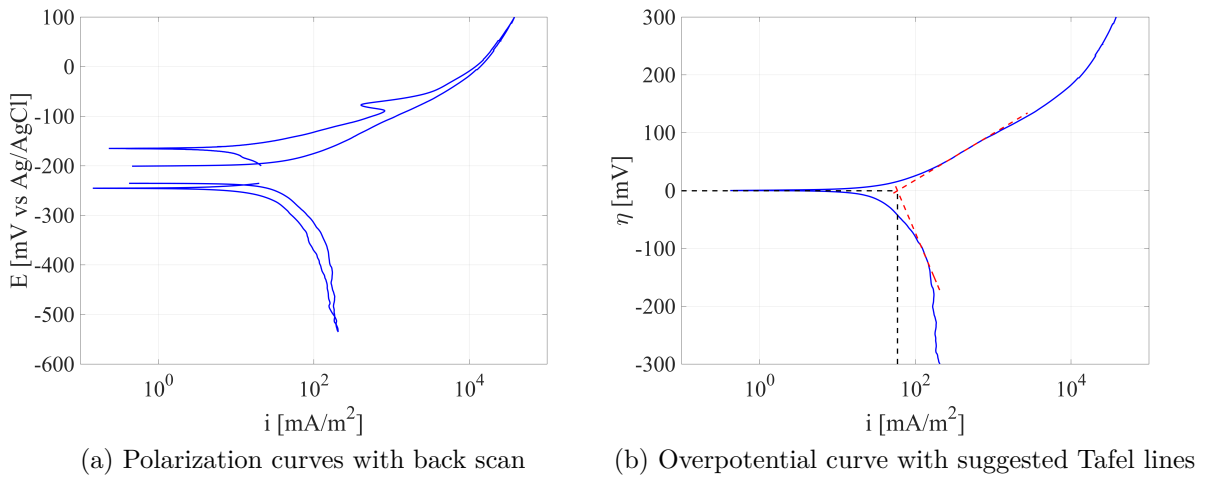
Figure 4.11: Polarization curves of the α phase in SSW with pH=8.2.

Table 4.8: Corrosion constants for the α phase in SSW with pH=8.2.

Constant	pH=8.2
E_{corr} [mV vs Ag/AgCl]	-210
i_{corr} [mA/m^2]	60
β_a [mV/decade]	81
β_c [mV/decade]	-318
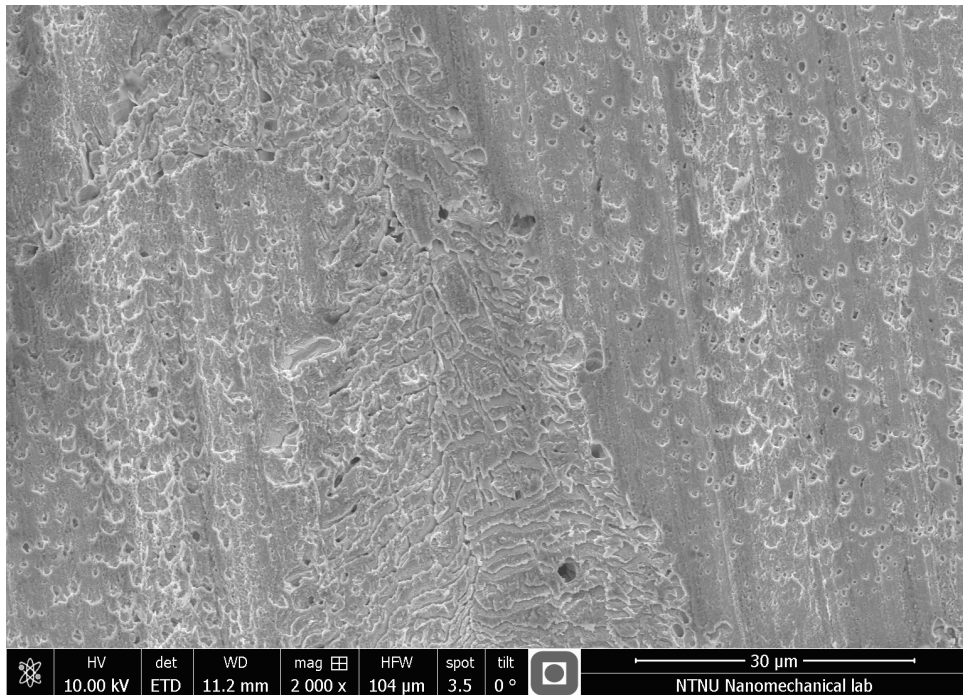
(a) Before polarization
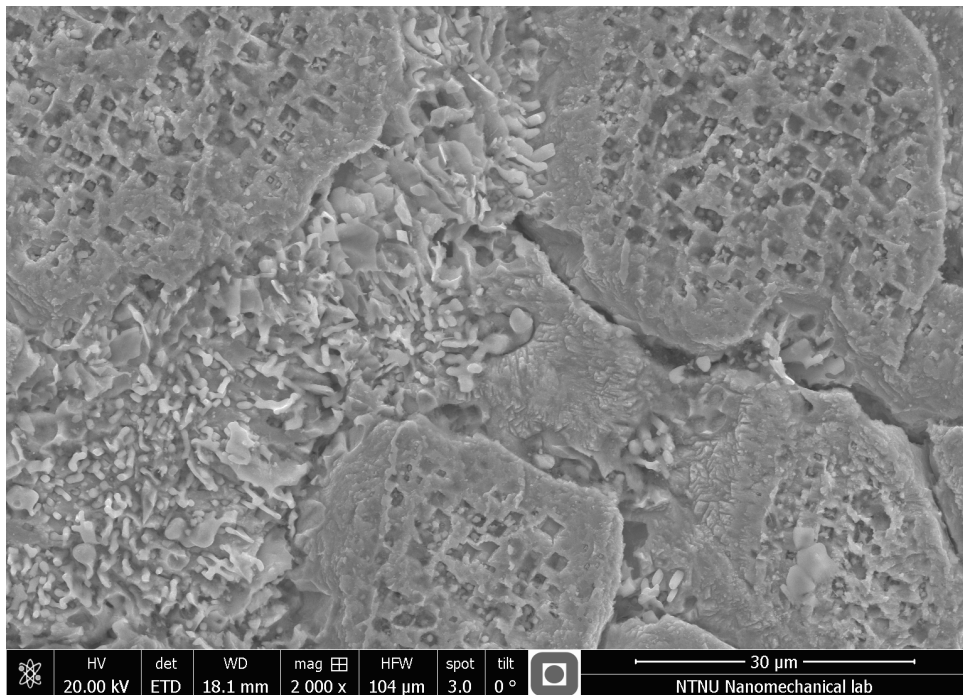
(b) After anodic polarization

Figure 4.12: Surfaces before and after anodic polarization of the α phase in SSW with pH=8.2.

4.4   Static anodic polarization of NAB in SSW with pH=3.5

This section contains graphs of the current densitiy development during static anodic polarization of NAB in SSW with pH=3.5 at different potentials and for different time durations, see Figure 4.14. The reader should note that the subfigures in Figure 4.14 are separate tests and not rescaled plots of the same test. SEM images of the test samples are given in figures 4.15, 4.16 and 4.17. The OCP measurements of NAB in SSW with pH=3.5, which can be seen in Figure 4.2, show that NAB has been stabilized at potentials ranging from about -280 to -350 mV vs Ag/AgCl. The last OCP measurements before static polarization to -300 mV vs Ag/AgCl display potentials -319, -306 and -292 mV vs Ag/AgCl, with the lowest OCP for the sample polarized for the shortest time and the highest OCP for the sample polarized the longest time. Thus, the static polarization experiments to -300 mV vs Ag/AgCl are of a cathodic character, i.e. negative anodic current, when the OCP is above the applied potential. The time and potential for each test was determined before the OCP measurement started, hence it was unknown that the applied potential would be cathodic for some of the samples, rather than anodic as the test name says. The results are still of interest and is included in this experiment, even though the polarization is cathodic rather than anodic. The static polarization measurements for 24 hours and 48 hours have been filtered in an attempt to make it easier to see the long term tendency. A description of the noice suppression procedure, as well as the original graphs, are given in Section A.4.
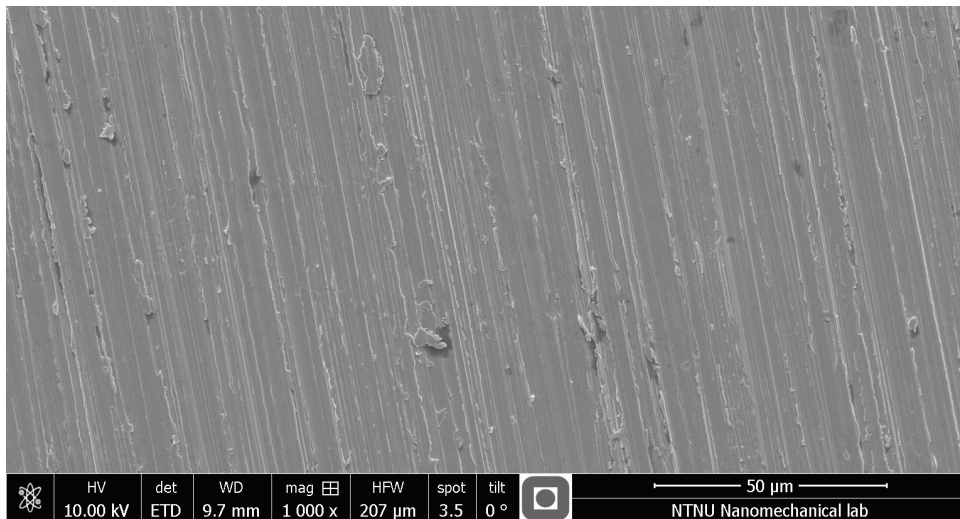
Figure 4.13: NAB exposed to SSW with pH=3.5 for one hour.

The SEM images to be presented in this section represent the surfaces well, however some observations are accentuated here.

- For all the potentials κ_{II} and κ_{IV} had started corroding after 30 minutes. Surfaces polarized at -150 and -250 mV vs Ag/AgCl had no κ_{IV} particles left. κ_{III} was, however, uncorroded.

- After 24 hours κ_{III} had started corroding on all surfaces, with the sample polarized to -300 mV vs Ag/AgCl being the least damaged. On the surface polarized to -150 mV vs Ag/AgCl α had started to corrode as well as the κ phases.

- After 48 hours the sample polarized to -250 mV vs Ag/AgCl had no visible κ phase on the surface. The α had developed a structure similar to the surface of copper after anodic polarization at high pH, see figures 4.5 and 4.12.

- After 48 hours all κ_{IV} particles had corroded from the surface polarized to -300 mV vs Ag/AgCl. κ_{II} and κ_{III} had corroded as well, however, small particles covered corroded areas. The depth of the corrosion attacks could not be seen due to the particles covering the corroded areas.

(a) 30 minutes
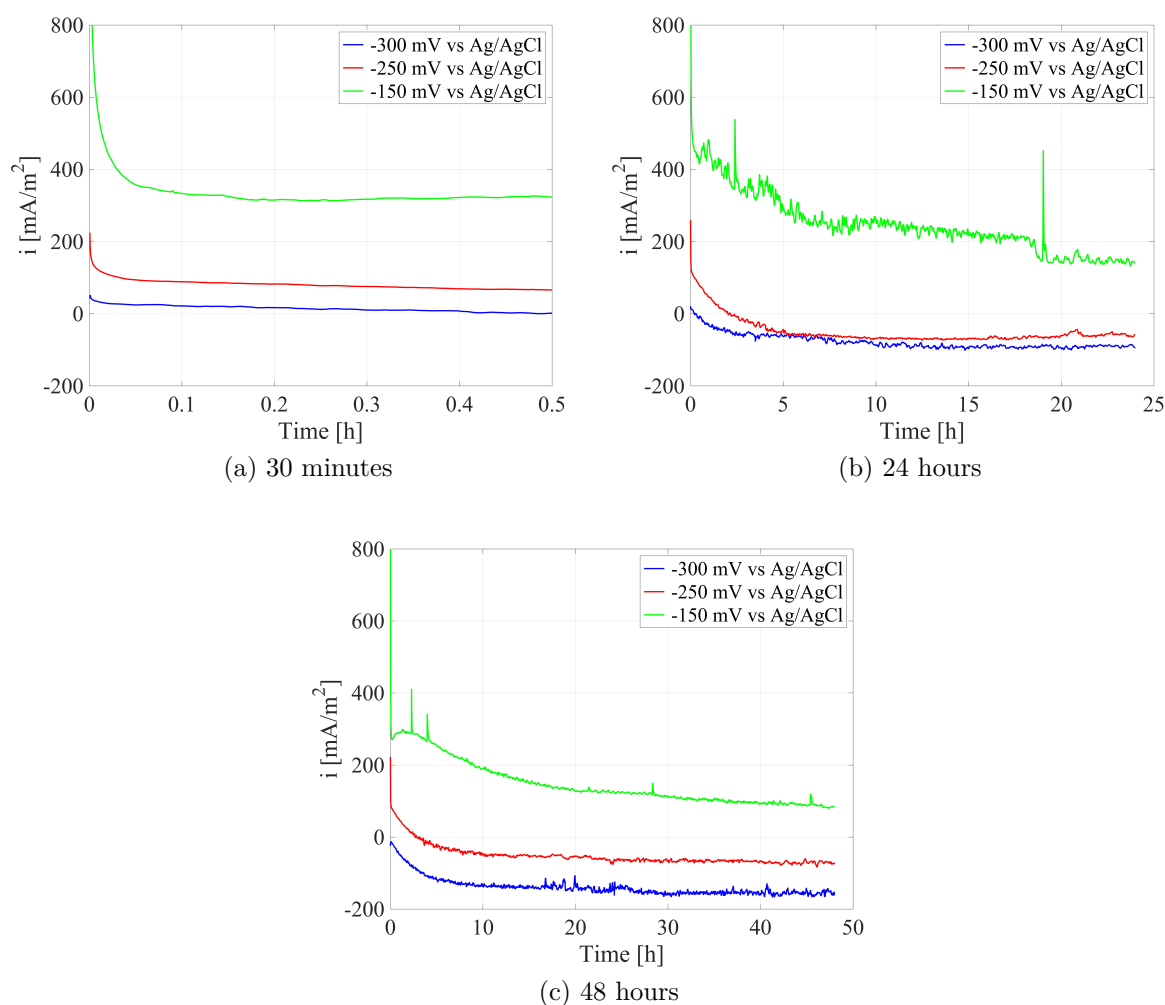
(b) 24 hours

(c) 48 hours

Figure 4.14: NAB polarized to potentials -150, -250 and -300 mV vs Ag/AgCl for 30 minutes, 24 hours and 48 hours, in SSW with pH=3.5.
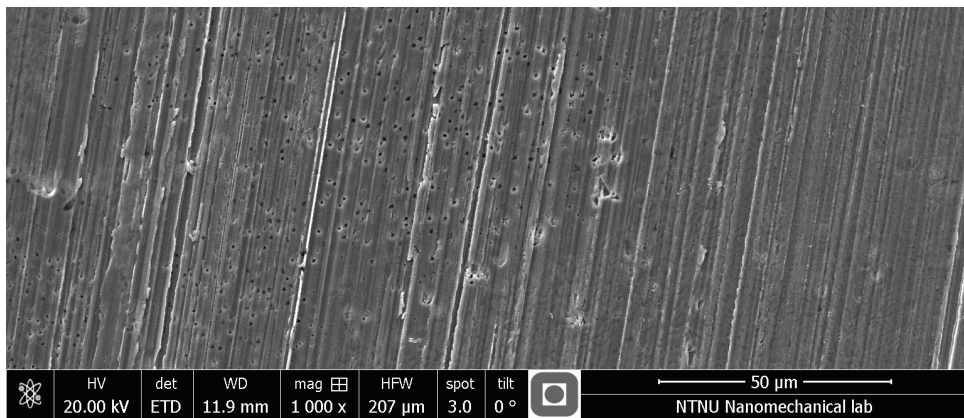
(a) 30 minutes
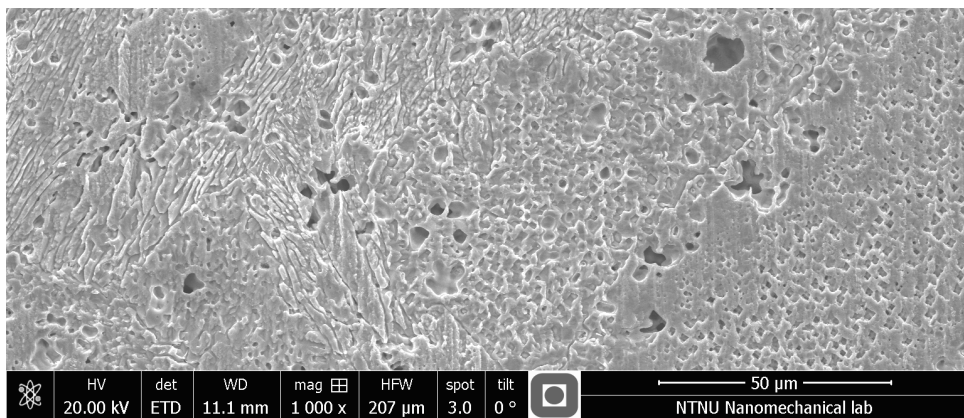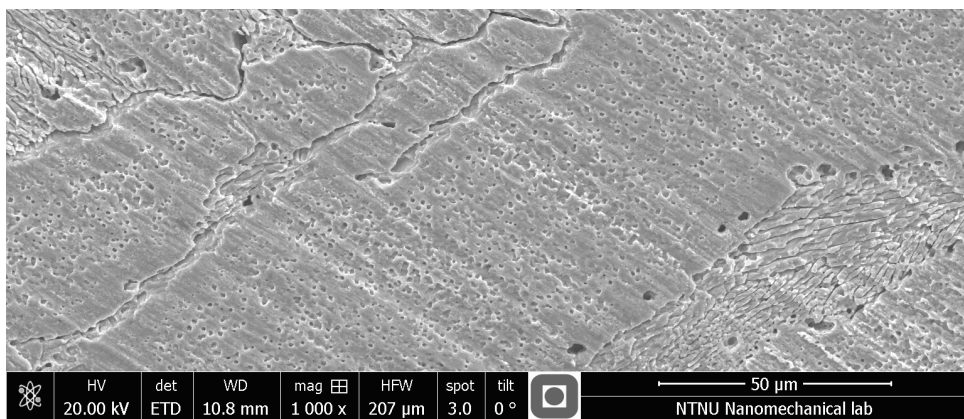
(b) 24 hours

(c) 48 hours

Figure 4.15: SEM images of NAB polarized to -150 mV vs Ag/AgCl in SSW with pH=3.5.
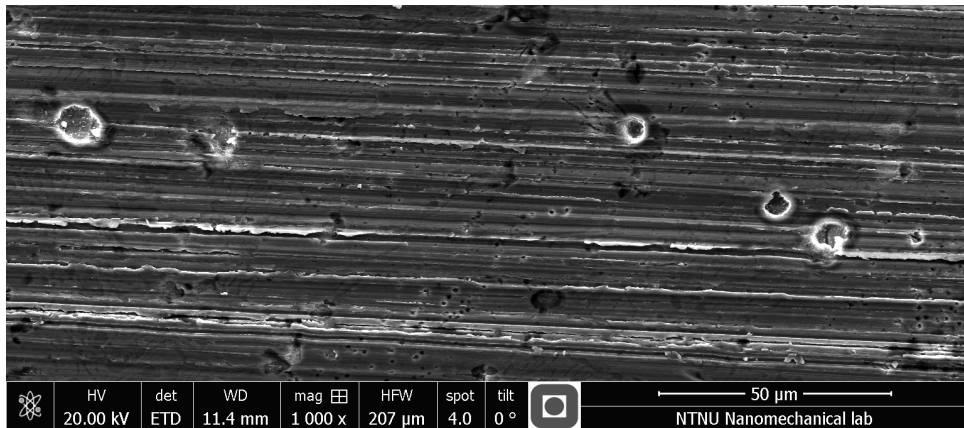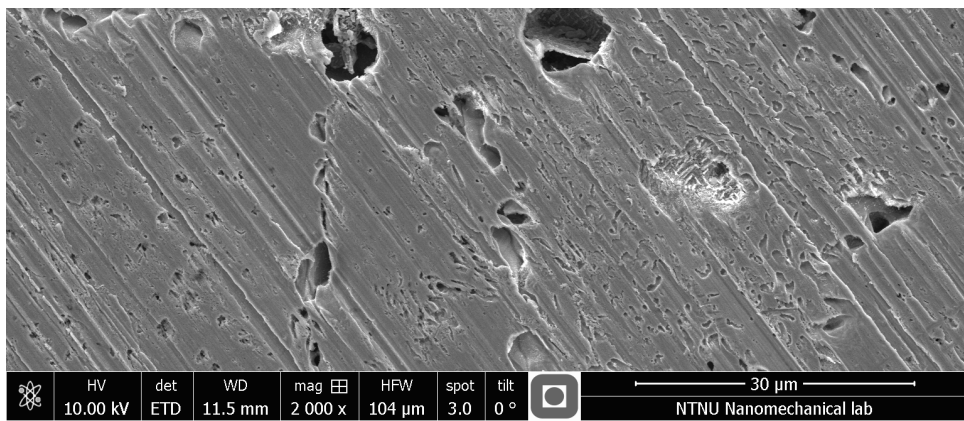
(a) 30 minutes
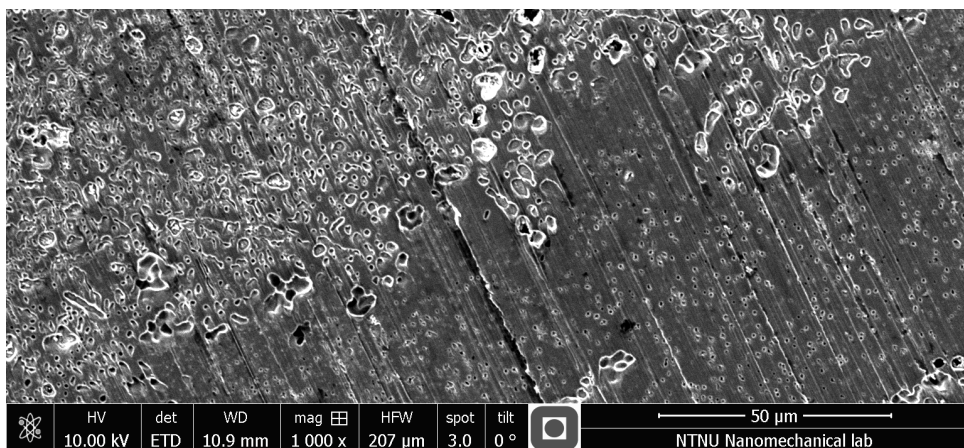
(b) 24 hours

(c) 48 hours

Figure 4.16: SEM images of NAB polarized to -250 mV vs Ag/AgCl in SSW with pH=3.5.
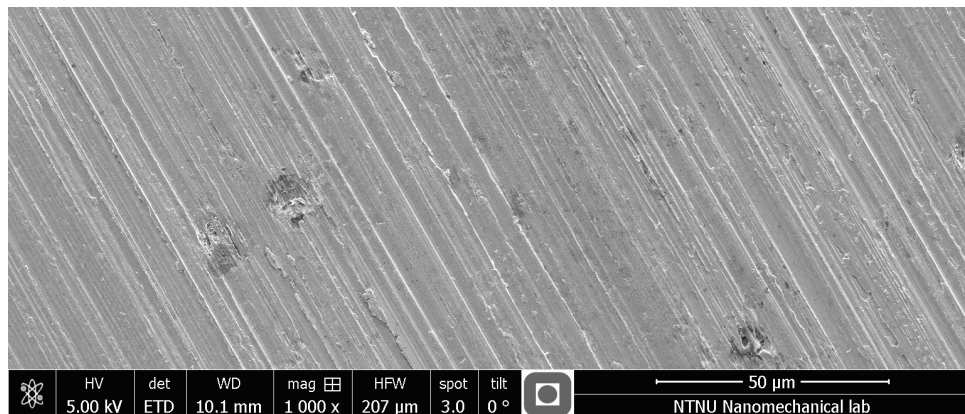
(a) 30 minutes
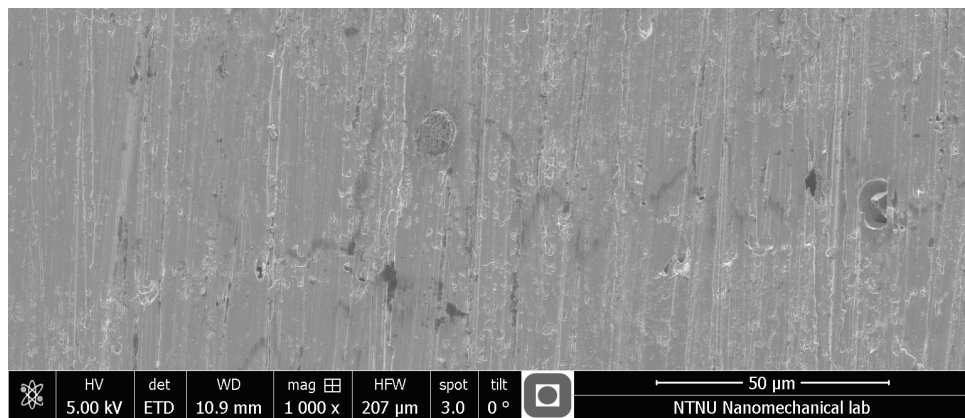
(b) 24 hours
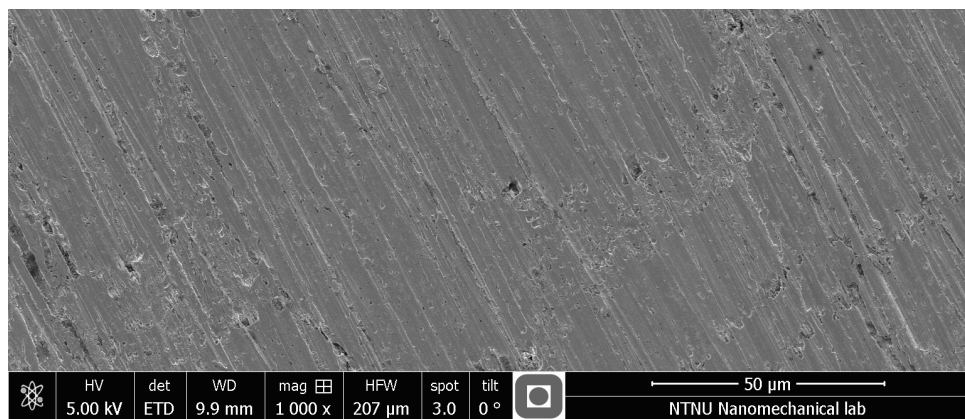
(c) 48 hours

Figure 4.17: SEM images of NAB polarized to -300 mV vs Ag/AgCl in SSW with pH=3.5.

4.5 Static anodic polarization of aluminium in SSW while reducing pH

A graphical presentation of the current density change with time during static anodic polarization of aluminium, while pH was reduced, is given in Figure 4.18. The pH measurements, which times are marked as black dots in Figure 4.18, are listed in Table 4.9.
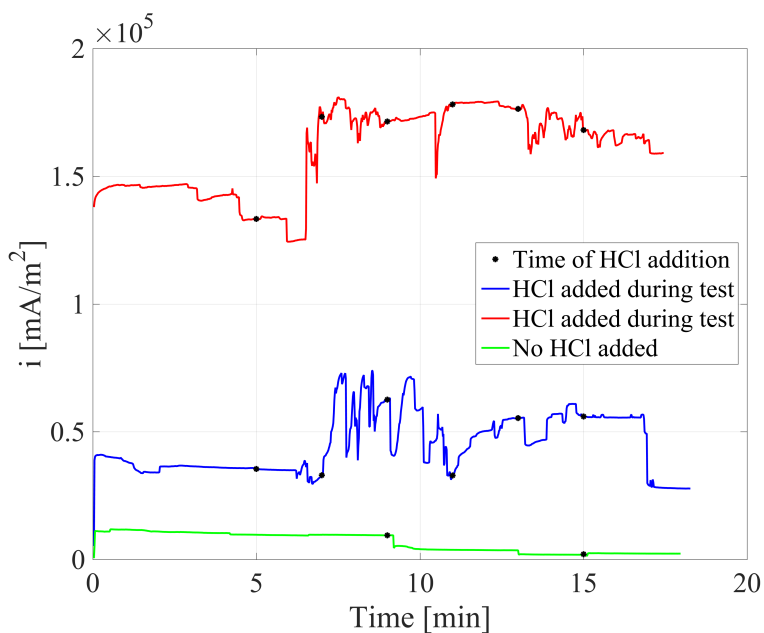
Figure 4.18: Static anodic poarization of aluminium in SSW at -200 mV vs Ag/AgCl, while the HCl is added.

Table 4.9: pH measurements during static anodic polarization of aluminium in SSW at -200 mV vs Ag/AgCl, while pH is reduced.

Time of HCl addition [min]	pH two minutes after addition		
	Blue curve	Red curve	Green curve
5	6.1	6.7	
7	6.0	5.9	
9	5.8	5.5	8.1
11	6.0	5.4	
13	5.6	4.5	
15	3.4	4.5	8.0

4.6   Long-time exposure of NAB in SSW with pH∈<3,4>

The long-time OCP measurements of NAB submerged in SSW with pH∈<3,4> are portrayed in Figure 4.19. The graphs in Figure 4.19 have been filtered to decrease the measurement noice. A description of the filtration procedure, as well as the original graphs, are given in Section A.4. The potential peaks coincided with the addition of destilled water and is expected to be caused by movements in the electrolyte, which disturbes the concentration gradients near the surfaces. The original graph is given in Appendix A. Figure 4.20 shows the weight loss of the samples, whereas the weight measurements are given in Table A.3. The samples were of similar dimentions and the weight loss measurements are concidered comparable. SEM images of the samples' surfaces are given in Figure 4.21, while SEM images of the samples' cross sections are given in figures 4.22 and 4.23.
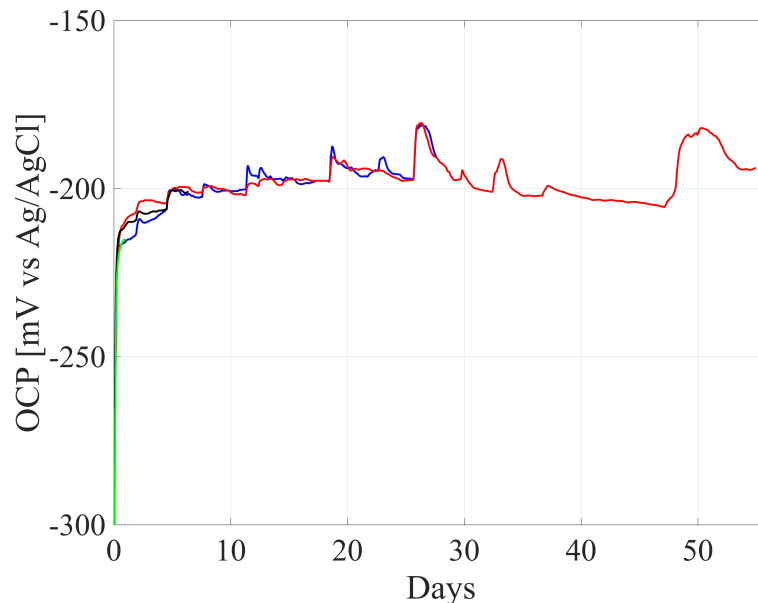
Figure 4.19: Measured OCP values of NAB samples immersed in SSW with pH∈<3,4> for up to eight weeks.

Some characteristics seen during SEM examination are listed here:

- After one day most of the κ_{IV} on the surface was corroded. Most of the κ_{II} and κ_{III} was uncorroded. The worst case found was corrosion attacks 10 μm below the surface, but most of the attacks occured above 5 μm below the surface.

- After one week, about half of the κ_{II} and κ_{III} 20 μm below the surface were corroded. No κ_{IV} was corroded below 10 μm. Some places κ_{II} particles 50 μm below the surface had corroded.

- After four weeks κ_{III} had mostly corroded to 30 μm below the surface. There were no signs of corroded κ_{IV} below 5 μm from the surface, however, some of the particles less than 5 μm from the surface had corroded. Some places entire grains had corroded. The craters from these grains were at the most 30 μm below the surface. Occasionally, single particles had corroded as far as 100 μm into the material.

- After eight weeks almost all the κ_{II} and κ_{III} closer than 60 μm from the surface had corroded. κ_{IV} was corroded to 10 μm below the surface in many places. Even more large grains had corroded and left craters on this sample, compared to the sample exposed four weeks.
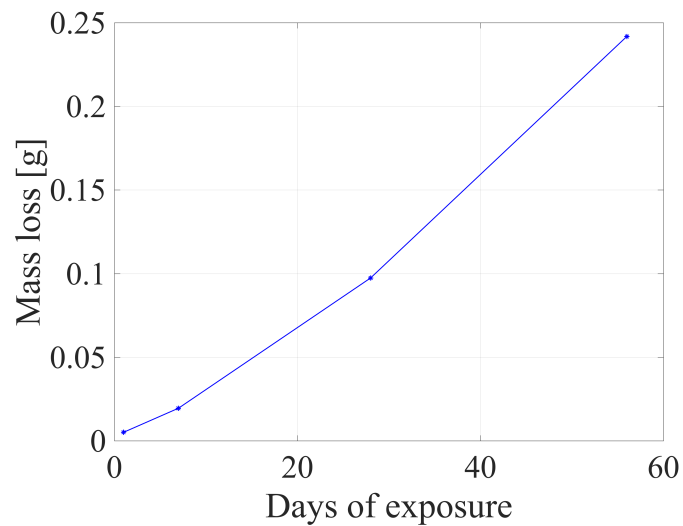
Figure 4.20: Weight loss of NAB during exposure to SSW with pH∈<3,4> for up to eight weeks.
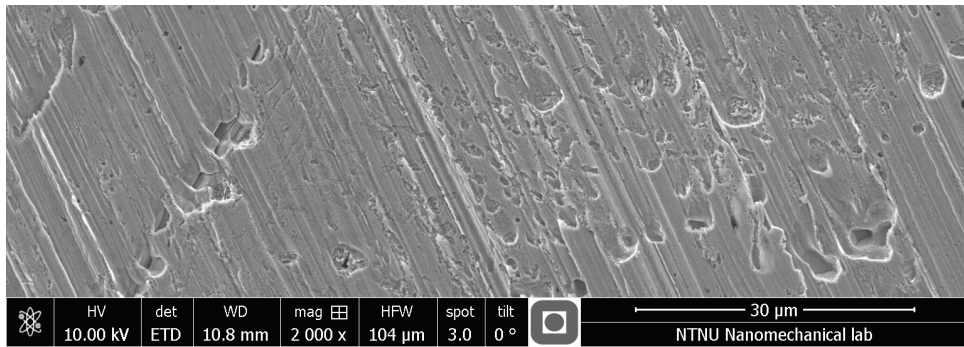
(a) Exposed one day
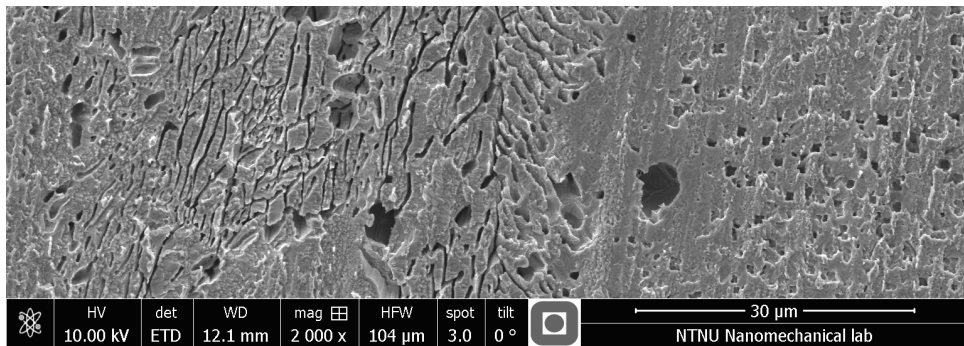
(b) Exposed one week
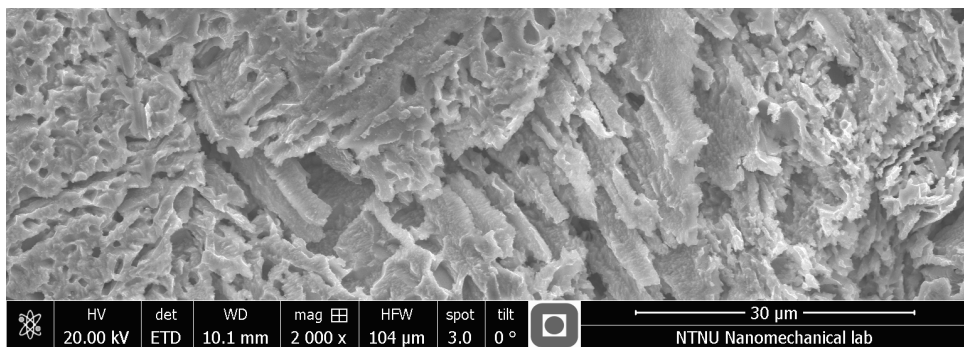
(c) Exposed four weeks
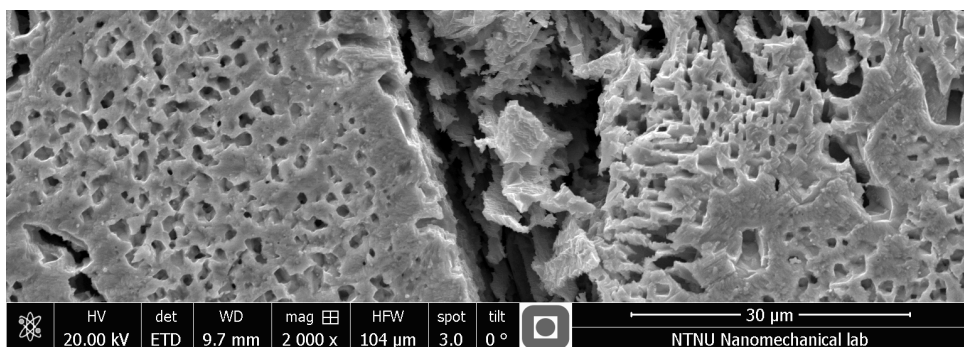
(d) Exposed eight weeks

Figure 4.21: SEM images of NAB surfaces exposed to SSW with pH∈<3,4>.
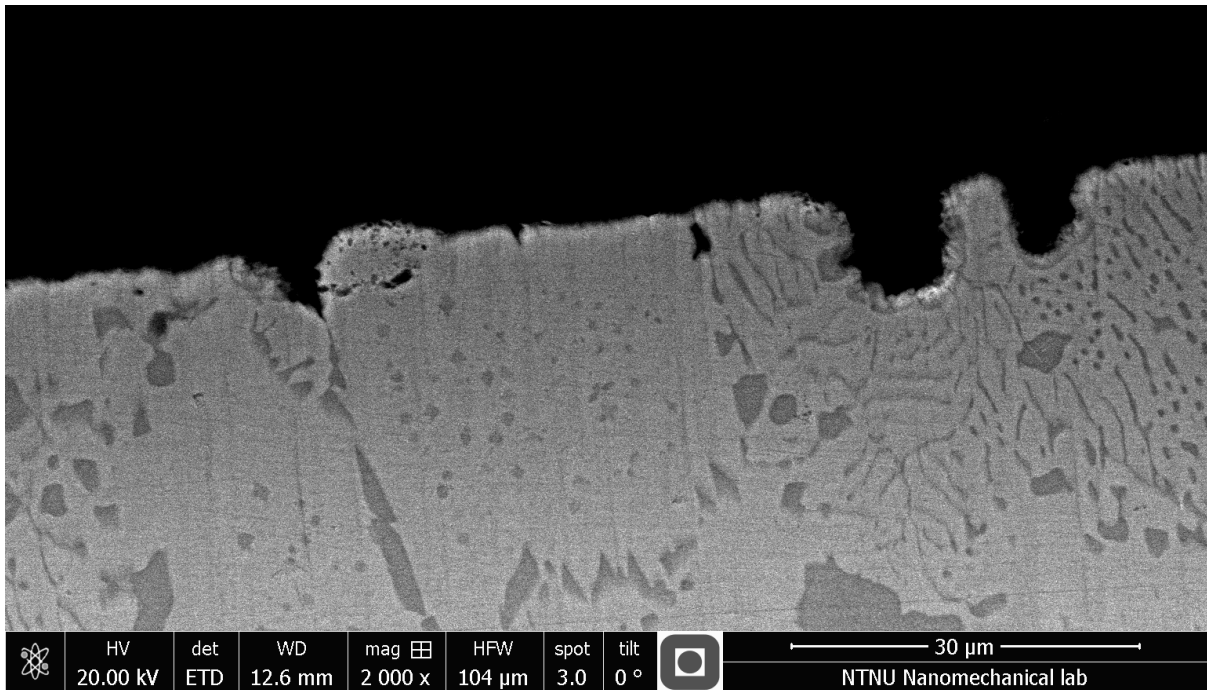
(a) Sample exposed one day.
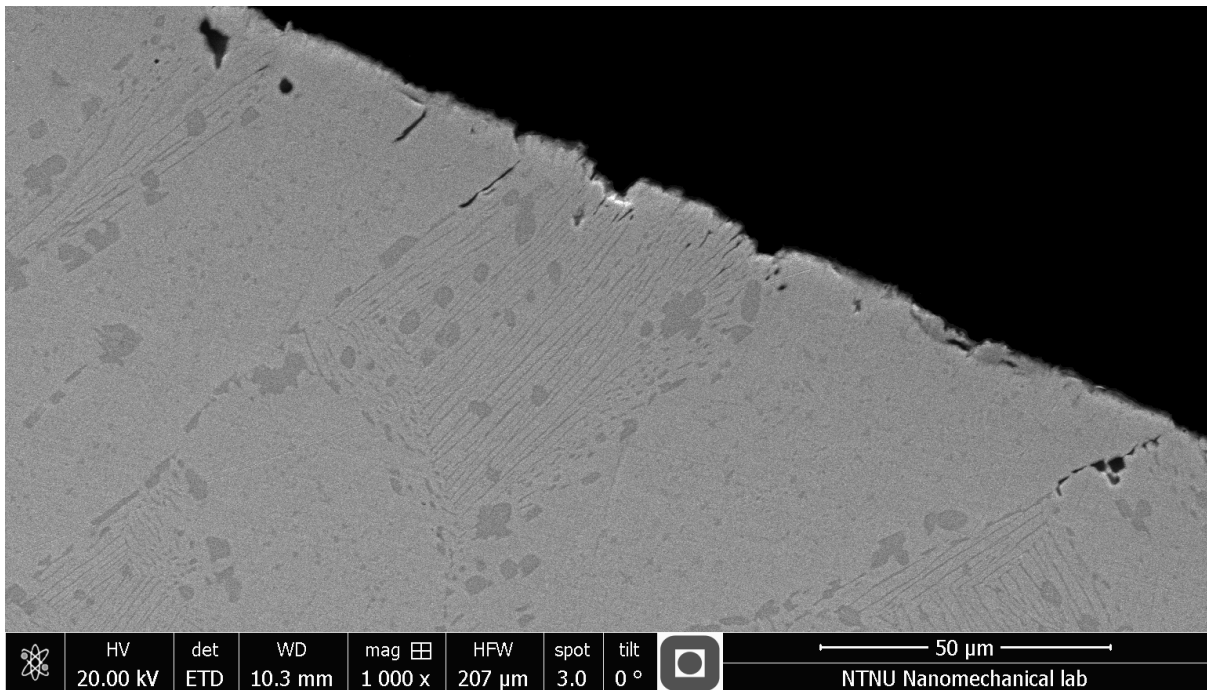
(b) Sample exposed one week.

Figure 4.22: SEM images of cross sections of NAB samples exposed to SSW with pH∈<3,4> for one day and one week.
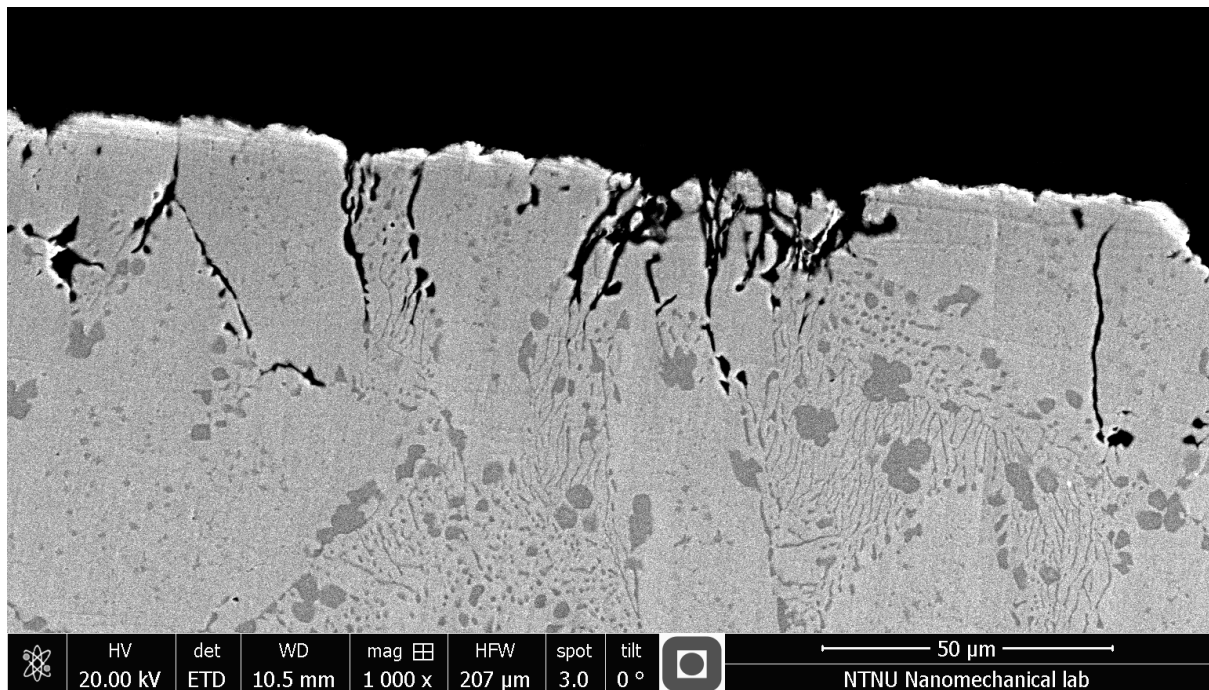
(a) Sample exposed four weeks.
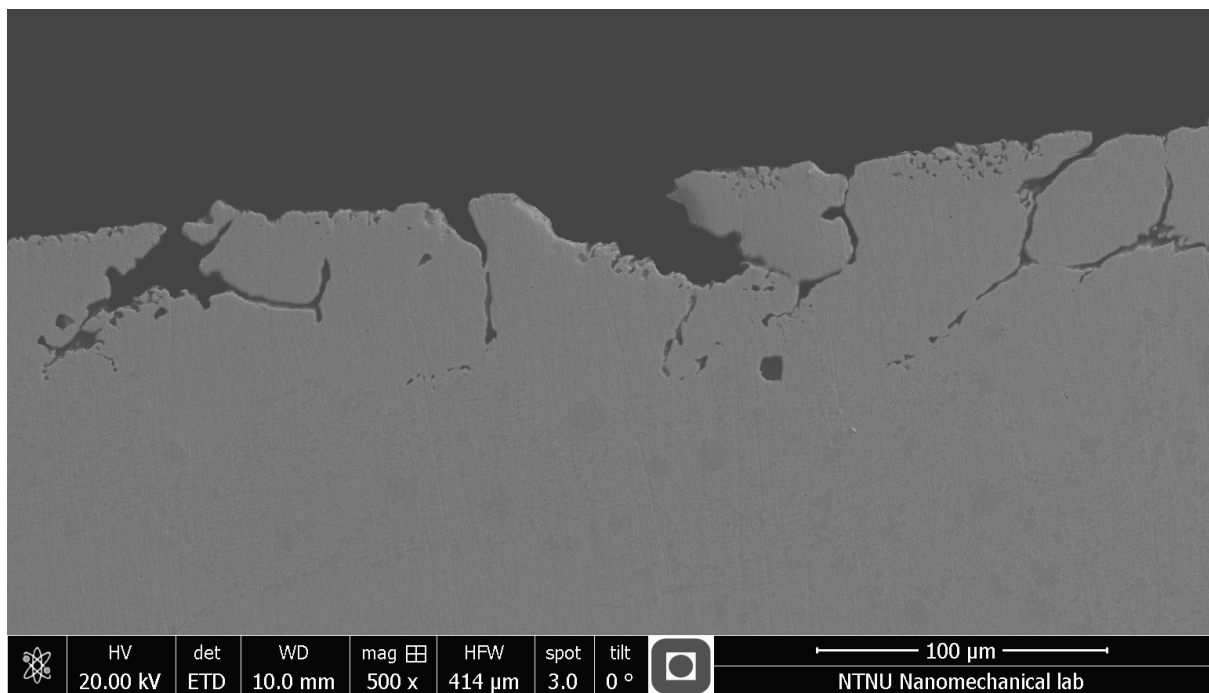
(b) Sample exposed eight weeks.

Figure 4.23: SEM images of cross sections of NAB samples exposed to SSW with pH∈<3,4> for four and eight weeks.

4.7   OCP variation with pH for NAB and nickel

The graph in Figure 4.24 displays the results of the test where the OCPs of nickel and NAB in SSW were measured while HCl was added to the electrolyte gradually to decrease the pH. SEM images of used test samples, as well as nickel and NAB in after 18 hours exposure in SSW, are given in Figure 4.25.
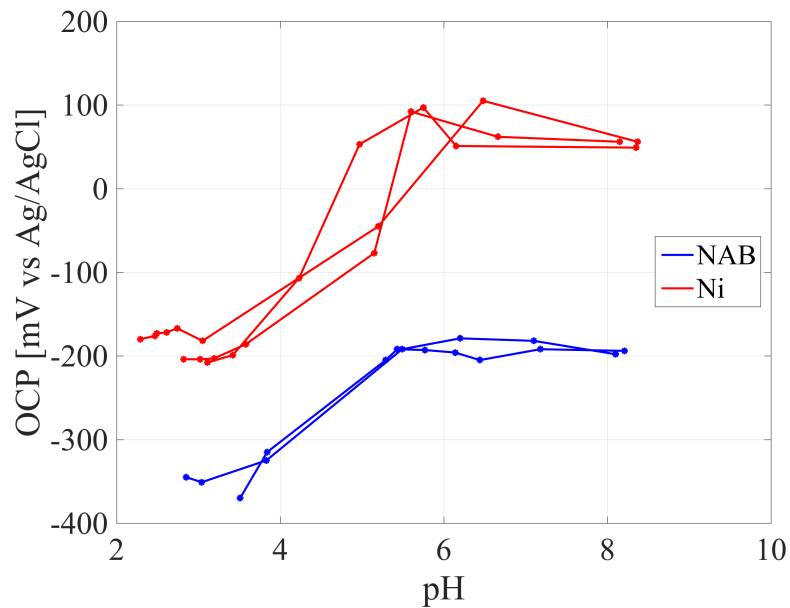
Figure 4.24: Measured relation between OCP and pH for NAB and nickel in SSW.
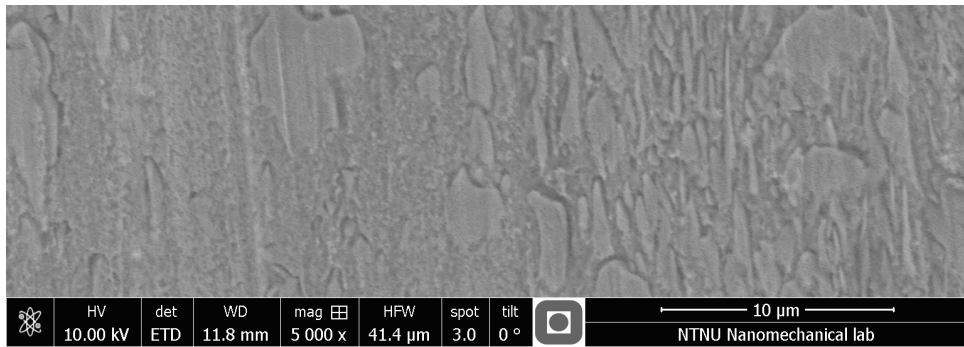
(a) NAB after 18 hours exposure.
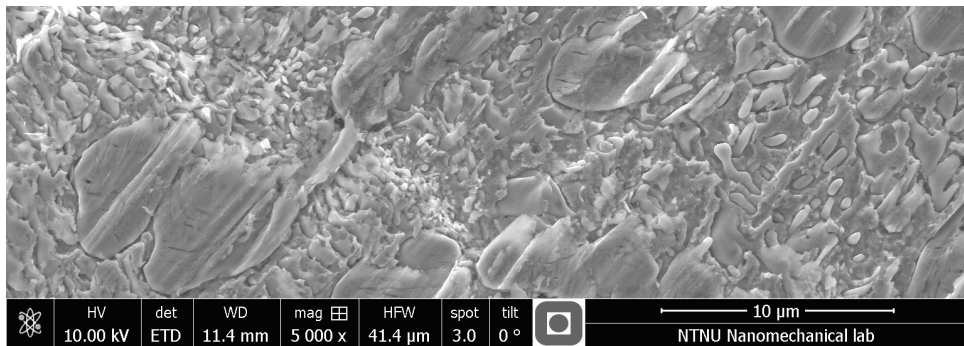
(b) NAB after test.
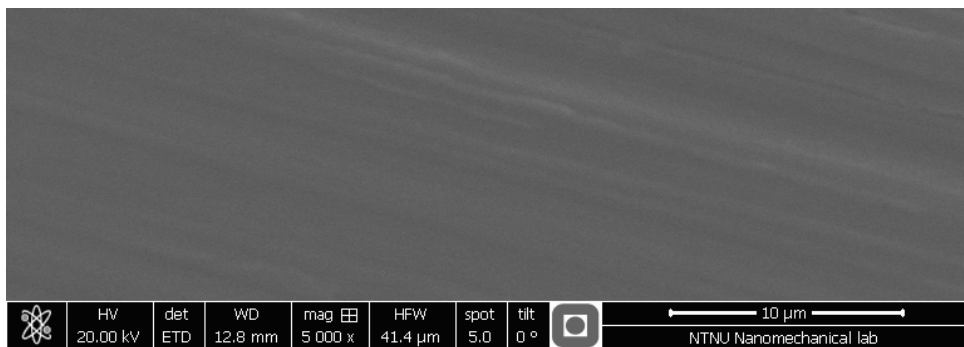
(c) Nickel after 18 hours exposure.
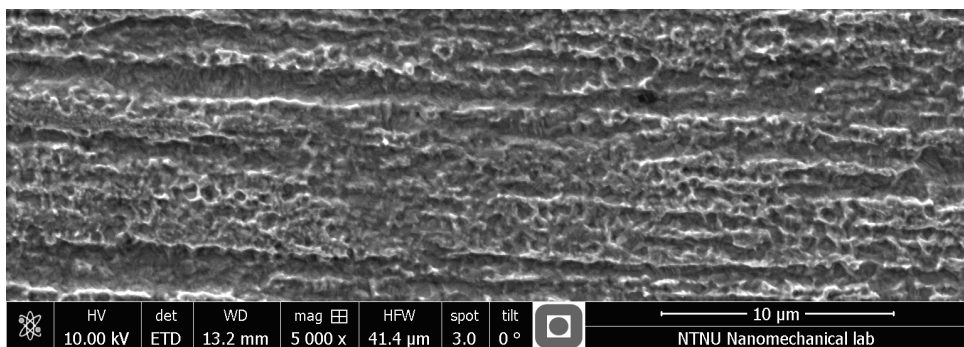
(d) Nickel after test.

Figure 4.25: SEM images of NAB and nickel samples before and after testing the pH-dependency of their OCPs in SSW.

Chapter 5

Discussion

This discussion is aimed to uncover the effect of the alloying elements on the corrosion properties of NAB. First, the microstructure of NAB is discussed to find which elements each phase is likely to be most influenced by. The corrosion properties of pure copper, aluminium and nickel are discussed based on the corrosion experiments performed for each of these materials. The corrosion properties of NAB are then discussed relative to the corrosion properties of the alloying elements.

5.1   Microstructure of NAB

The microstructure of NAB is indeed complex [2, 5, 8, 11]. The SEM observations of the **CuAl**10**Fe5Ni**5 alloy revealed a microstructure consisting of α, κ_{II}, κ_{III} and κ_{IV}. No β phase or κ_{I} particles were found. The contents of the elements were estimated with high standard deviation for the κ phases, which makes sence given the various possibilities of substitutional elements in the Fe_3Al and NiAl bases of the κ phases. However, the main characteristics of the phases were confirmed to be as reported earlier in [2, 4–8]; κ_{II} and κ_{IV} displayed far higher contents of iron than the other phases, κ_{III} was the most nickel-rich phase and α the phase richest in copper. The contents of aluminium, iron and nickel were lowest for the α phase.

The surface-area fraction of κ in NAB was estimated to 18% ± 8%, i.e. 10%-26% of the NAB surface is κ. A similar relation is expected for the volume fraction of κ in NAB. Hence, if only α corrodes actively, at least 74% of the surface will be active, whereas if only κ corrodes actively, less than 26% of the area will be active. Thus, in a hypothetical situation where either α or κ is working as a cathode, and the other as an anode, and there are no other anodes or cathodes affecting them, the current density of κ will be almost three times as large as the current density of α at OCP, assuming 26 % κ in the surface. For lower κ contents, the difference in current density will be even larger.

5.2   Corrosion properties of alloying elements

In this section the corrosion properties of pure copper, aluminium and nickel in pH=3.5 and pH=8.2 are discussed. Polarization curves, potensiostatic anodic polarization test for aluminium and OCP variation with pH test for nickel, where the tests are applicable, are the basis of the discussion.

5.2.1 Copper

Copper displayed quite similar polarization behaviour in SSW with pH=3.5 and pH=8.2. The characteristic $b_a \approx$60 mV/decade and OCP$\approx$-200 mV vs Ag/AgCl were displayed in both environments. The variations in i_{corr} and b_c are expected to be caused by errors in the cathodic Tafel extrapolation caused by limiting current conditions during cathodic polarization. The corroded surfaces were seemingly similarly attacked by corrosion as well.

The negative current densities of the back scans of the copper curves are related to the reversal of the copper oxidation process. This will only occur for dissolved species and not for oxides or other stable chemical compounds. The anodic curve at pH=8.2 is expected to start with a transformation of copper to Cu(I) complexes followed by dissolution of copper to Cu(II) complexes [18]. According to Figure 2.7, the Cu(I) and Cu(II) species formed are $CuCl_2^-$ and CuO, respectively. As the potential is lowered, the dissolved $CuCl_2^-$ complexes will be unstable and start reducing. This increases the cathodic current on the sample and the net current of the surface becomes cathodic. The potential of the reduction reactions are higher during the back scan than the polarization before back scan due to the increased amount of metal ions in the solution. Reduction of $CuCl_2^-$ is probably causing the higher region of negative i, whereas the lower region is caused by an increase of OCP. The OCP increases as a consequence of the increased amount of copper ions in the solution and changed surface properties, caused by the polarization. The back scan of the anodic curve at pH=3.5 is negative from E=-57 mV vs Ag/AgCl until OCP was reached. According to the pourbaix diagram in Figure 2.7, and other pourbaix diagrams for copper in chloride media [18,19], copper oxides are not stable at pH=3.5. $CuCl_2^-$ and Cu^{2+} are the stable species during anodic polarization at pH=3.5. These become unstable when the potential is lowered, causing a cathodic current in the anodic back scan. The copper surfaces had similar appearances in SEM, though oxide formation was only expected for the surface exposed to pH=8.2. This is probably caused by the copper that redeposited during the back scan, which evens the dissimilarities of the surfaces' compositions and appearences.

5.2.2 Aluminium

The aluminium polarization curves were relatively similar near OCP, but rather different in the higher anodic region. However, the SEM images of the surfaces display a similar corrosion mechanism, with servere pitting attacks in both environments. Aluminium had a sligthly lower OCP in SSW with pH=3.5 compared to SSW with pH=8.2, -720 and -700 mV vs Ag/AgCl respectively. The negative i for E <-706 mV vs Ag/AgCl in the back scan of the anodic curve at pH=3.5 is occuring very close to the OCP. This cathodic current is probably attributed an increase of OCP, for similar reasons as described for copper in Section 5.2.1. Both b_a and b_c were steeper for the low pH environment. The cathodic curve at pH=3.5 had generally much higher i than the cathodic curve at pH=8.2. This is probably a direct consequence of the increased H^+ concentration at low

pH, which increases the reduction potential of the hydrogen evolution reaction, given in (2.2). i_{corr} was almost seven times higher at pH=3.5 than at pH=8.2. Al_2O_3 is expected to be more stable at pH=8.2 than pH=3.5, and is probably causing the difference in i_{corr}.

During the anodic polarization of aluminum, bubbles developed rapidly on the aluminium surface and drifted to the electrolyte surface. At high potentials in chloride media, pits, are created in the Al_2O_3 film and the electrolyte comes closer to the metal surface in the pits. The large potential difference between the surface and electrolyte causes H_2 evolution [28]. This implies consumption of H^+ ions, which increases the pH. Thus, the pH during the anodic scans are unknown. The anodic polarization curve of aluminium at low pH had a typical passive shape, which is not expected at low pH. The pH is thus assumed to have been altered, during the test, to a level where Al_2O_3 is stable. Unfortunately, no pH measurements were conducted during this test.

The potentiostatic tests of aluminium displayed much less stable i values for the samples subject to HCl addition compared to the sample exposed to stable pH. The differences in i for the experiments are assumed to be caused by a difference in OCP, as the OCP of pure aluminium spans a large range of values, see Figure 2.6. Thus, the samples are anodically polarized to different potentials relative to their OCP. The variation of i during each separate test is emphasized, while the difference of i for different tests is not discussed. The experiments where HCl was added, displayed their highest and least stable i values at pH<6. The pH measurements in Table 4.9 show that for HCl additions after 7, 9 and 11 minutes of exposure, the pH level was restored within two minutes. This tendency was not seen for NAB and nickel during HCl addition in the OCP variation with pH test. Bubbles developed on the surfaces of the samples in the same manner as during anodic polarization curve measurements. The bubble development and increased pH are assumed to be attributed the reduction of H^+ ions during the experiment.

5.2.3 Nickel

Nickel displayed the largest transformation in corrosion properties from high to low pH. The OCP was -160 mV vs Ag/AgCl at pH=8.2, and -380 mV at pH=3.5. i_{corr} was 2 mA/m^2 at pH=8.2, and 54 mA/m^2 at pH=3.5. b_a at pH=3.5 was twice the size of b_a at pH=8.2, while the b_c at pH=3.5 was smaller than the b_c at pH=8.2.

The expected corrosion products for nickel are NiO and $Ni(OH)_2$, or partially hydrated NiO, as mentioned in Section 2.5.4. In the test where nickel was exposed to SSW while HCl was added, the OCP remained relatively stable until pH=5.5. At pH$\in$<4,5.5> the OCP gradually decreased, until it became stable for pH<4. This behaviour is expected to be caused by the breakdown of partially hydrated NiO, which increases with increasing H^+ concentration. It is suggested that partially hydrated NiO is protecting the surface satisfactorily above pH≈5.5 and not at all below pH≈4. The OCP of nickel, after 18 hours of exposure in SSW with pH=8.2, was higher than the OCP before polarization tests in SSW with pH=3.5 and pH=8.2. At pH=8.2 a passive film is not expected to

be formed during one hour of submersion, due to the low corrosion rate. Thus, the OCP of nickel after one hour exposure in SSW is representative for a submerged, but not passivated surface. The surface submerged for 18 hours in SSW seemed to have developed a protective passive film, thus the OCP of nickel at pH=8.2 in the OCP as a function of pH test is more representative for passivated nickel. The passive potential of nickel is then ~30 mV vs Ag/AgCl.

The anodic polarization curves of nickel exhibited linear dependence on the logarithm of the current density for a relatively wide range of current densities. Hence, b_a, for both environments, was determined with ease and the differences in Tafel slopes cannot be attributed to errors. With the OCP as a function of pH test indicating stable OCP at pH=3.5 and pH=8.2, it is suggested that the anodic reaction of nickel at pH=3.5 is related to formation of Ni^{2+}, wheras b_a at pH=8.2 is related to the formation of NiO and/or $Ni(OH)_2$. Oxides have low solubility and the OCP of the nickel surface is expected to be changed by the formation of an oxide layer. The negative i in the back scan of nickel at pH=8.2 indicates that the OCP of the surface is changed to -70 mV vs Ag/AgCl due to the formation of a passive film. This is ~100 mV lower than the potential measured for nickel exposed to SSW for 18 hours, which suggests that the protective film formed during 18 hours of exposure is more protective than the film formed during the polarization test at pH=8.2. The relative amount of NiO vs Ni(OH), and the thickness of the film, are some of the factors that might give reason to such a difference.

5.3   The corrosion properties of NAB

The corrosion properties of NAB is discussed in this section with basis in the results of NAB characterization and corrosion experiments conducted in this work. The main topics of the section are the behaviour of NAB when polarized, OCP variation with pH and corrosion development in low pH environments.

5.3.1   Polarization behaviour

The polarization curves of NAB in SSW with pH=8.2 and pH=3.5 had very different appearences. The curves are plotted with the polarization curves of α in Figure 5.1. At both pH levels tested, the OCP measurements before polarization indicated dealloying of aluminium on NAB as described in Section 2.5.2. The OCP of NAB was much lower at pH=3.5 than at pH=8.2, and the potential was not as stable at pH=3.5 as pH=8.2. This has been attributed to the loss of passivity by Al_2O_3, which makes κ corrode at low pH [4, 10]. The OCP at low pH is thus representative for the OCP of κ phases at this pH, whereas the OCP at pH=8.2 is representative for α at this pH.

The polarization curves of α behaved very similarly to NAB at pH=8.2. The SEM images before and after the anodic polarization curve of α, which can be seen in Figure 4.12, show that only α corroded significantly during the test, as the κ phases seem intact.

Thus, the presence of κ in the surface is trivial to the polarization properties of NAB at pH=8.2, and the properties of the anodic and cathodic polarization curves of NAB at pH=8.2 reflects the properties of α. The similarity between the NAB and α polarization curves at high potentials indicate that the corrosion properties of NAB at high anodic potentials are dominated by corrosion of α, independently of pH. This similarity has been documented before in [4], see Figure 2.4. When α starts corroding at pH=3.5, the anodic curve starts deviating from Tafel kinetics. Between the anodic Tafel region at pH=3.5 and the potential where NAB starts being independent of pH, both corrosion of α and κ contributes significantly to the corrosion current, for NAB at pH=3.5. For potentials where the polarization curves behave relatively similarily, the current density is higher for NAB at pH=3.5 compared to pH=8.2. This potential difference is caused by the active corrosion of κ, which only occurs for the low-pH curve. At pH=3.5, only κ corrodes significantly below the upper part of the anodic Tafel region. The b_a, b_c, i_{corr} and OCP found for NAB at pH=3.5 are thus representative for the κ phases of a freshly prepared NAB surface. Since $κ_{II}$ and $κ_{IV}$ have much higher contents of iron than $κ_{III}$, and both are discontinuous, the corrosion constants are not expected to be the same for a sample where $κ_{II}$ and $κ_{IV}$ have corroded.
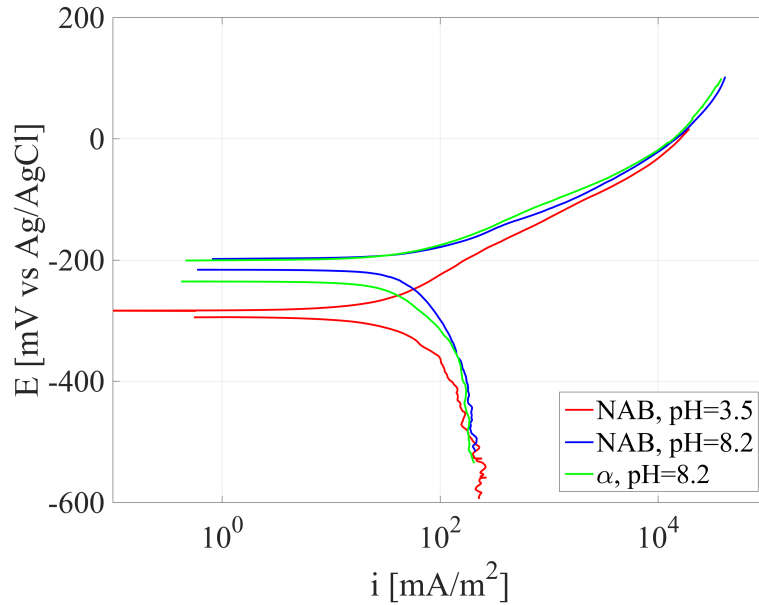
Figure 5.1: Polarization curves of NAB, in SSW with pH=3.5 and pH=8.2, and α, in SSW with pH=8.2.

The anodic back scan for NAB in SSW with pH=8.2 displayed negative current densities for E<-185 mV vs Ag/AgCl, while the entire anodic back scan of NAB at pH=3.5 was positive. The negative current densities in the anodic back scan start at similar potentials as the negative values found in the anodic polarization back scan of copper at pH=8.2, which were attributed to a change of OCP. At $E \approx$-70 mV vs Ag/AgCl, the current density decreased for the NAB anodic back scan curve at pH=8.2. This is

probably caused by the reduction of previously oxidzed species on the surface, but with a cathodic current being lower than the anodic current of the surface. Hence, the current is still positive. The back scan of the anodic polarization curve of copper at pH=8.2 was negative for $-84 < E < -58$ mV vs Ag/AgCl, which is in the region where the NAB curve exhibited a reduction of current density. A similar reduction of current was not observed for aluminium or nickel, nor was it observed for iron during the preliminary project [1]. The region is thus connected to the reduction of $CuCl_2^-$.

The corrosion current density for NAB was twice as large in SSW with pH=8.2 than SSW with pH=3.5. However, the current is not evenly distributed over the surface during corrosion. At OCP conditions, the κ phases are not corroding at pH=8.2, while α is not corroding at pH=3.5, given a relatively freshly polished surface. Using the area fractions of α and κ phases found in Section 4.1, the estimated corrosion current densities for the active areas on NAB at pH=3.5 and pH=8.2 are

$$
\begin{aligned}
\text{pH=3.5}: \quad & i_{\text{corr},\kappa} = 28 \cdot 100/18 = 156 \ \text{mA/m}^2 \\
\text{pH=8.2}: \quad & i_{\text{corr},\alpha} = 70 \cdot 100/82 = 85 \ \text{mA/m}^2
\end{aligned}
\tag{5.1}
$$

Thus, the corrosion attack is expected to be much more severe at pH=3.5 than at pH=8.2, even though the i_{corr} is larger when concidering the entire surface to be active. In (5.1), $i_{\text{corr},\kappa}$ is calculated for a surface where κ_{II} and κ_{IV} are uncorroded. As κ_{II} and κ_{IV} dissapear from the surface due to corrosion, the active area will be smaller and $i_{\text{corr},\kappa}$ will increase.

The SEM images of the polarized NAB samples, given in Figure 4.3, show that α has corroded to a slightly larger degree at pH=8.2 than at pH=3.5. The κ_{IV} particles are intact at pH=8.2, whereas the κ_{IV} particles visible at pH=3.5 are partially corroded. The particles visible on the sample polarized in SSW with pH=3.5 have probably been covered by α for most of the test, and first exposed when overlying α has corroded. κ_{II} is partially corroded in both environments, but more severely at low pH. κ_{III} seems to be uncorroded in both environments. In Table 4.3 the measured current densities of the pure elements at the OCP of NAB are listed. The net current densities generated by aluminium and iron when polarized are much larger than the net current densities generated by nickel and copper. The difference is most distinct at high pH. However, the relative difference between iron and aluminium is most marked at low pH. Iron has more than ten times as high current density at the OCP of NAB at pH=3.5 as aluminium, which explains why κ_{II} and κ_{IV} particles corrode much faster than κ_{III} at low pH.

The samples subject to static anodic polarization tests had few signs of corrosion after one hour exposure in SSW with pH=3.5, i.e. right before polarization started. After 30 minutes κ_{IV} and κ_{II} had started corroding for all three potentials, while κ_{III} had not. This means that a rather small area is corroding in the beginning of the static polarization, and removal of κ_{IV} and κ_{II} from the surface is expected to go fast. The three samples exposed for 30 minutes had positive currents, except for the polarization to -300 mV vs

Ag/AgCl, where the current was slightly negative at the end. A negative current means that the current from the sample is cathodic, rather than anodic. With iron rich particles corroding away, the anodic current is largely reduced, since the applied potentials are much higher than the OCP of iron. Also, the α area of the surface is increased, since α is covering the κ_{IV} particles, and κ_{II} particles to a large extent as well. This is likely to be causing the net current of the anodically polarized surfaces to be cathodic. The current was positive for all the static polarization tests at -150 mV vs Ag/AgCl, which is expected, as this potential is anodic for both κ and α. During static polarization at -300 mV vs Ag/AgCl, the current was below zero less than halv an hour into the polarization for all the samples. Samples polarized to the same potential displayed quite different current densities. This is especially evident for tests conducted for 24 and 48 hours. The difference is assumed to be caused by variation of phases present on the surfaces. The OCP measurements of NAB during one hour of exposure in SSW with pH=3.5, see Figure 4.13, indicate that the corrosion properties of NAB vary a lot when κ is corroding.

5.3.2   OCP variation with pH

The OCP of nickel varied in a similar manner as the OCP of NAB in the OCP variation with pH test, indicating there might be a link between the pH-dependency of the two materials. NAB is expected to be dealloyed from aluminium within 20 minutes of exposure, thus, the similarity was observed for an NAB surface dealloyed from aluminium. The potential difference between aluminium and copper is the driving force behind the dealloying of aluminium. Iron has an OCP conciderably lower than copper, see Figure 2.6, and the surface is expected to be dealloyed from iron within the hour as well. The SEM images of the NAB samples show that both α and κ have corroded during the test. α suffered from corrosion to a larger extent than the κ phase, which is reasonable given that the sample has been exposed to pH>4 for a much longer time than pH<4. During the 18 hours of exposure, before polarization, the surfaces had to some degree developed oxides. The nickel surface looked passivated in the SEM, and was difficult to image, which is typical for nonconducting materials. The EDS analyses detected a small fraction of oxygen on nickel the surface, below 5 wt%. The emission depth of the electron beam was probably longer than the thickness of the passive layer, which makes sence as partially hydrated NiO protects the substrate materials when only nanometers thick [25]. Hydrogen cannot be detected with EDS, and the ratio between NiO and $Ni(OH)_2$ has not been determined. The surface is assumed to be covered with a thin layer of partially hydrated NiO after 18 hours immersion in SSW. The EDS analyses of NAB displayed higher concentrations of oxygen, but still below 10 wt%. NAB is expected to need more than 200 hours for creating a passive film when exposed to seawater at ambient temperature [9]. Thus, a fully developed film was not the starting point for NAB in this test.

Both materials had relatively stable potentials at pH$\in$<5.5,8.2]. The OCP variation for nickel in this region is assumed to be temporary and stabilization might have been acchieved if the test was conducted with a slower frequency of HCl addition. Nickel has

in general been observed to be especially easily affected by introduction of flow to still electrolytes. At pH<4 the potential seems to start stabilizing for both materials. The nickel curves display a gradual decrease of OCP from pH=5.5 to pH=3.5. The NAB curve lacks measurements at pH$\in$[4,5] and OCP$\in$[-200,-300] mV vs Ag/AgCl. Thus, it is not clear whether the change of OCP is sudden or gradual. However, the stability of the OCP of NAB until pH=5.5 can not be attributed to the stability of Al_2O_3 alone, as Al_2O_3 has been proven to be unstable at pH<6, see Figure 4.18 and Table 4.9.

5.3.3 Corrosion development in low pH environment

The potential of the NAB samples exposed in SSW, with pH$\in$<3,4> for up to eight weeks, stabilized around -190 mV vs Ag/AgCl after five days. This is not far from the OCP of NAB in SSW with pH=8.2, where α is corroding. However, the cross sections of the samples indicate that κ is corroding at much higher velocity than α. The OCP of NAB is thus expected to be affected by corrosion of κ as well. The corroded grains seen in the cross section images, see Figure 4.23, did probably contain α lamellas that loosened when the surrounding κ_{III} corroded. Due to the cleaning of the surface before SEM imaging, any loose material within the crevices is expected to be washed away. Thus, the SEM images do not show whether α lamellas have loosened or not.

The SEM images of the corroded surfaces display marked corrosion attacks of α on the samples exposed for four and eight weeks. The sample exposed for one week has distinct enlargened craters where κ has corroded and the surrounding α has started to corrode too, thus increasing the crater sizes beyond the volume previously occupied by κ. The only sample with seemingly undamaged α is the one exposed for one day. As the potential of the samples increased during the first day and stabilized a bit later, α is indeed not expected to be a main contributor to corrosion during the first day.

In the long exposure experiment, the $\alpha + \kappa_{III}$ eutecotid zone is relatively isolated from the electrolyte at the deepest corroded areas. Wharton and Stokes [12] found deposited copper inside crevices where κ_{III} had corroded on NAB samples subject to crevice corrosion for one month. Copper deposition is thus possible for the samples exposed over long time, due to the creation of channels where κ_{III} has corroded. However, the long exposure test of NAB revealed no redeposition of copper on the surfaces. Redeposited copper may mask corrosion damage, but also support the attack of κ_{III}. The absence of copper deposits in the experiment could mean that the crevices are not as islolated from the electrolyte as they seem to be in the cross section images. Also, high Cl^- concentrations may prevent copper from depositing. Either the environment inside the corroded lamellar areas is contaning too much Cl^- for solid copper to be stable, or the corrosion products within the crevice contain too little copper, or the environment is open enough to prevent pile-up of copper ions.

During the long exposure test the pH increased and had to be adjusted several times to maintain pH<4. The increase in pH is expected to be caused by the cathodic corrosion

reactions, as both O_2 reduction and H_2 evolution consume H^+ ions from the electrolyte.

5.4   Effect of alloying elements in NAB

Copper is the main element in NAB and is thus expected to affect the corrosion properties to a large extent. The polarization experiments in SSW with pH=8.2 for NAB, α and pure copper have a clear resemblance and verify the existing theory that corrosion of NAB in seawater is largely dominated by copper oxidation, when the surface has been dealloyed from aluminium. At pH=3.5, the elemental copper only contributes significantly to the corrosion current of NAB at $E>$-100 mV vs Ag/AgCl. For longer exposure in pH=3.5, however, the potential of NAB increased from below -300 mV vs Ag/AgCl to -220 mV vs Ag/AgCl during the first day, which was caused by the loss of all κ_{II} and κ_{IV} particles on the surface. The potential of the NAB surface stays close to the potential of pure copper during further exposure, and the anodic reactions of α increase while the cathodic decrease.

Al_2O_3 is one of the main components of a fully developed passive film on NAB [9]. The potetiostatic test for aluminium indicated that Al_2O_3 is stable at pH=8.2 and unstable at pH<6. Copper is known to reduce the stability of Al_2O_3, thus, NAB is not expected to form a passive Al_2O_3 film at pH<6. The current of aluminium at pH$\in<6,8.2>$ was not measured, thus, the instability of Al_2O_3 could have started above pH=6. One of the tests, drawn as a blue curve in Figure 4.18, displayed a stable and low current at the end of the test, at pH=3.4. This stability may be caused by complete dissolution of the Al_2O_3 film. For the other test, the lowest measured pH was 4.5, and the current did not decrease towards the end of the test. As the pH was altered, due to H_2 evolution during the test, even lower pH levels were probably reached between the sampling points. In the OCP as a function of pH test, NAB displayed stable behaviour until pH=5.5, i.e. below the pH where Al_2O_3 was unstable in the potentiostatic test for aluminium. Thus, Al_2O_3 must either be stabilized by the presence of other elements in NAB, or other elements must have created passive oxides. The main candidates are copper and nickel.

Nickel is added to aluminium bronzes to allow higher aluminium content in the alloy without formation of corrodable phases [3]. Nickel is an FCC stabilizer and increases the stability of the α phase while the stability of γ_2 is decreased. The nickel-rich κ_{III} is a weakness in NAB at low pH, due to its continuous nature, but avoiding γ_2 is more beneficial than avoiding κ_{III}. The disadvantage of κ_{III} may be reduced if the lamellar structure is avoided near the surface. This may be acchieved by heat treatment [5]. To the author's knowledge, the effect nickel might have on NAB film formation has not been examined before. In the thorough analysis of the passive film of NAB performed by Schüssler and Exner [9], profiles of varying contents of different elements, like copper, aluminium, iron and oxygen, were determined, however, the content of nickel was not. As partially hydrated NiO is able to protect a nickel substrate when only nanometer

thick, there is a possibility that nickel is more important to the passive protection of NAB than assumed. However, nickel is cathodically protected at the OCP of NAB at pH=8.2, which means it is not likely that a partially hydrated NiO film will be formed on NAB in SSW at OCP conditions. At pH=3.5, the OCP of NAB is anodic to nickel and such a film may be formed. However, the OCP as a function of pH test proved no passivity of pure nickel at such a low pH. The presence of other species is known to affect passive film formation. Hence, the presence of nickel may affect the formation of aluminium, copper and iron oxides, and the presence of copper, iron and aluminium may affect the stability of the NiO in different environments. The presence of copper in Al_2O_3 is known to reduce the protective properties of Al_2O_3 [22]. However, the presence of copper also increase the pitting potential of Al_2O_3 [23]. Similar connections are possible for the other elements in NAB. As iron oxides are not known to contribute to passive protection of alloyed steels in seawater, corrosion of iron in NAB is assumed to be unaffected by the presence of other species in other ways than polarizing the surface and thus altering the current densities of iron corrosion.

Iron has not been a major subject in this thesis, due to the stable behaviour iron displayed in the preliminary project [1]. Iron is still of great importance for the corrosion properties of NAB as κ_{II} and κ_{IV} are based on Fe_3Al. κ_{II} and κ_{IV} have the lowest nobility of the phases found in as-cast $CuAl10Fe5Ni5$ [10], and it is thus expected that κ_{II} and κ_{IV} are the first phases to corrode in the static anodic polarization tests. Due to the discontinuous nature of the κ_{II} and κ_{IV} particles, iron is not considered to be very detrimental to the corrosion properties of the NAB structure examined in this work.

Chapter 6

Conclusion

The main objectives of this work have been:

- To examine the stability of aluminium oxide at different pH levels.

- To determine whether nickel effect SPC of NAB.

- To examine the corrosion behaviour of NAB and its constituent phases at different potentials and pH levels.

- To connect the corrosion behaviour of the NAB phases to their main elements.

- To evaluate the extent of corrosion attacks on NAB at low pH.

The OCP of NAB is stable for pH>5.5, due to sufficient passive protection of the κ phases. The OCP is also stable about pH<4, where corrosion is first dominated by oxidation of the κ phases. Al_2O_3 is unstable at pH<6, wheras partially hydrated NiO displays stability in the same region as NAB. Nickel is cathodic to NAB when NAB is passivated, and the formation of an NiO film on NAB is thus expected to be very slow, if film formation is possible. However, the presence of nickel in the Al_2O_3 layer may stabilize the Al_2O_3 to the pH range where NAB is passivated.

At OCP conditions the corrosion properties of freshly polished NAB is mainly determined by corrosion of the copper-rich α phase at pH=8.2 and corrosion of the intermetallic κ phases at pH=3.5. The corrosion properties of the α phase are seemingly independent of pH, while the κ phases are passivated at pH>5.5. The volume fraction of κ is estimated to $18\% \pm 8\%$. For exposure of freshly grinded NAB surfaces, exposed one hour in SSW, i_{corr} for the active areas are

$$i_{corr, \; \kappa, \; pH=3.5} = 156 \; mA/m^2$$
$$i_{corr, \; \alpha, \; pH=8.2} = 85 \; mA/m^2$$

When freshly prepared NAB is anodically polarized in SSW with pH=3.5 corrosion is dominated by oxidation of κ for E<-200 mV vs AgAgCl. For $E \in$<-200,-100> mV vs Ag/AgCl, the corrosion of both α and κ contribute considerably to the anodic current. For E>-100 mV vs Ag/AgCl, both α and κ are corroding, but the difference in area makes corrosion of α overshadow the contribution from κ corrosion when concidering i for the entire NAB surface.

For long time exposure to pH<4 the corrosion properties of NAB are first established by corrosion of the intermetallic κ phases. The surface becomes depleted from the dis-continuous κ phases, κ_{II} and κ_{IV}, as these corrode and the potential of the surface increases as the iron-rich phases disappear. As the potential of the surface is moving closer to the OCP of copper, also α starts corroding significantly. For exposure between one day and eight weeks both α and κ corrodes significantly. Corrosion of κ_{II} and κ_{IV} is then dependent on the corrosion of α, as these particles are embedded within α. Thus, the presence of iron-rich phases is not very detrimental. The OCP seems little effected by the corrosion of these particles after it is stabilized at a potential close to the OCP of copper. Even though corrosion of α is the main reaction at OCP conditions for NAB at pH<4 after a day of exposure, the corrosion of κ_{III} is more likely to cause disintegration of NAB at pH<4, due to its continuous nature, high corrosion rate and small area of exposure.

The effect of the main alloying elements in a NAB structure, consisting of α, κ_{II}, κ_{III} and κ_{IV}, can be summarized as follows:

- Iron only affects the corrosion properties of NAB to a minor extent by lowering the OCP during the first day of exposure in low pH environments.

- Copper is the element with most pronounced effect of the corrosion properties of NAB at pH=8.2. For exposure in SSW with pH<4, copper dominates the corrosion properties of NAB when polarized above -100 mV vs Ag/AgCl, and controls the OCP after depletion of κ_{II} and κ_{IV}.

- Aluminium is passive at pH=8.2 and protects the κ phases at this pH. Al_2O_3 is unstable below pH=6, but is assumed to keep the κ phases stable until pH=5.5 due to stabilization of the Al_2O_3 layer by the presence of other elements.

- Nickel prevents the formation of the corrodable γ_2 phase, but stabilizes the continuous κ_{III} phase, which may lead to severe corrosion attacks at low pH. However, nickel and NAB have both been documented to be stable until pH=5.5, which suggests that nickel might strengthen the stability of Al_2O_3. Heat treatment of NAB may lead to discontinuous κ_{III} near the surface [5], and thus reduce the undesired effect of nickel.

Chapter 7

Further Work

This chapter lists topics and issues that could be of interest for further examination.

- **Characterization of the passive film of NAB including the nickel content:** Previous analyses of the passive film on NAB have been established without concidering the content of nickel, due limitations in the method used [9]. An analysis that detects all the elements within the passive layer may confirm or discard the theory that nickel, or possibly other elements, increases the passivity of Al_2O_3 on NAB.

- **Corrosion experiments on alloys with the composition of α and κ_{III}:** The corrosion properties of the constituent phases themselves are of interest due to the selective corrosion properties of NAB. However, it is difficult to isolate the corrosion properties of one phase due to the presence of the others. If an alloy with similar contents as κ_{III} is created, the critical pH, where κ_{III} is no longer corrosion resistant, could be determined. Corrosion experiments on pure α could be interesting to find out whether the the presence of κ phases is positive for the corrosion properties of α in seawater or not.

- **Corrosion tests on heat treated NAB where κ_{III} is no longer continuous close to the surface:** The continuous nature of κ_{III} makes NAB especially susceptible to deep corrosion attacks. A heat treatment could remove this weakness from the material. Jahanafrooz et al. [6] reports that κ_{III} may be spheroidized, and as κ_{III} is the last κ phase to solidify, the κ_{II} and κ_{IV} particles are not expected to be dissolved by this transformation. However, such a heat treatment will affect the other phases as diffusion increases with increasing temperature. Thus, the mechanical properties, as well as the corrosion properties, of heat treated NAB are not necessarily better than the as-cast structure. If the properties are better for heat treated NAB, development of a heat treatment suitable for large components is of interest.

Appendices

Appendix A

Experimental Details

In this appendix additional information about the experiments and results is given.

A.1 Composition of SSW

The SSW was mixed according to the ASTM D1141 standard. The resulting composition is given in Table A.1.

Table A.1: Composition of SSW.

Compound	Concentration [g/L]
NaCl	24.53
$MgCl_2$	5.20
Na_2SO_4	4.09
$CaCl_2$	1.16
KCl	0.695
$NaHCO_3$	0.201
KBr	0.101
H_3BO_3	0.027
$SrCl_2$	0.025
NaF	0.003
$Ba(NO_3)_2$	0.0000994
$Mn(NO_2)_2$	0.0000340
$Cu(NO_3)_2$	0.0000308
$Zn(NO_3)_2$	0.0000096
$Pb(NO_3)_2$	0.0000066
$Ag(NO_3)$	0.00000049

A.2   pH-variation during long-time exposure of NAB in SSW with pH∈<3,4>

The pH variation during the long-time exposure of NAB is listed in Table A.2. HCl was added five times during the experiment in order to maintain pH<4. The pH was logged before and after HCl addition, and both values are noted in Table A.2.

Table A.2: pH during exposure of NAB in SSW with pH∈<3,4> for up to eight weeks. HCl has been added where two pH values are given.

Days after immersion	pH
0	3.42
5	3.55
7	3.60
12	3.70, 3.29
14	3.30
15	3.51
20	3.71
22	3.73
23	3.81, 3.48
26	3.66
30	3.83, 3.39
33	3.43
35	3.53
37	3.58, 3.25
48	3.40
49	3.68
51	3.62, 3.24
54	3.42
56	3.62

A.3   Weight loss during long-time exposure of NAB in SSW with pH∈<3,4>

The measured weight losses of the NAB samples exposed to SSW with pH∈<3,4> for different time instances are given in Table A.3. The weight loss is plotted in Figure 4.20.

Table A.3: Weight loss of NAB samples exposed to SSW with pH∈<3,4> for one day to eight weeks.

Exposure time	Weight, start [g]	Weight, end [g]	Total weight loss [g]	Average weight loss [g/day]
One day	33.8334	33.8283	0.0051	0.0051
One week	30.8883	30.8688	0.0195	0.0028
Four weeks	31.9682	31.8708	0.0974	0.0035
Eight weeks	24.9920	24.7502	0.2418	0.0043

A.4   Noice reduction of sampled measurements using IIR low-pass filtering

Infinite Impulse Response (IIR) filters are a type of frequency filters that may be used for noice suppression in a sampled signal. A first order IIR-filter is given on the form [29]

$$y[n] = a_1 y[n-1] + (1-a_1)x[n] \tag{A.1}$$

where $x[n]$ is the input signal, $y[n]$ is the filtered output signal and a_1 is the feedback filter coefficient. In this thesis a filter on the form given in (A.1) has been applied to reduce the effect of noice during measurement sampling. The only filtered measurements are the plots of the static polarization test and the long exposure test for NAB in SSW with pH$\in$<3,4>. For the long exposure test, a_1=0.95 was used. a_1=0.97 was used for the 24 hour and 48 hour long static polarization tests for NAB. The original graphs are given alongside the filtered measurements in Figures A.1 and Figure A.2.

(a) Original   (b) Filtered
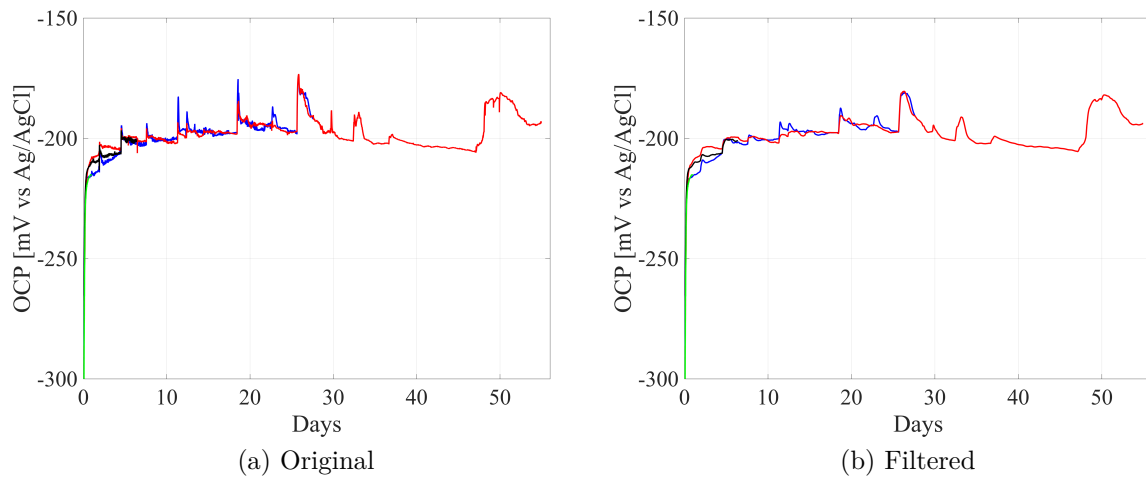
Figure A.1: Original and filtered OCP measurements of NAB samples exposed up to eight weeks in SSW with pH$\in$<3,4>.

(a) Original

(b) Filtered

(c) Original
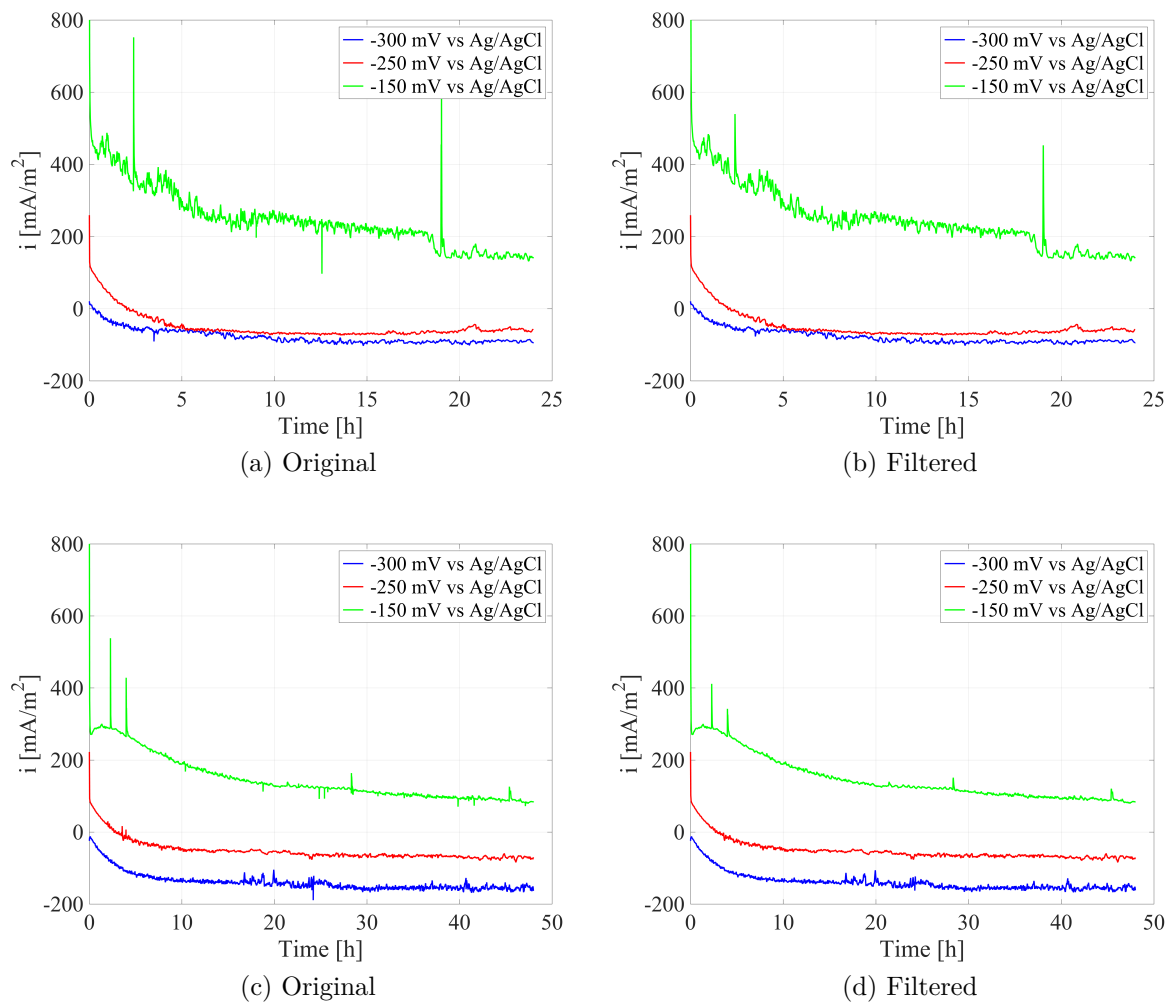
(d) Filtered

Figure A.2: Original and filtered measurements from the static polarization test of NAB in SSW with pH=3.5.

Appendix B

Calculation of Chloride Content in Electrolytes

The change of pCl, due to addition of HCl to SSW, is calculated here.
A mixture of SSW and HCl with pH=3.5 consisted of about 14 mL 12 M HCl added to 25 L of SSW.
Complete dissolution of salts is assumed.

Molar masses [g/mol]	
Cl	35,45
Na	22,99
Mg	24,31
Ca	40,08
K	39,1
Sr	87,62
H	1,008

Species in SSW that contain chloride	Concentration [g/L]	Molar weight [g/mol]	Concentration [mol/L]	[mol Cl/L]
NaCl	24,53	58,44	0,4197	0,4197
MgCl2	5,2	95,21	0,0546	0,1092
CaCl2	1,16	110,98	0,0105	0,0209
KCl	0,695	74,55	0,0093	0,0093
SrCl2	0,025	158,52	0,0002	0,0003
Cl concentration in SSW				0,5595

In mixture	
Volume SSW [L]	25
Volume of 12 M HCl [L]	0,014
Moles Cl	14,1560
Concentration Cl [mol/L]	0,5659

Concentration difference [mol/L]	0,0064
pCl, SSW	0,2522
pCl, mixture	0,2472
pCl decrease from SSW to mixture	1,96 %

Appendix C

Photos of Experiments

This section includes photoes from some of the corrosion experiments. A polarization experiment is imaged in Figure C.1. This equipment and configuration was used for polarization curves, static polarization of NAB and the static polarization of aluminium, except the latter was performed in a smaller container. Figure C.3 shows a photo of the OCP variation with pH test. A similar container was used for the static polarization test of aluminium. The long exposure experiment for NAB in SSW with pH∈<3,4> is portrayed in Figure C.2.

Figure C.1: Experimental configuration of polarization experiments. Here with an aluminium sample installed.

Figure C.2: Experimental configuration for the long-time exposure test for NAB in SSW with pH<4.
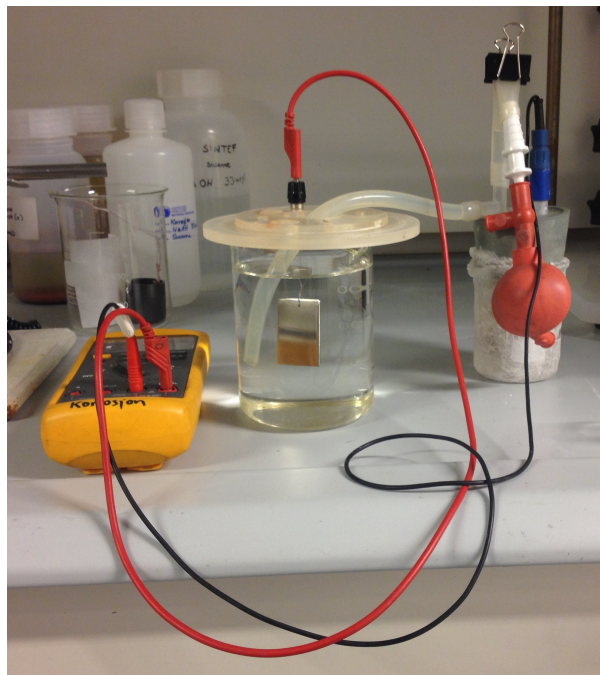
Figure C.3: Experimental configuration for the experiment of OCP variation with pH. Here with a nickel sample installed.

Appendix D

Project Description and Risk Assessment

MASTEROPPGAVE VÅR 2016

FOR

STUD.TECHN. ELLEN SYNNØVE SKILBRED

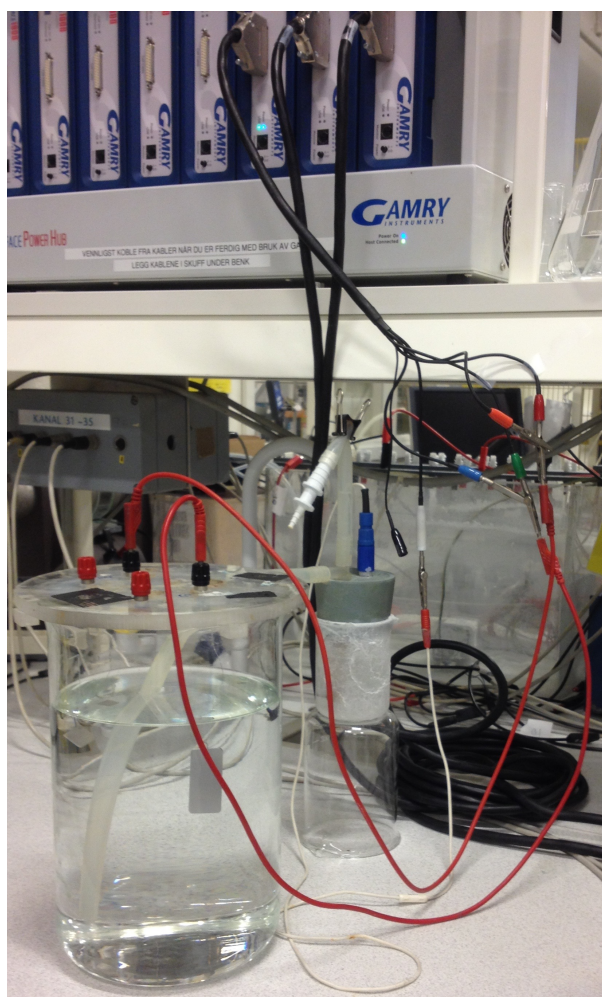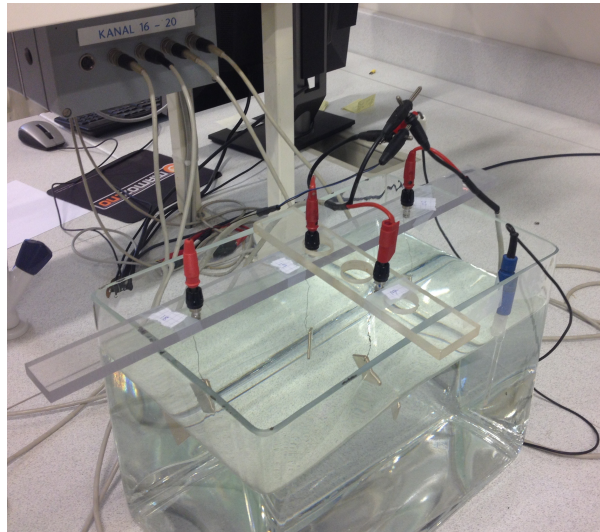**Korrosjon av Nikel Aluminium Bronse i sjøvann – Hvordan påvirker de ulike legeringselementene korrosjonsegenskapene?**

Corrosion of Nickel Aluminium Bronze (NAB) in seawater – How does the different alloying elements effect the corrosion properties?

Beskrivelse:

I prosjektoppgaven har studenten dokumentert at korrosjonsegenskapene til Ni-Al Bronse endres med pH i syntetisk sjøvann (SSV). En kompleks mikrostruktur med flere intermetalliske faser, med et høyt innhold av bl.a. Ni og Al i forhold til matriksen (alfa-matriks Cu 9wt% Al), ser ut til å være årsaken til den markante forskjellen i korrosjonsangrep ved pH 8 og pH 3 i SSV.

OCP-målinger og polarisasjonskurver av Cu, Ni, Al og Ni-Al Bronse viste at Ni-Al Bronse oppfører seg i stor grad likt som Cu ved pH 8, mens ved pH 3 er det Ni-Al Bronse og Ni som har flest likheter.

Litteratur på Ni-Al Bronse hevder at det er Al-innholdet som avgjøre pH-avhengigheten av legeringen sine korrosjonsegenskaper. Dette pga. Al sin evne til å danne passivsjikt ved midlere pH-verdier, og ustabilitet ved lave pH. Al-oksidet vil derfor beskytte de intermetalliske fasene ved midlere pH, mens ved lave pH vil ikke Al forme noe slikt sjikt, men aktivt korrodere.

I denne masteroppgaven er målsettingen å forsøke å oppnå en god forståelse av hvordan legeringselementene påvirker korrosjonsegenskapene til Ni-Al Bronse, og hvordan fasene i materialet oppfører seg ved forskjellige potensial og pH. Det vil legges særlig fokus på korrosjonsegenskapene ved lav pH, og hvorvidt Ni-innholdet har en signifikant rolle på de pH-avhengig korrosjonsegenskapene til Ni-Al Bronse.

Følgende eksperimentelle oppgaver vil bli prioritert:

1. En analyse av mikrostrukturen av Ni-Al Bronse med tilhørende bestemmelse av fasekomposisjon ved bruk av SEM og EDX.

2. Undersøke korrosjonsegenskapene til alfa-fasen ved midlere pH. Til dette kan studenten benytte en prøve som er utsatt for lav pH i lengere tid, der de intermetalliske fasene er korrodert vekk.

3. Nye forsøk med Al, Ni og Ni-Al Bronse ved varierende pH, med den hensikt å klargjøre legeringselementenes rolle i pH-avhengigheten. Det er ønskelig å oppnå et estimat for pH verdien der Ni-Al Bronse går fra selektiv korrosjon av alfa-fasen til korrosjon av de intermetalliske fasene.

4. Repetisjon av noen av eksperimentene fra prosjektoppgaven med endrede parameter. Dette for å oppnå høyere kvalitet på kurver med tanke på publisering. Kurvene for Al, Cu, Ni og Ni-Al Bronse vil bli prioritert.

5. Anodisk polarisering av Ni-Al Bronse til forskjellige potensial i lav pH for å se hva som skjer når de intermetalliske fasene er korroderer bort.

6. SEM-analyse av korrodert Ni-Al Bronse ved lav pH – tverrsnitt.

Formelle krav:

Senest 3 uker etter oppgavestart skal et A3 ark som illustrerer arbeidet leveres inn. En mal for dette arket finnes på instituttets hjemmeside under menyen masteroppgave (https://www.ntnu.no/web/ipm/masteroppgave-ved-ipm). Arket skal også oppdateres en uke før innlevering av masteroppgaven.

Risikovurdering av forsøksvirksomhet skal alltid gjennomføres. Eksperimentelt arbeid definert i problemstilling skal planlegges og risikovurderes innen 3 uker etter utlevering av oppgavetekst. Konkrete forsøksvirksomhet som ikke omfattes av generell risikovurdering skal spesielt vurderes før eksperimentelt arbeid utføres. Risikovurderinger skal signeres av veileder og kopier skal inngå som vedlegg til oppgaven.

Besvarelsen skal ha med signert oppgavetekst, og redigeres mest mulig som en forskningsrapport med et sammendrag på norsk og engelsk, konklusjon, litteraturliste, innholdsfortegnelse, etc. Ved utarbeidelse av teksten skal kandidaten legge vekt på å gjøre teksten oversiktlig og velskrevet. Med henblikk på lesning av besvarelsen er det viktig at de nødvendige henvisninger for korresponderende steder i tekst, tabeller og figurer anføres på begge steder. Ved bedømmelse legges det stor vekt på at resultater er grundig bearbeidet, at de oppstilles tabellarisk og/eller grafisk på en oversiktlig måte og diskuteres utførlig.

Besvarelsen skal leveres i elektronisk format via DAIM, NTNUs system for Digital arkivering og innlevering av masteroppgaver.

Kontaktperson: Roy Johnsen
Medveileder: Hedda Nordby Krogstad

Torgeir Welo
Instituttleder

Roy Johnsen
Faglærer

NTNU
Norges teknisk-
naturvitenskapelige universitet
Institutt for produktutvikling
og materialer

NTNU		Risikovurdering			Utarbeidet av	Nummer	Dato	
					HMS-avd.	HMSRV2601	22.03.2011	
HMS					Godkjent av		Erstatter	
					Rektor		01.12.2006	

Enhet: Institutt for produktutvikling og materialer   **Dato: 13.01.16**

Linjeleder: Torgeir Welo

Deltakere ved kartleggingen (m/ funksjon): Ellen Synnøve Skilbred (student), Roy Johnsen (hovedveileder), Hedda Krogstad (medveileder)

Kort beskrivelse av hovedaktivitet/hovedprosess: Masteroppgave Ellen Synnøve Skilbred. Korrosjon av Nikkel Aluminium Bronse i sjøvann.

Er oppgaven rent teoretisk? Nei

Signaturer: *Ansvarlig veileder:*   *Student:* Ellen Synnøve Skilbred

ID nr.	Aktivitet/prosess	Ansvarlig	Eksisterende dokumentasjon	Eksisterende sikringstiltak	Lov, forskrift o.l.	Kommentar
1	Preparere prøver til korrosjonstester	Student	HMS håndbok, opplæring på laboratoriet.	Vernebrillepåbud, labfrakk, førstehjelp- og brannslukningsutstyr tilgjengelig.	Arbeidsmiljøloven	
2	Utføre korrosjonstester	Student	HMS håndbok, opplæring på laboratoriet.	Vernebrillepåbud, labfrakk, førstehjelp- og brannslukningsutstyr tilgjengelig.	Arbeidsmiljøloven	
3	Opprydding etter korrosjonstester	Student	HMS håndbok, opplæring på laboratoriet.	Vernebrillepåbud, labfrakk, førstehjelp- og brannslukningsutstyr tilgjengelig.	Arbeidsmiljøloven	
4	Undersøkelse av prøver i SEM	Student	HMS håndbok, opplæring på laboratoriet.	Opplæring om bruk av utstyret.	Arbeidsmiljøloven	

NTNU		Utarbeidet av	Nummer	Dato
	Risikovurdering	HMS-avd.	HMSRV2601	22.03.2011
		Godkjent av		Erstatter
HMS		Rektor		01.12.2006

Enhet: Institutt for produktutvikling og materialer

Linjeleder: Torgeir Welo

Deltakere ved kartleggingen (m/ funksjon): Ellen Synnøve Skilbred (student), Roy Johnsen (hovedveileder), Hedda Krogstad (medveileder)

Dato: 13.01.16

Risikovurderingen gjelder hovedaktivitet: Masteroppgave Ellen Synnøve Skilbred. Korrosjon av Nikkel Aluminium Bronse i sjøvann.

Signaturer: *Ansvarlig veileder:* [signatur]   *Student:* Ellen Synnøve Skilbred

ID nr	Aktivitet fra kartleggings-skjemaet	Mulig uønsket hendelse/ belastning	Vurdering av sannsyn-lighet (1-5)	Vurdering av konsekvens: Menneske (A-E)	Ytre miljø (A-E)	Øk/ materiell (A-E)	Om-dømme (A-E)	Risiko-Verdi (menn-eske)	Kommentarer/status Forslag til tiltak
1	Sliping av prøver og boring av hull i dem.	Skade på fingre.	3	A	A	A	A	A3	Vær forsiktig med fingrene, følg med når du bruker utstyret.
2	Bruk av 12M HCl.	Søl av HCl og innhalering av HCl-gass.	3	D	B	A	A	3D	Bruk briller, hansker og dekkende klær (lange ermer og lange bukser). Arbeid under avtrekk. Fjern søl øyeblikkelig, bruk åndedrettsvern hvis sølet skjer utenfor avtrekk. Små søl kan nøytraliseres med større mengder vann.
4	Bruk av SEM.	Skade på utstyr.	1	A	A	D	A	A1	Vær forsiktig med utstyret. Spør erfarne brukere eller teknikere når du er usikker.

Risikovurdering

Sannsynlighet vurderes etter følgende kriterier:

Svært liten 1	Liten 2	Middels 3	Stor 4	Svært stor 5
1 gang pr 50 år eller sjeldnere	1 gang pr 10 år eller sjeldnere	1 gang pr år eller sjeldnere	1 gang pr måned eller sjeldnere	Skjer ukentlig

Konsekvens vurderes etter følgende kriterier:

Gradering	Menneske	Ytre miljø Vann, jord og luft	Øk/materiell	Omdømme
E Svært Alvorlig	Død	Svært langvarig og ikke reversibel skade	Drifts- eller aktivitetsstans >1 år.	Troverdighet og respekt betydelig og varig svekket
D Alvorlig	Alvorlig personskade. Mulig uførhet.	Langvarig skade. Lang restitusjonstid	Driftsstans > ½ år Aktivitetsstans i opp til 1 år	Troverdighet og respekt betydelig svekket
C Moderat	Alvorlig personskade.	Mindre skade og lang restitusjonstid	Drifts- eller aktivitetsstans < 1 mnd	Troverdighet og respekt svekket
B Liten	Skade som krever medisinsk behandling	Mindre skade og kort restitusjonstid	Drifts- eller aktivitetsstans < 1uke	Negativ påvirkning på troverdighet og respekt
A Svært liten	Skade som krever førstehjelp	Ubetydelig skade og kort restitusjonstid	Drifts- eller aktivitetsstans < 1dag	Liten påvirkning på troverdighet og respekt

Risikoverdi = Sannsynlighet x Konsekvens
Beregn risikoverdi for Menneske. Enheten vurderer selv om de i tillegg vil beregne risikoverdi for Ytre miljø, Økonomi/materiell og Omdømme. I så fall beregne disse hver for seg.

Til kolonnen "Kommentarer/status, forslag til forebyggende og korrigerende tiltak":
Tiltak kan påvirke både sannsynlighet og konsekvens. Prioriter tiltak som kan forhindre at hendelsen inntreffer, dvs. sannsynlighetsreduserende tiltak foran skjerpet beredskap, dvs. konsekvensreduserende tiltak.

NTNU			utarbeidet av	Nummer	Dato
⬛		Risikomatrise	HMS-avd.	HMSRV2604	08.03.2010
HMS/KS			godkjent av		Erstatter
			Rektor		09.02.2010

MATRISE FOR RISIKOVURDERINGER ved NTNU

		Svært liten	Liten	Middels	Stor	Svært stor
KONSEKVENS	Svært alvorlig	E1	E2	E3	E4	E5
	Alvorlig	D1	D2	D3	D4	D5
	Moderat	C1	C2	C3	C4	C5
	Liten	B1	B2	B3	B4	B5
	Svært liten	A1	A2	A3	A4	A5
				SANNSYNLIGHET		

Prinsipp over akseptkriterium. Forklaring av fargene som er brukt i risikomatrisen.

Farge		Beskrivelse
Rød		Uakseptabel risiko. Tiltak skal gjennomføres for å redusere risikoen.
Gul		Vurderingsområde. Tiltak skal vurderes.
Grønn		Akseptabel risiko. Tiltak kan vurderes ut fra andre hensyn.

Bibliography

[1] E. S. Skilbred. Corrosion of Nickel Aluminium Bronze (NAB) in seawater - How does the different alloying elements effect the corrosion properties, December 2015.

[2] F. Hasan, A. Jahanafrooz, G. W. Lorimer, and N. Ridley. The Morphology, Crystallography, and Chemistry of Phases in As-Cast Nickel-Aluminum Bronze. *Metallurgical Transactions A*, 13(8):1337–1345, 1982.

[3] H. J. Meigh. *Cast and Wrought Aluminium Bronzes: Properties, Processes and Structure*. Book (Institute of Materials (Great Britain))). IOM Communications, 2000.

[4] S. Neodo, D. Carugo, J. A. Wharton, and K. R. Stokes. Electrochemical behaviour of nickel–aluminium bronze in chloride media: Influence of pH and benzotriazole. *Journal of Electroanalytical Chemistry*, 695:38 – 46, 2013.

[5] E. A. Culpan and G. Rose. Microstructural characterization of cast nickel aluminium bronze. *Journal of Materials Science*, 13(8):1647–1657, 1978.

[6] A. Jahanafrooz, F. Hasan, G. W. Lorimer, and N. Ridley. Microstructural Development in Complex Nickel-Aluminum Bronzes. *Metallurgical Transactions A*, 14(10):1951–1956, 1983.

[7] P. Weill-Couly and D. Arnaud. Influence de la composition et de la structure des cupro-aluminiums sur leur comportement en service. *Fonderie*, 322, 1973.

[8] D. Nakhaie, A. Davoodi, and A. Imani. The role of constituent phases on corrosion initiation of NiAl bronze in acidic media studied by SEM–EDS, AFM and SKPFM. *Corrosion Science*, 80:104 – 110, 2014.

[9] A. Schüssler and H. E. Exner. The corrosion of nickel-aluminium bronzes in seawater—I. Protective layer formation and the passivation mechanism. *Corrosion Science*, 34(11):1793 – 1802, 1993.

[10] Q. N. Song, Y. G. Zheng, D. R. Ni, and Z. Y. Ma. Studies of the nobility of phases using scanning Kelvin probe microscopy and its relationship to corrosion behaviour of Ni–Al bronze in chloride media. *Corrosion Science*, 92:95 – 103, 2015.

[11] Y. Wang. Evaluation of long term seawater exposure corrosion specimens and electrochemical studies of nickel aluminium bronze alloys. *NACE International Corrosion Conference and Expo*, 2009.

[12] J. A. Wharton and K. R. Stokes. The influence of nickel–aluminium bronze microstructure and crevice solution on the initiation of crevice corrosion. *Electrochimica Acta*, 53(5):2463 – 2473, 2008.

[13] J. A. Wharton and K. R. Stokes. Analysis of nickel–aluminium bronze crevice solution chemistry using capillary electrophoresis. *Electrochemistry Communications*, 9(5):1035 – 1040, 2007.

[14] B. G. Ateya, E. A. Ashour, and S. M. Sayed. Corrosion of α-Al Bronze in Saline Water. *J. Electrochem. Soc.*, 141:71–78, 1994.

[15] Naval Surface Treatment Centre. `http://www.nstcenter.biz/navy-product-approval-process/approved-exterior-ship-coatings/marine-cathodic-protection/`. Accessed: 2015-06-04.

[16] F. W. Fink and W. K. Boyd. *The corrosion of metals in marine environments.* DMIC report. Bayer & Co., 1970.

[17] C. W. Jr. Hummer, C. R. Southwell, and A. L. Alexander. Corrosion of Metals in Tropical Environments. *Materials Protection*, 7:41–47, 1968.

[18] G. Kear, B. D. Barker, and F. C. Walsh. Electrochemical corrosion of unalloyed copper in chloride media—a critical review. *Corrosion Science*, 46(1):109 – 135, 2004.

[19] R. C. Barik, J. A. Wharton, R. J. K. Wood, and K. R. Stokes. The environmental factors affecting the performance of nickel aluminum bronze. *NACE International*, 2004.

[20] A. L. Bacarella and J. C. Griess. The Anodic Dissolution of Copper in Flowing Sodium Chloride Solutions Between 25°C and 175°C. *Journal of the Electrochemical Society.*, 120, 1973.

[21] A. M. Alfantazi, T. M. Ahmed, and D. Tromans. Corrosion behavior of copper alloys in chloride media. *Materials & Design*, 30(7):2425–2430, 2009.

[22] C. Vargel. *Corrosion of Aluminium.* Referex Engineering. Elsevier, 2004.

[23] A. M. Zossi, A. Morales Torres, S. M. Micheli, and H. Biloni. Effect of Solidification Microstructure on Corrosion Behavior of the Chill Zone in Aluminum Binary Alloys. *Metallurgical Transactions A*, 7(10):1489–1496, 1976.

[24] J. A. Beavers, G. H. Koch, and W. E. Berry. *Corrosion of Metals in Marine Environments.* MCIC report. Metals and Ceramics Information Center, 1986.

[25] M. Iida and T. Ohtsuka. Ellipsometry of passive oxide films on nickel in acidic sulfate solution. *Corrosion Science*, 49(3):1408 – 1419, 2007.

[26] S. C. Tjong. SIMS / XPS studies of the passive film on nickel. *Materials Research Bulletin*, 17(10):1297 – 1304, 1982.

[27] C. R. Southwell and A. L. Alexander. Corrosion of Metals in Tropical Environments. Part 8 - Nickel and Nickel-Copper Alloys. Technical Report 6597, Naval research laboratory Washington, D.C., 1967.

[28] M. Curioni and F. Scenini. The Mechanism of Hydrogen Evolution During Anodic Polarization of Aluminium. *Electrochimica Acta*, 180:712 – 721, 2015.

[29] J. H. McClellan, R. W. Schafer, and M. A. Yoder. *Signal Processing First.* Pearson/Prentice Hall, 2003.